

# Locomotor rhythm and pattern generating networks of the human lumbar spinal cord

DISSERTATION

submitted in partial fulfillment of the requirements for the degree of

**Doktor der technischen Wissenschaften**

by

**Simon M. Danner**

Registration Number 0526996

to the Faculty of Informatics  
at the Vienna University of Technology

Advisor: Prof. Frank Rattay

The dissertation has been reviewed by:

---

(Prof. Milan R. Dimitrijevic)

---

(Prof. Frank Rattay)

Vienna, August 19, 2013

---

(Simon M. Danner)



---

*Erklärung zur Verfassung der Arbeit*

Simon M. Danner  
Glasergergasse 9/11  
1090 Wien

Hiermit erkläre ich, dass ich diese Arbeit selbständig verfasst habe, dass ich die verwendeten Quellen und Hilfsmittel vollständig angegeben habe und dass ich die Stellen der Arbeit – einschließlich Tabellen, Karten und Abbildungen –, die anderen Werken oder dem Internet im Wortlaut oder dem Sinn nach entnommen sind, auf jeden Fall unter Angabe der Quelle als Entlehnung kenntlich gemacht habe.

---

(Ort, Datum)

---

(Unterschrift)





---

## Abstract

The view on the neural control of human locomotion has undergone changes in the past decades. In spite of the encephalization and the erect, bipedal mode of walking characteristic for human beings, independent observations imply that unperturbed locomotor patterns can be generated by similar spinal neural circuits as in other vertebrates. However, little is known about the organization of these rhythm and pattern generating networks in humans.

It has been shown that the human lumbar spinal cord isolated from supraspinal control due to traumatic spinal cord injury (SCI) can generate rhythmic, locomotor-like activity in response to sustained epidural spinal cord stimulation (SCS) of certain frequencies. The rhythmic activities consist of a series of stimulus time-related and rhythmically modulated posterior-root muscle (PRM) reflexes, each initiated in posterior root afferents and electromyographically recorded as compound muscle action potentials (CMAPs). The relation between individual stimuli and responses, as well as their electromyographic (EMG) characteristics, allow for the identification of mechanisms in addition to the information gained from the overall EMG patterns.

This thesis aims at uncovering the locomotor capabilities and their underlying mechanisms intrinsic to the human lumbar spinal cord. In the first part, rhythmic EMG data in response to SCS were analyzed, both, regarding overall patterns and the constituent units. Based on the information gained, in the second part, computer models were formulated to test hypotheses, to learn about their implications to primary and secondary phenomena and to generate research questions.

EMG activities of quadriceps, hamstrings, tibialis anterior and triceps surae, bilaterally in response to epidural stimulation at  $\leq 42$  Hz were analyzed in 10 individuals with motor complete posttraumatic SCI. Thirty-nine segments (duration: 10 s) of rhythmic activities found in all four-muscle groups of one lower limb were identified in 7 subjects. Phases of bursting and suppressed activities were recognized. Latencies of PRM reflexes were calculated.

A computational network model of neurons with Hodgkin-Huxley-like membrane dynamics was developed to test whether hypothesized rhythm and pattern generating networks would reproduce the recorded data. A core rhythm-generating network model was extended by adding conduction delays, presynaptic inhibition and disinhibition of parallel central pathways.

Within a given 10-s segment, rhythmic activities of all muscle groups had a constant phase relation. Dimensionality reduction by non-negative matrix factorization revealed that all expressed activity patterns of individual muscle groups can be best reproduced by a linear combination of 3 to 4 basic patterns, while two basic patterns that are similar to those seen in fictive locomotion (co- and reciprocal activity) already explain 83.2% of the variance. PRM reflexes constituting bursts during the extension phases had predominantly monosynaptic latencies. During flexion phase, a suppression of these responses was often observed. In such cases these

---

monosynaptic reflexes were replaced by delayed, oligosynaptic PRM reflexes.

Computer simulation showed that the activation of the rhythm and pattern generating circuits with persistent sodium channels as the source for rhythm generation is frequency dependent and this frequency dependence matches the electrophysiological data beyond the hypotheses. Stimulus time-locked motoneuron firing (resulting in the PRM reflexes) was explained by the interplay of relatively strong and highly synchronized afferent input and the relatively diffuse and weaker influence of the interneurons. This afferent influence of the motoneurons was presynaptically, rhythmically gated and postsynaptically modulated by excitatory input from the pattern formation and inhibitory input from last-order interneurons. Together with the selection of alternative interneuronal pathways (within the flexor side) the model reliably reproduced electrophysiological findings.

The electrophysiological data, as well as the computer simulations, give insight into the organization of the human spinal rhythm and pattern generating networks and reveal common control characteristics with the central pattern generators for locomotion described in animal experimental work. The constant phase relation of rhythmic outputs to one lower limb suggests a common, plurisegmental rhythm generator, and the various EMG patterns indicate separate stereotypic pattern formation modules. These neural circuitries possess many of the necessary components to generate functional locomotion. Yet, there is a lack of coordination in and between the muscles. Such coordination may require inputs from supraspinal centers, as well as feedback from the periphery.

---

## Kurzfassung

Die Sicht auf die neuronale Kontrolle der menschlichen Fortbewegung hat sich im Laufe der letzten Dekaden stark gewandelt. Trotz der Enzephalization und dem aufrechten, zweifüßigen Gang haben unabhängige Beobachtungen gezeigt, dass Bewegungsmuster der Beine von Nervenschaltkreisen im Rückenmark – ähnlich denen anderer Wirbeltiere – erzeugt werden können. Es ist jedoch wenig über die Organisation der Netzwerke zur Rhythmus- und Mustererzeugung im Menschen bekannt.

Es wurde gezeigt, dass das lumbale Rückenmark des Menschen – in Isolation von supraspinalen Einflüssen in Folge einer Rückenmarksverletzung – auf Stimulation mit einer epidural platzierten Elektrode mit der Generierung von Bewegungsmustern reagieren kann, die der menschlichen Fortbewegung ähneln. Die entsprechenden rhythmischen elektromyographischen (EMG) Aktivitäten bestehen aus einzelnen stimulationskorrelierten ‘posterior root-muscle’ (PRM) Reflexen, die rhythmisch moduliert sind. Die Reflexe werden in den Hinterwurzeln initiiert und von den Muskeln elektromyographisch aufgezeichnet. Der eindeutige Zusammenhang zwischen einzelnen Stimulationsimpulsen und den jeweiligen Muskelantworten erlaubt – zusätzlich zur Analyse der allgemeinen Muster – einen detaillierten Einblick in das dynamisch modifizierte Netzwerk im Rückenmark.

Das Ziel dieser Arbeit ist es, die Eigenschaften und zugrundeliegende Mechanismen jener neuronalen Rhythmus- und Mustergeneratoren im menschlichen Lumbalmark zu untersuchen, die der Fortbewegung dienen. Im ersten Teil werden rhythmische, durch Rückenmarkstimulation initiierte EMG Aktivitäten analysiert. Die Analyse umfasst sowohl allgemein die EMG Muster als auch die einzelnen Komponenten (die PRM Reflexe). Basierend auf dieser Analyse werden im zweiten Teil der Arbeit Computermodelle formuliert, um Hypothesen zu testen, den Einfluss von Annahmen auf primäre und sekundäre Phänomene zu verstehen und neue Fragestellungen zu finden.

Bei 10 Probanden mit motorisch kompletter Querschnittslähmung wurden EMG Aktivitäten der Ober- und Unterschenkelmuskulatur beider Beine bei epiduraler Rückenmarkstimulation mit Stimulationsfrequenzen  $\leq 42$  Hz analysiert. Für die weitere Analyse wurden 10 Sekunden lange Abschnitte in den EMG Aufzeichnungen ausgewählt, in denen rhythmische Aktivitäten in allen 4 abgeleiteten Muskelgruppen eines Beines auftraten. Insgesamt konnten 39 solcher Beispiele in 7 der 10 Probanden identifiziert werden. Die Relation der rhythmischen Aktivitäten der verschiedenen Muskelgruppen untereinander wurde festgestellt, und Latenzzeiten der PRM Reflexe wurden berechnet.

Ein Netzwerkmodell von Neuronen mit Hodgkin-Huxley-ähnlichen Membraneigenschaften wurde entwickelt, um zu testen, ob die angenommenen rhythmischen und mustererzeugenden Netzwerke elektrophysiologische Daten reproduzieren können. Ein rhythmischer erzeugendes ‘half-center’ Modell wurde mit Signallaufzeiten, präsynaptischer Inhibition und Disinhibition von parallelen, zentralen Pfaden erweitert.

In jedem der identifizierten 10 Sekunden Abschnitte hatten die rhythmischen Aktivitäten aller Muskelgruppen eine konstante Phasenrelation.

---

Die Dimensionsreduktion mittels nicht-negativer Matrix-Faktorisierung zeigte, dass die EMG Muster aller Muskelgruppen mit einer Linearkombination von 3 bis 4 Grundmustern optimal reproduziert werden können. Zwei Faktoren – ähnlich zur fiktiven Lokomotion in Tierexperimenten (sinusoid und reziprok zueinander) – beschreiben bereits 83.2% der Varianz. Die PRM Reflexe in der Extensionsphase hatten hauptsächlich monosynaptische Latenzzeiten, während in der Flexionsphase oft eine Suppression der monosynaptischen Reflexkomponente bei gleichzeitiger Entstehung oligosynaptischer PRM Reflexe beobachtet wurde.

Die Computersimulation zeigte, dass die Aktivierung von rhythmus- und mustergenerierenden Netzwerken, die auf einem anhaltenden, langsam sich selbst inaktivierenden Natriumstrom basieren, frequenzabhängig ist und dass diese Frequenzabhängigkeit mit den elektrophysiologischen Beobachtungen übereinstimmt.

Der eindeutige Zusammenhang von Stimulationspuls und EMG Antwort wurde durch das Zusammenspiel von relativ starker, hochsynchroner Aktivierung der Hinterstränge nahe der Motoneurone mit diffusem und relativ schwachem Einfluss der Interneurone am Motoneuron erklärt. Der afferente Einfluss auf die Motoneurone wurde präsynaptisch rhythmisch inhibiert und postsynaptisch von exzitatorischem Input von Interneuronen des mustererzeugenden Netzwerks und inhibitorischem Input von Ia Interneuronen und Renshaw Zellen moduliert. Zusammen mit der Selektion von alternativen zentralen Pfaden innerhalb des ‘Flexor-half-centers’ konnte das Modell verlässlich elektrophysiologische Phänomene nachvollziehen.

Die elektrophysiologischen Daten und das darauf aufbauende Computermodell gewähren Einblicke in die Organisation der rhythmus- und mustererzeugenden Netzwerke des menschlichen Rückenmarks. Gemeinsamkeiten mit den Mechanismen der zentralen Mustergeneratoren (‘central pattern generators’), die aus Tierversuchen bekannt sind, konnten nachgewiesen werden. Die konstante Phasenbeziehung der rhythmischen Aktivitäten in einem Bein legt einen gemeinsamen, multisegmentalen Rhythmusgenerator nahe. Die unterschiedlichen EMG Muster sind ein Indikator für separate Mustergeneratoren. Es wurde gezeigt, dass diese neuronalen Schaltkreise eine Vielzahl der notwendigen Komponenten besitzen, um funktionelle Fortbewegungsmuster zu erzeugen. Jedoch fehlt deren adäquate Koordination in und zwischen den einzelnen Muskeln. Eine derartige Koordination kann sowohl von Inputs von supraspinalen Zentren als auch von peripherem Feedback abhängen.

---

## *Acknowledgements*

Over the past few years I have received support and encouragement from a great number of individuals. Prof. Frank Rattay was able to guide and advise me in all matters of (academic) importance. Prof. Milan R. Dimitrijevic mentored me to attain knowledge about restorative neurology, neurology of spinal cord (injury) and human neural control of movement and locomotion. He and his family supported me during my stays in Houston and Bohinj. Dr. Karen Minassian, with his detailed knowledge about and his sincere interest in the subject, was instrumental in the design, implementation and completion of this thesis. Their guidance has made this a thoughtful and rewarding journey.

My colleagues, Dr. Ursula Hofstötter, DI Matthias Krenn, DI Thomas Halmetschlager, Ahmad Amini, MSc and Prof. Winfried Mayr, were always helpful in discussing topics of importance and solving problems at hand. Dr. Birgit Köchl provided encouragement and insights.

Above all, I want to thank my parents, who from a very early age on have fostered my inquisitiveness and who have always supported me throughout my studies.



---

*Contents*

<b>Abstract</b>	<b>v</b>
<b>Kurzfassung</b>	<b>vii</b>
<b>Acknowledgements</b>	<b>ix</b>
<b>Contents</b>	<b>xi</b>
<b>Abbreviations</b>	<b>xiii</b>
<b>I Electrophysiology</b>	<b>1</b>
<b>1 Introduction</b>	<b>3</b>
<b>2 Methods</b>	<b>5</b>
2.1 Subjects . . . . .	5
2.2 Stimulation and recording . . . . .	6
2.2.1 Stimulation protocol . . . . .	8
2.3 Data analysis . . . . .	8
2.3.1 Data selection . . . . .	8
2.3.2 Analysis of the overall rhythm pattern . . . . .	9
2.3.3 Analysis of phase relations . . . . .	15
2.3.4 Analysis of single CMAPs . . . . .	16
2.3.5 Statistical analysis . . . . .	18
<b>3 Results</b>	<b>19</b>
3.1 Identification of primitives . . . . .	22
3.2 Phase lags . . . . .	29
3.3 CMAP parameters . . . . .	32
<b>4 Discussion</b>	<b>43</b>
4.1 Rhythms and patterns . . . . .	44
4.2 Reflex latencies . . . . .	45
4.3 Clues to the human locomotor networks . . . . .	47
4.4 Significance . . . . .	50

<b>II Computer simulation</b>	<b>53</b>
<b>5 Introduction</b>	<b>55</b>
5.1 Aims . . . . .	61
<b>6 Methods</b>	<b>63</b>
6.1 Neuron models . . . . .	63
6.2 Population and network model . . . . .	68
6.3 Simulation . . . . .	71
6.4 Parameters . . . . .	71
6.4.1 Replication of Rybak’s model . . . . .	71
6.4.2 Model A . . . . .	74
6.4.3 Model B . . . . .	75
6.4.4 Model C . . . . .	76
<b>7 Results</b>	<b>77</b>
7.1 Model A . . . . .	82
7.2 Model B . . . . .	87
7.3 Model C . . . . .	87
<b>8 Discussion</b>	<b>93</b>
8.1 Conclusion . . . . .	96
8.2 Model limitations . . . . .	97
<b>Bibliography</b>	<b>99</b>
<b>A Appendix</b>	<b>109</b>
A.1 Tables . . . . .	109
A.2 Source code . . . . .	116
A.3 Curriculum vitae . . . . .	132



---

## *Abbreviations*

- AIC** Akaike information criterion
- ASIA** American Spinal Injury Association
- CMAP** Compound muscle action potential
- CPG** Central pattern generator
- EMG** Electromyography, electromyographic
- EPSP** Excitatory post synaptic potential
- H/Ham** Hamstrings
- Ia** Ia inhibitory neurons
- InPath** Inhibitory neurons of the inhibition of the polysynaptic flexor pathway
- InPf** Inhibitory neurons of pattern formation network
- InPs** Inhibitory neurons of presynaptic inhibition
- InRg** Inhibitory neurons of the rhythm generation network
- NaP** Slowly inactivating, persistent sodium
- LLPG** Lumbar locomotor pattern generator
- M** Mean
- MLR** Mesencephalic locomotor region
- NMF** Non-negative matrix factorization
- PF** Pattern formation neurons
- PRM** Posterior root-muscle (reflex)
- Q** Quadriceps
- R** Renshaw cell

## ABBREVIATIONS

---

**RG** Rhythm generation neurons

**SD** Standard deviation

**SE** Standard error

**SCI** Spinal cord injury

**SCS** Spinal cord stimulation

**SRES** Standardized residual

**TA** Tibialis anterior

**TS** Triceps surae

**-E** Postfix for neurons that are part of the extensor side

**-F** Postfix for neurons that are part of the flexor side

**Part I**

**Electrophysiology**



## Chapter One

---

### *Introduction*

The capability of the lumbar spinal cord to produce rhythmic motor outputs in the absence of supraspinal control has been demonstrated across fish and mammals, including humans (Brown, 1914; Grillner, 1981, 1985, 2011). In quadrupedal mammals, central rhythm and pattern generators have been demonstrated within the lumbar spinal cord segments for hindlimb control, which can produce alternating activity to groups of flexors and extensors in absence of (patterned) signals from descending and movement related afferent sources (Pearson & Gordon, 2000; Grillner, 2006). The human lumbar spinal cord networks can be activated by different types of externally generated inputs to produce rhythmic motor outputs to the paralyzed lower limbs. Patterned sensory feedback generated by the mechanical events during imposed, passive stepping movements on a treadmill can evoke rhythmic electromyographic (EMG) activities in the paralyzed lower limbs (Wernig & S. Müller, 1992; V. Dietz, Colombo, Jensen, & Baumgartner, 1995; Dobkin, Harkema, Requejo, & Edgerton, 1995; Harkema et al., 1997). Non-patterned sustained drive provided by continuous electrical stimulation over the lumbar spinal cord in supine, motor complete spinal cord injured (SCI) individuals at a frequency within the range of 25 Hz–60 Hz can generate rhythmic EMG activities in the lower limbs without manual manipulations of the legs (Dimitrijevic, Gerasimenko, & Pinter, 1998b; Gerasimenko, Daniel, Regnaud, Combeaud, & Bussel, 2001; Minassian, Gilge, et al., 2004).

The present study bases on these previous findings that the human lumbar cord can generate a variety of motor outputs, including rhythmic, locomotor-like patterns in response to sustained non-patterned input. A systematic examination of the intrinsic capabilities of the human lumbar spinal cord to process neural input signals with a predominant tonic character to produce rhythmic and patterned efferent activity is presented. The focus lies on the features and varieties of the rhythmic activities that can be produced by the human lumbar spinal cord in the absence of supraspinal control due to SCI and reduced sensory feedback input in the supine position. The analysis was not restricted to locomotor-like patterns, i.e. patterns of reciprocal activation of flexors and extensors. The main interest was to identify common principles of rhythm and pattern generation underlying the variety of motor outputs generated.

The lumbar spinal cord was isolated from supraspinal, volitional motor

control due to traumatic spinal cord injury. The supine position of the subjects limited (axial) lower limb loading and hip extension and thus the influence of sensory feedback thought to be essentially contributing to rhythm-generation (V. Dietz, R. Müller, & Colombo, 2002). A tonic, driving input to lumbar and upper sacral segments of the spinal cord is provided by continuous epidural SCS at a fixed frequency. Whereas the site of activation is through sensory afferents of posterior roots (Rattay, Minassian, & Dimitrijevic, 2000; Minassian, Persy, Rattay, Pinter, et al., 2007), the sustained, tonic nature of the neural input signals to the spinal cord is thought to be similar to that of the (missing) non-patterned components of brainstem descending excitatory drive (Dimitrijevic et al., 1998b).

Specifically, EMG activities of quadriceps, hamstrings, tibialis anterior and triceps surae in response to epidural stimulation at  $< 42.5$  Hz in 10 individuals with motor complete posttraumatic SCI were analyzed. A semi-automatic search for 10-second segments of stable rhythmic activities produced in all four studied unilateral limb muscles with a cycle frequency between 0.2 and 3 Hz was performed, without restriction of the specific patterns produced. By applying a decomposition technique, I sought to identify basic components of the patterns underlying the rhythmic activities. The EMG activities recorded from the lower limb muscles further consist of individual compound muscle action potentials (CMAPs) time-related to each stimulus, i.e. series of posterior root-muscle reflexes, which are rhythmically modulated (Minassian, Jilge, et al., 2004). In the second step of the analysis, I examined in detail the EMG characteristics of the responses to each pulse of repetitive stimulation during the 10-second segments of stable rhythmic activities. The EMG activity in response to pulsed posterior root stimulation is comprised of stimulus time-locked CMAPs, which have been identified as reflexes and termed after their initiation and recording sites—posterior root muscle (PRM) reflexes. In the case when rhythmic EMG activities were generated the reflex pathways were modified, resulting in modulation of CMAP amplitude, morphology and latency. This modulation gives insight into the spinal circuitries involved. Prolonged CMAP latencies were previously reported to exist in tibialis anterior during flexion phase (Minassian, Jilge, et al., 2004). Here, the change of latencies are systematically investigated throughout different phases of rhythmicity in functionally different muscle groups. The rationale was to find out whether there are systematic modifications of the individual EMG responses that are correlated to distinct phases of rhythmicity. The analysis was performed with the aim of formulating a model of the underlying neural circuits that can reproduce, both the overall patterns and their constituent units, the synchronous motoneuron firing.

*Methods*

## 2.1 Subjects

Ten subjects (mean age  $28.2 \pm 11.8$  years; 3 females) with post-traumatic, clinically motor complete SCI were studied (table 2.1). The participants were otherwise healthy adults with closed spinal cord lesions in a chronic ( $4.2 \pm 3.6$  years post-onset) and stable condition. All subjects had preserved stretch and cutaneomuscular reflexes of the lower limbs. Neurologic status was evaluated according to the American Spinal Injury Association (ASIA) standard neurological classification and the ASIA Impairment Scale (AIS; table 2.1). Seven subjects were classified as AIS A, and three as AIS B. Additionally, a surface EMG-based neurophysiological method was applied for the identification of sub-clinical, translesional activation of motor units (Sherwood, McKay, & Dimitrijevic, 1996). Here, two markers for the presence of such residual, supraspinal influence were used, first, the ability to induce task-related traces of EMG activity by the attempt of isolated ankle dorsi- and plantar-flexion (even in the absence of muscle contractions), and secondly, the ability to diffusely activate muscles below the lesion in response to reinforcement maneuvers, including forceful neck flexion against resistance and the Jendrassik maneuver (table 2.2). None of the subjects produced EMG activities in the lower limb muscles by the volitional attempt of performing left and right ankle movements (vlak, vrak). Six subjects generated EMG activity in the lower limb muscles in responses to reinforcement maneuvers and were thus classified as having a discomplete SCI (a lesion which is clinically complete but which is accompanied by neurophysiological evidence of residual supraspinal influence on spinal cord function below the lesion; Sherwood, McKay, & Dimitrijevic, 1996). The maximum number of recruited muscle groups (adductors, quadriceps (Q), hamstrings (Ham), tibialis anterior (TA), triceps surae (TS) bilaterally) in response to various types of reinforcement maneuvers is given in table 2.2. Subject 6 did not demonstrate translesional EMG generation during this neurophysiological evaluation, but had the ability to voluntarily enhance SCS-induced rhythmic activity and thus retained some preservation of distal brain influence. The remaining three subjects (subjects 1, 4, 8) showed neither clinical or subclinical signs of suprasegmental influence upon the lower limb muscles. All subjects had SCS systems implanted for the control of spinal spasticity affecting the lower limbs (Pinter, Gerstenbrand, &

Dimitrijevic, 2000). SCS system implantation and stimulation protocols were approved by the local ethics committee. All subjects signed written informed consent to participate.

### 2.2 Stimulation and recording

The stimulation system consisted of a cylindrically-shaped percutaneous lead (Pisces-Quad electrode, Model 3487A, Medtronic Inc, Minneapolis, MN, USA) connected to an implanted pulse generator (Itrel 3, Model 7425, Medtronic). The lead had four independent contacts, each 1.27 mm in diameter and 3 mm long, with an inter-contact spacing of 6 mm. For their identification, the contacts were labeled as 0 to 3, 0 being the most rostral one. The lead was located in the dorso-medial epidural space, i.e. inside the vertebral canal but outside of the meninges covering the spinal cord. Rostro-caudal positions of the 4 epidural contacts ranged from vertebral levels T11–L1 (see table 2.3). Stimulation was thus applied to the posterior aspect of the lumbosacral spinal cord from a close distance, approximately 1.5 mm–4.5 mm for electrodes at T12-vertebral levels in supine individuals (Holsheimer, den Boer, Struijk, & Rozeboom, 1994). The pulse generator, located subcutaneously in the abdominal wall, delivered quasi-monophasic, charge balanced stimuli. The pulse shape was approximately a rectangular pulse set at a width of 210  $\mu$ s that was followed by a long second phase of small amplitude which prevented charge accumulation, but was irrelevant for the stimulation process. Stimulus intensities of up to 10.5 V, and frequencies of 2.1 Hz–130 Hz at steps given by the pulse generator were programmable. Each lead contact could be set as cathodes, anodes or inactive, allowing for various bipolar or multi-polar stimulation modes. Monopolar stimulation was applied with one of the lead contacts selected as cathode and the active area of the pulse generator case as anode.



Table 2.1: Demographic data and clinical neurological evaluation

Subject	Gender	Age (years)	Years post injury	Vertebral level(s) of fracture	ASIA standard neurological classification of SCI				
					AIS	Neurological level of injury	Motor score	Pin prick score	Light touch score
1	f	20.1	3.3	T4, T5	A	T4	50	48	44
2	m	24.3	1.0	T3, T4	A	T5	50	50	50
3	m	58.4	3.3	T7, T8	B	T9	50	88	86
4	m	25.3	1.6	C5, C6	B	C8	27	68	68
5	f	33.0	2.7	T4T6, T10	A	T5	50	50	54
6	m	33.1	13.5	T5T8	B	T8	50	86	86
7	f	26.2	5.7	T7	A	T5	50	50	50
8	m	21.9	5.1	C5	A	C6	16	23	23
9	m	21.2	2.6	T7, T8	A	T7	50	61	61
10	m	18.0	3.0	C4,C5, T7	B	C6	16	64	64

ASIA, American Spinal Injury Association; SCI, spinal cord injury; AIS, ASIA Impairment Scale

Table 2.2: Neurophysiological evaluation of translesional EMG generation

Subject	Number of activated muscles (max = 10)		
	Vlak	Vrak	Reinforcement
1	0	0	0
2	0	0	10
3	0	0	10
4	0	0	0
5	0	0	10
6	0	0	0
7	0	0	4
8	0	0	0
9	0	0	5
10	0	0	7

Vlak, vrak, volitional attempt of left and right ankle movements, respectively.

### 2.2.1 Stimulation protocol

The study protocol was conducted for assessment of the SCS effect on the excitability of spinal motoneurons associated with the lower limbs (Pinter et al., 2000). Subjects assumed a comfortable supine position. For a given selection of active electrodes, stimulation was initially applied at 2.1 Hz, and the stimulus intensity was increased in 1-V increments until muscle twitch responses (Murg, Binder, & Dimitrijevic, 2000) were detected in all lower limb muscles studied. At this stimulus intensity, the stimulation frequency was gradually increased up to 100 Hz, with steps given by the pulse generator. Frequency variation from 2.1 Hz to 100 Hz was repeated for graded stimulus intensities up to a maximum of 10 V.

## 2.3 Data analysis

### 2.3.1 Data selection

Data segments of rhythmic activities with 10-s duration were selected semi-automatically from the data pool. Both lower limbs were treated independently, rhythmic activity had to be constantly present in all four ipsilateral muscle groups. The maximum stimulation frequency that allows analysis based on individual CMAPs is  $\approx 40$  Hz, thus higher frequencies were excluded

Table 2.3: Electrode array position

Subject	Vertebral position (X ray)		Muscle twitch thresholds for 0+3- configuration			
	Electr. 0	Electr. 3	RQ	RTS	LQ	LTS
1	middle T12	middle L1	6	6	6	10
2	upper L1	L1/L2 disc	2	4	3	6
3	upper T11	T11/T12 disc	4	8	3	7
4	lower T11	lower T12	2	4	2	4
5	T11/T12 disc	upper L1	2	3	3	3
6	middle T11	upper T12	3	4	4	4
7	T11/T12 disc	T12/L1 disc	3	3	3	4
8	upper T12	upper L1	2	2	3	3
9	lower T12	middle L1	1	1	2	1
10	lower T12	lower L1	5	5	3	5

Electr., electrode, RQ, LQ, right and left quadriceps, RTS, LTS, right and left triceps surae.

(maximal included frequency was 41.8 Hz). All possible 10-s data segments containing a unique set of consecutive CMAPs were extracted from all data segments with constant stimulation conditions (i.e. frequency, intensity and electrode configuration) and ranked for every recording session. The ranking parameter  $r$  was calculated for both lower limbs independently as follows:

$$r = \prod_{i=1}^4 \max f_i \quad (2.1)$$

where  $i$  is the index of the muscle group and  $f$  is the frequency spectrum between 0.2 Hz and 3 Hz as calculated by a Fast Fourier transform based on the peak-to-peak amplitudes of the CMAPs. Afterwards all 10-s windows of one recording session were sorted in descending order of  $r$ , sighted by the author and visually confirmed. Samples for further analysis were selected based on the value  $r$  with the constraint that only one example with the same pattern of co-activation and reciprocity between the muscle groups was selected from a recording segment where the stimulation conditions were constant.

### 2.3.2 Analysis of the overall rhythm pattern

For all samples of rhythmic activities an envelope was calculated (the process of calculating the rhythm cycles and phases is summarized in figure 2.1). This envelope was created by lowpass filtering the series of peak-to-peak amplitudes of the constituent CMAPs. For filtering a zero-phase Equiripple filter with

## 2. METHODS

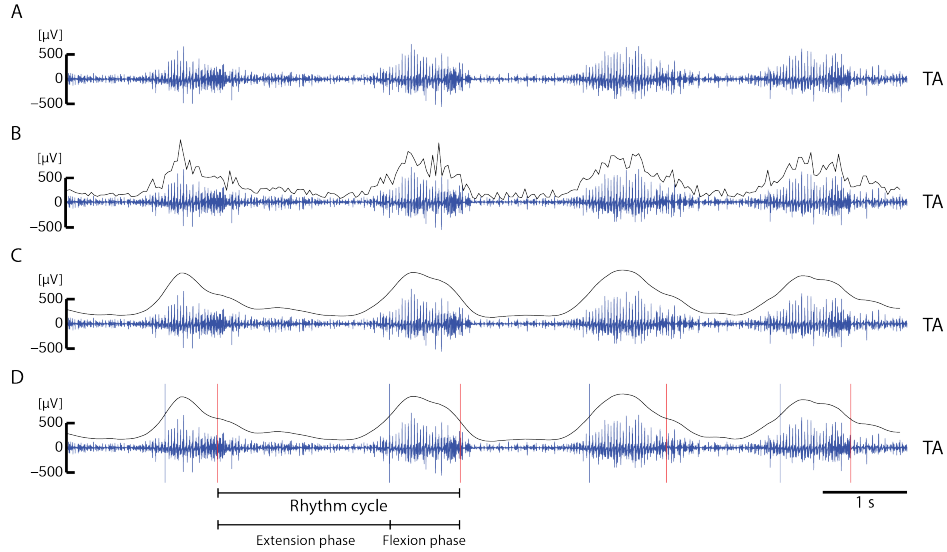


Figure 2.1: Identification and definition of rhythm cycles, and extension and flexion phases. *A.* A trace of electromyographic (EMG) activity of the tibialis anterior (TA). Note that the rhythm cycle as well as the extension and flexion phases are defined for all muscle groups based on the TA activity. *B.* The peak-to-peak amplitudes of the compound muscle action potentials, comprising the EMG activity, were calculated in the next step (black line). *C.* The signal of the peak-to-peak amplitudes were lowpass filtered with a zero-phase Equiripple filter. *D.* Bursting and silent phases were defined depending on the half-maximum of the individual peaks of the lowpass filtered signal of the peak-to-peak amplitudes. The extension phase was defined as the phase between two consecutive half-maxima with lower activity than the two neighboring phases, which were defined as the flexion phase. Thus, the flexion phase was the phase where TA is bursting and the extension phase when TA is in a silent period or exhibits relative to the flexion phase a low amplitude EMG activity.

following parameters was applied:  $F_{pass} = 0.125$ ,  $F_{stop} = 0.167$  in normalized frequency units and  $A_{pass} = 2$ ,  $A_{stop} = 5$  in dB. Peaks and valleys of the filtered data of TA were identified and the onset of the burst or active phase  $t_{TA-act-start}$  was defined as the time between a valley and the following peak when the value of the filtered data exceeds 50% of their relative difference. Similarly, the end of the burst or active phase  $t_{TA-act-end}$  was defined as the time between a peak and valley were the filtered value deceeds 50% of their relative difference. A *rhythm cycle* was defined as the time between two successive  $t_{TA-act-end}$ .

In order to identify underlying primitives of the rhythmic activities sur-

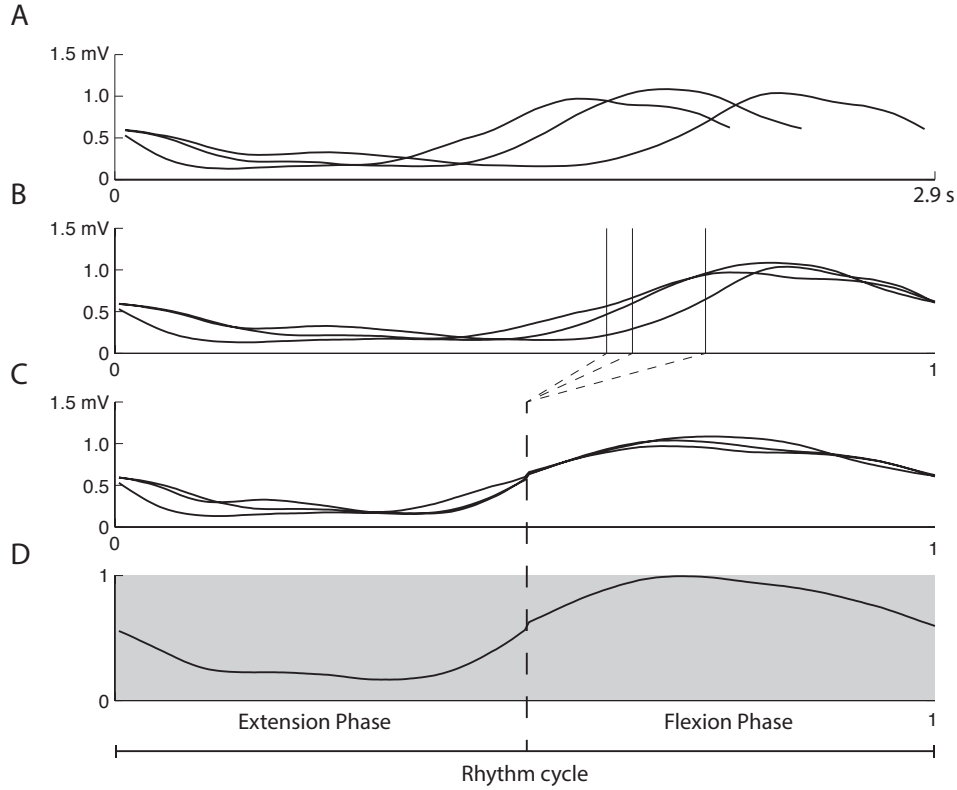


Figure 2.2: Processing of the rhythm cycles of a recording for the non-negative matrix factorization (NMF). *A*. All (here three) filtered envelopes of the electromyographic activity of individual rhythm cycles in one muscle group of one sample. These data form the basis for the further calculation. *B*. The duration of the rhythm cycles was normalized. *C*. The phase duration of the extension and flexion phases, respectively, were normalized. *D*. Finally the individual signals were averaged and normalized. This signal forms the basis for the NMF calculation.

passing all muscle groups a non-negative matrix factorization (NMF; D. D. Lee & Seung, 1999) was applied (cf. Dominici et al., 2011). The filtered data of all four ipsilateral muscle groups was split into rhythm cycles, interpolated to 200 samples per cycle, so that the phases between  $t_{TA-act-end}$  and  $t_{TA-act-start}$  as well as between  $t_{TA-act-start}$  and  $t_{TA-act-end}$  both account for 100 data points and averaged for every muscle group and data sample.

Thus resulting in 4 averaged rhythm cycles per data sample. All rhythm cycles were normalized to their maximum amplitude. These data were assembled into a matrix  $X$ , where a column is an observation (i.e. averaged gait cycle), is the input for the NMF (see figure 2.2).

## 2. METHODS

---

NMF is a method where  $X$  is factorized into two matrices,  $W$  and  $H$ :

$$\text{NMF}(X, k) \rightarrow WH \quad (2.2)$$

so that

$$X = WH \quad (2.3)$$

where  $X$  is an  $n$ -by- $m$ ,  $W$  an  $n$ -by- $k$  and  $H$  a  $k$ -by- $m$  matrix;  $k$  is the number/index of basic activation patterns,  $m$  is the number of EMG profiles,  $n$  are the 200 data points (time samples) of each EMG profiles over the rhythm cycle.

All matrices are strictly non-negative. Since there is generally no exact solution to equation 2.3 the problem has to be formalized as

$$X = WH + U \quad (2.4)$$

$$U \rightarrow \min \quad (2.5)$$

where  $U$  is the residual and is minimized. Here an NMF algorithm is applied that minimizes the function

$$F(W, H) = \|X - WH\|_F^2 \quad (2.6)$$

where the norm is calculated as the Frobenius norm

$$\|A\|_F = \sqrt{\sum_{i=1}^m \sum_{j=1}^n |a_{ij}|^2}. \quad (2.7)$$

For the purpose of interpretation,  $W$  will represent  $k$  primitives that multiplied with their respective loadings in  $H$  will best reproduce the data  $X$  with respect to the optimization criterion.

Several models with different values for  $k$  were calculated ( $k=1-8$ ). In order to assess how well one model describes the data, two values were calculated, the coefficient of determination ( $R^2$ ) and the Akaike Information Criterion (AIC; Akaike, 1974). The  $R^2$  is simply calculated as the relation between the explained variance of the model and the total variance and can be written as a function of the total ( $SS_T$ ) and the residual sum of squares ( $SS_R$ )

$$R^2 = 1 - \frac{SS_R}{SS_T} \quad (2.8)$$

since

$$SS_R + SS_M = SS_T \quad (2.9)$$

where  $SS_M$  is the sum of squares explained by the model. The three sums of squares are defined as follows:

$$SS_T = \sum_i (x_i - \bar{x})^2 \quad (2.10)$$

$$SS_M = \sum_i (f_i - \bar{x})^2 \quad (2.11)$$

$$SS_R = \sum_i (x_i - f_i)^2 \quad (2.12)$$

where  $f$  are the values predicted by the model and  $x$  the values of the real data. In the present case the averaged rhythmic cycles can be interpreted as data points in a 200-dimensional space, while the sum of squares are derived from the euclidian distance between two points. Thus, the minus in the equations above have to be seen as operator for the euclidian distance. This geometric interpretation is also fulfilled by the optimisation criterion (eqn. 2.6). Let

$$U = X - WH \quad (2.13)$$

be the difference between the data and the reproduced data of the model. Then

$$\|U\|_F = \sqrt{\sum_{i=1}^m \sum_{j=1}^n |r_{ij}|^2} \quad (2.14)$$

$$= \sqrt{\sum_{j=1}^n \sum_{i=1}^m |r_{ij}|^2} \quad (2.15)$$

$$= \sqrt{\sum_{j=1}^n \left( \sqrt{\sum_{i=1}^m |r_{ij}|^2} \right)^2} \quad (2.16)$$

and under assumption that all elements of  $U$  are real

$$\|U\|_F = \sqrt{\sum_{j=1}^n \left( \sqrt{\sum_{i=1}^m r_{ij}^2} \right)^2} \quad (2.17)$$

and since

$$\sqrt{\sum_{i=1}^n r_{i,j=c}^2} \quad (2.18)$$

is the euclidian distance between the the  $c$ -th column of  $X$  and  $WH$ , and

$$u_{i,j} = x_{i,j} - (WH)_{i,j} \quad (2.19)$$

the NMF can be also be interpreted as minimizing the sum of squares of the euclidian distance, or more accurately its square root, of the real data  $X$  and the data reproduced by the factorization into  $W$  and  $H$ .

This leads to the second criterion for the goodness of fit of the proposed NMF models, the AIC. The AIC is a criterion rooted in information theory and represents an estimate of the relative information loss by representing the reality with a given model (Burnham & Anderson, 2002). The AIC is defined by

$$\text{AIC} = 2K - 2\ln(\mathcal{L}(\hat{\theta})) \quad (2.20)$$

where  $K$  is the number of parameters in the statistical model and  $\mathcal{L}(\hat{\theta})$  is the maximized value of the likelihood function and  $\hat{\theta}$  is the vector of parameters that maximizes the function with respect to the model the data. The maximum of the likelihood function for least-square approaches is

$$\mathcal{L}(\hat{\theta}) = \left[ \frac{1}{\sqrt{2\pi\hat{\sigma}^2}} \right]^n e^{-\frac{1}{2}n}, \quad (2.21)$$

or

$$\ln(\mathcal{L}(\hat{\theta})) = -\frac{1}{2}n \ln(\hat{\sigma}^2) - \frac{n}{2} \ln(2\pi) - \frac{n}{2} \quad (2.22)$$

where  $\hat{\sigma}^2$  is the maximum likelihood estimator,

$$\hat{\sigma}^2 = SS_R/n, \quad (2.23)$$

and  $n$  the sample size. Additive constants are often discarded since they do not influence likelihood based inference, thus for all standard linear models equation 2.22 can be simplified to

$$\ln(\mathcal{L}) \approx -\frac{1}{2}n \ln(\hat{\sigma}^2). \quad (2.24)$$

For small values of  $K$  the second order information criterion or AIC with correction ( $\text{AIC}_c$ ) was proposed (Hurvich & Tsai, 1989).

$$\text{AIC}_c = \text{AIC} + \frac{2K(K+1)}{n-K-1}. \quad (2.25)$$

The  $\text{AIC}_c$  should be always used unless the sample size is large with respect to the number of estimated parameters (Burnham & Anderson, 2002). A single value of the AIC (or  $\text{AIC}_c$ ; note that from now on both values can be used interchangeably) has little meaning, but it is helpful for comparing several a priori specified models. The model with the lowest AIC value can be interpreted as the best one of the proposed models according to the data. Note that if all models are poor the AIC criterion only helps to identify the best of the poor models, it does not offer any information on the overall, objective quality of the model. There are two generally accepted measures based on the AIC for comparing several models, the  $\Delta\text{AIC}$  and the Akaike



weights ( $w_i$ ). The  $\Delta\text{AIC}$  is simply the difference between the AIC of a model and the minimum AIC of all investigated models or for the  $i$ -th model

$$\Delta\text{AIC}_i = \text{AIC}_i - \min \text{AIC}. \quad (2.26)$$

As a rule of thumb values of  $\Delta\text{AIC}$  smaller than 2 indicate substantial evidence for the model and values higher than 10 suggest that the model is very unlikely to be the true model. Alternatively, the Akaike weight  $w_i$  is a measure of how likely a given model is the best of all models. In other words,  $w_i$  is the weight of evidence in favor of model  $i$  being the actual best model (according to the K-L distance) of all investigated models (Burnham & Anderson, 2002). The Akaike weight is defined as:

$$w_i = \frac{e^{-\frac{1}{2}\Delta\text{AIC}_i}}{\sum_{r=1}^N e^{-\frac{1}{2}\Delta\text{AIC}_r}}, \quad (2.27)$$

where  $N$  is the number of models.

Here, both criteria, the AICc and the  $R^2$ , were calculated for the 8 different NMF models with  $k$ , the number of primitives, ranging from 1 to 8. The Akaike weight was used to choose the best model and the  $R^2$  was used in addition to describe the fit, according to the explained variance, of all models.

Furthermore, all rhythmic samples were categorized based on the co- and reciprocal activity between tibialis anterior and any other muscle group. Therefore the lowpass filtered signals were correlated and the categorization was based on the sign of the correlation (if significant). In case any correlation was not significant the pattern was called **-1**, **1** if all muscle groups were correlated positively with tibialis anterior, **2** if quadriceps and hamstrings were correlated positively and triceps surae negatively with tibialis anterior, **3** if all muscle groups except hamstrings were correlated positively with tibialis anterior, **4** if only quadriceps was correlated positively with tibialis anterior, **5** if only quadriceps was correlated negatively with tibialis anterior, **6** if only hamstrings was correlated positively with tibialis anterior, **7** if only triceps surae was correlated positively with triceps surae and **8** if all correlations with tibialis anterior were negative.

### 2.3.3 Analysis of phase relations

Phase relations between co-active muscle groups were calculated using cross correlations, which is defined for two discrete functions  $f$  and  $g$  as:

$$(f * g)[n] = \sum_{m=-\infty}^{\infty} f^*[m]g[n + m], \quad (2.28)$$

where  $f^*$  denotes the complex conjugate of  $f$ . The cross correlations were calculated for every pair of muscle groups of one recording using the lowpass

filtered signal. If the correlation between any two muscle groups was negative the pair was excluded, since it indicates that they are reciprocally active. The phase lags were defined as the value  $n$  relative to the cycle period of the same recording where the cross correlation ( $f * g$ ) is maximal. These phase lags were pooled by muscle group and reported as histograms. Furthermore, the relation of the pairwise co-active muscle groups of the subjects with phase lags larger than 15% of the cycle period were reported.

### 2.3.4 Analysis of single CMAPs

Control PRM reflexes responses were obtained from the PRM response elicited by the first pulse of the stimulation train that eventually lead to the generation of the rhythmic activities analyzed here. Alternatively, when data were not available from the same recording session as well as with same lead polarity and stimulus intensity, control PRM reflexes were also derived from a series of single pulses at the lowest available stimulation frequency (Minassian, Gilge, et al., 2004), i.e. 2.1-Hz stimulation, in order to build a large enough distribution of control responses to be compared statistically with PRM responses during rhythmic activity.

Peak-to-peak amplitude, onset and offset latencies, and widths of the CMAPs associated with these PRM reflexes were calculated. All these parameters were calculated for a time window that started 7 ms and 15 ms after the stimulus artifact for the thigh and leg muscle groups, respectively, and had a duration equal to the inter-stimulus interval. The time offsets were chosen to neglect responses that were clearly not related to the stimulus that is being analyzed and to capitalize on the whole response time where the responses can be traced back to a given stimulus. The onset latency was defined as the time between the preceding stimulus and the first EMG deflection from baseline larger than 25% of the largest deflection of the CMAP from zero of the same sign. Accordingly, the CMAP offset was defined as the last deflection from baseline larger than 25% of the largest deflection of the CMAP from zero of the same sign. The CMAP width was the duration between the onset latency and the offset. Additionally, the "weighted latency" or "center of gravity"  $cg$  of the response was calculated. This value,  $cg$ , was defined by the first time point where the cumulative sum of the absolute value of the EMG signal in the time window from the beginning to this time point is bigger or equal to 50% of the respective cumulative sum of the total time window to be analyzed.

All CMAP latency parameters were visually confirmed. This was done by a MATLAB application (see figure 2.3). Manual conformation followed following rules. i) In order to determine the onset latency there should have been a clear separation of the CMAP related to the previous stimulus and the CMAP under investigation and ii) noise or other artifacts did not interfere with the the latency detection. iii) If (i) and (ii) were given but the onset latency was calculated wrongly due to a too short offset for latency detection (e.g. during

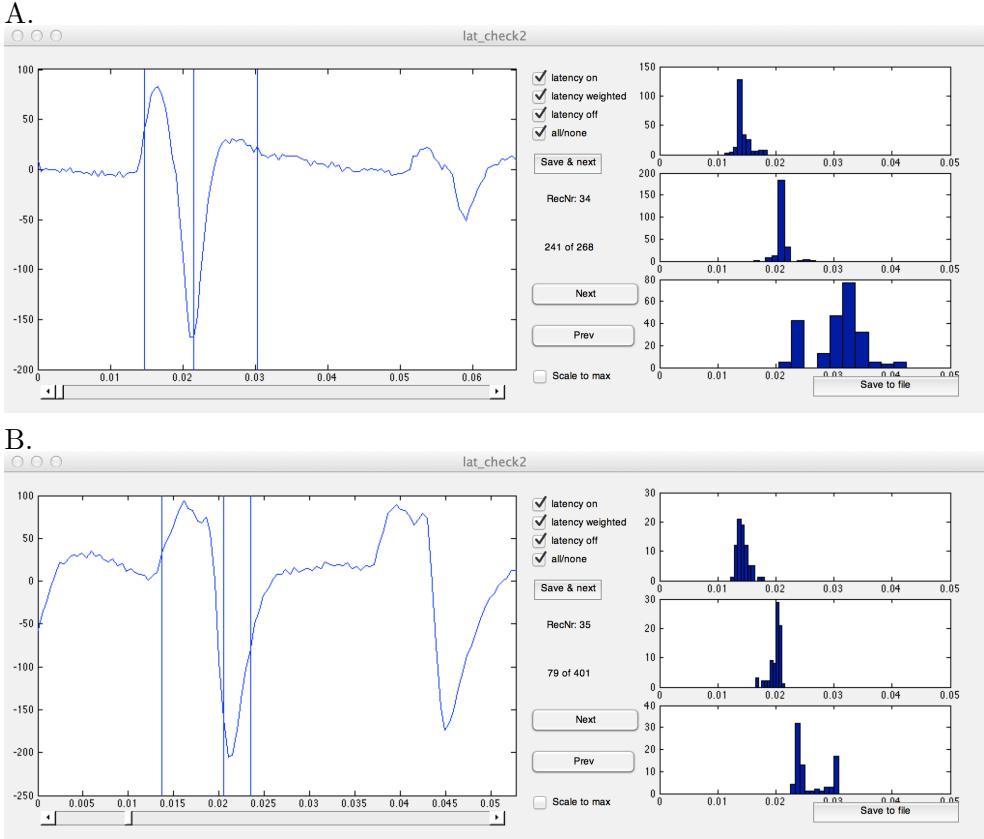


Figure 2.3: Semi-automatic detection of latency parameters. The application window of the semi-automatic detection of the compound motor action potential (CMAP) specific latency parameters. The left side shows a stimulus triggered time window with the electromyographic activity as the blue (non-vertical) line. The blue vertical lines illustrate the calculated onset, weighted (*cg*) and offset latencies (from left to right). Each value was visually confirmed and if not clearly correct rejected or if possible corrected by changing the offset (see text to *B.*). *A.* Shows a case where all parameters were calculated correctly. *B.* Shows a case where it was necessary to increase the offset that specifies how long after the stimulus the deflections will be ignored by the calculation. Note that the deflections from zero before the 10 ms post stimulus clearly correspond to the previous response.

prolonged latency response the previous response can be well present in the normal identification window but there is still a clear separation between previous and current response) the offset was shifted until the previous response did not influence the latency detection any more. iv) The detection of the weighted latency or center of gravity *cg* should not be obviously influenced by the previous response. v) Off-set latencies were selected according rules (i) and (ii) but not (iii). vi) If the latency parameters did not match they were removed from the analysis and declared as missing values. For statistical comparisons between the flexion and extension phases, only the parameters of the central 50% of the CMAPs in every phase were used.

### 2.3.5 Statistical analysis

Mean values were compared using Student's t-tests or analyses of variance or their non-parametric equivalents, i.e. Whitney-Mann U test and Kruskal-Wallis test. Categorical data was analyzed using Pearson's  $\chi^2$ -test and if the expected count was lower than 5 in any one cell, Fisher's exact test was used instead. Correlations were calculated to investigate the relation of two scalar values and linear regressions were calculated to investigate whether one scalar value predicts the outcome of another one. Similarly, logistic regressions were used to analyze scalar predictors on categorical values. Furthermore, analyses of covariances were used to compare mean values while controlling for the effects of scalar variables, as well as to investigate their effect. In order to counteract the problem of multiple comparisons all post-hoc tests were Bonferroni corrected. An  $\alpha$  error of  $p < .05$  was regarded as significant.

## Chapter Three

---

### *Results*

The semi-automatic selection of the data yielded in 39 10-s windows of rhythmic activities of one limb (3.1) in 7 out of 10 subjects. In all subjects except in subjects 3 and 6, rhythmic EMG segments were discovered in both limbs. Four to nine EMG segments were identified in the different subjects. The patterns and stimulation parameters of the samples are listed in table 3.1. The effective stimulation frequency was  $29.5 \pm 4.85$  Hz, with a range of 22.5 Hz–41.8 Hz (the latter being the highest singular frequencies considered). The stimulation voltage and electrode configuration and position varied considerably (see table 2.3).

The frequency of rhythmic activity was identical across all muscle groups in a given EMG segment. The rhythm frequency of the selected samples was in mean  $0.71$  Hz  $\pm$   $0.41$  Hz and varied considerably across the samples (min=0.27, max=1.84). Furthermore, an analysis of variances revealed that the burst frequency varied significantly between the subjects (S1: M=0.63 Hz, SD=0.25 Hz; S2: M=0.59 Hz, SD=0.26 Hz; S3: M=0.48 Hz, SD=0.95 Hz; S4: M=0.44 Hz, SD=0.33 Hz; S5: M=1.31 Hz, SD=0.40 Hz; S6: M=0.80 Hz, SD=0.25 Hz; S7: M=0.94 Hz, SD=0.28 Hz;  $F(6,32)=6.551$ ,  $p < .001$ ). Bonferroni corrected post-hoc tests revealed that subject 5 had significantly higher burst frequencies than subjects 1–4. All other post-hoc tests did not yield significant results.

The stimulation frequency was not significantly correlated with the burst frequency (Pearson's  $r = .125$ ,  $p = .450$ ). The duration of the extension phase was  $1.29$  s  $\pm$   $0.75$  s (min=0.28 s, max=2.94 s) and was not significantly correlated to the stimulation frequency ( $r = -.069$ ,  $p = .677$ ). The duration of the flexion phase was in  $0.59$  s  $\pm$   $0.27$  s (min=0.26 s, max=1.44 s) and was, although not significantly, negatively correlated to the stimulation frequency ( $r = -.291$ ,  $p = .072$ ). The extension phase amounted in mean to  $65.6\% \pm 10.4\%$  (min=45%, max=84%) of the total cycle duration.

A linear regression showed that the rhythm frequency significantly predicted the relative extension phase duration with respect to the rhythm cycle duration (constant: B=0.780, SE=0.025; rhythm frequency: B=-0.174, SE=0.031,  $\beta = -.684$ ,  $t(37) = -5.698$ ,  $p < .001$ ;  $R^2=.467$ ,  $F(1,37)=32.466$ ,  $p < .001$ ). The rhythm frequency also predicted the absolute flexion phase duration (constant: B=0.908, SE=0.065; rhythm frequency: B=-0.453, SE=-0.080,  $\beta = -.682$ ,  $t(37) = -5.677$ ,  $p < .001$ ;  $R^2=.466$ ,  $F(1,37)=32.230$ ,

### 3. RESULTS

---

Table 3.1: Selected 10-s windows of rhythmic activity

SID	RID	Elect. <sup>†</sup>	Fq. [Hz]	V	Leg	Pat.	Burst fq. [Hz]
1	1	0+3-	22.5	10	L	1	0.27
	2	0+3-	33.6	10	R	1	0.47
	3	0+3-	33.6	10	R	1	0.59
	4	0+3-	27.0	10	L	1	0.48
2	5	0+1-	30.1	7	R	1	1.00
	6	0+1-	30.1	8	R	1	0.93
	7	0+1-	30.1	9	R	4	0.88
	8	1+3-	27.7	9	R	1	0.33
	9	1+3-	27.7	10	R	1	0.40
	10	1+3-	27.7	10	L	1	0.44
3	11	0+3-	22.5	10	L	4	0.54
	12	0+3-	22.5	10	L	4	0.53
	13	0-2+	24.1	10	L	8	0.47
	14	2+3-	24.1	10	L	8	0.56
4	15	0+3-	28.3	6.5	L	1	0.35
	16	0+3-	28.4	6	L	6	0.33
	17	0+3-	28.4	6	L	8	0.36
	18	0+3-	28.4	7.5	R	-1	0.36
	19	0+3-	28.4	7	L	-1	0.35
	20	0+3-	28.4	7	L	1	0.30
	21	0+3-	28.4	7	R	1	0.33
	22	0+3-	31.5	6	L	6	0.28
	23	0+3-	33.6	8	R	2	0.30
5	24	0+3-	22.5	9	R	4	1.32
	25	0+3-	33.6	9	R	2	1.40
	26	0+3-	22.5	10	R	2	1.41
	27	0+3-	33.6	10	L	2	1.31
	28	0+3-	33.6	10	R	2	1.32
	29	2-3+	33.6	10	R	1	1.84
6	30	3-c+	27.0	3	R	7	0.61
	31	0+3-	27.0	5	R	-1	0.80
	32	0+3-	33.6	5	R	7	0.74
	33	1+3-	27.0	5	R	7	0.80
	34	2+3-	41.8	5	R	8	0.49
7	35	0-3+	23.0	10	L	1	1.19
	36	0-3+	34.1	10	L	3	1.16
	37	0-3+	34.1	10	R	1	0.94
	38	0-3+	34.1	10	R	3	1.09
	39	0-3+	41.8	9	R	3	0.54

<sup>†</sup>contact acting as cathodes (-) and anodes (+), c stands for case;  
SID/RID subject/recording identification number

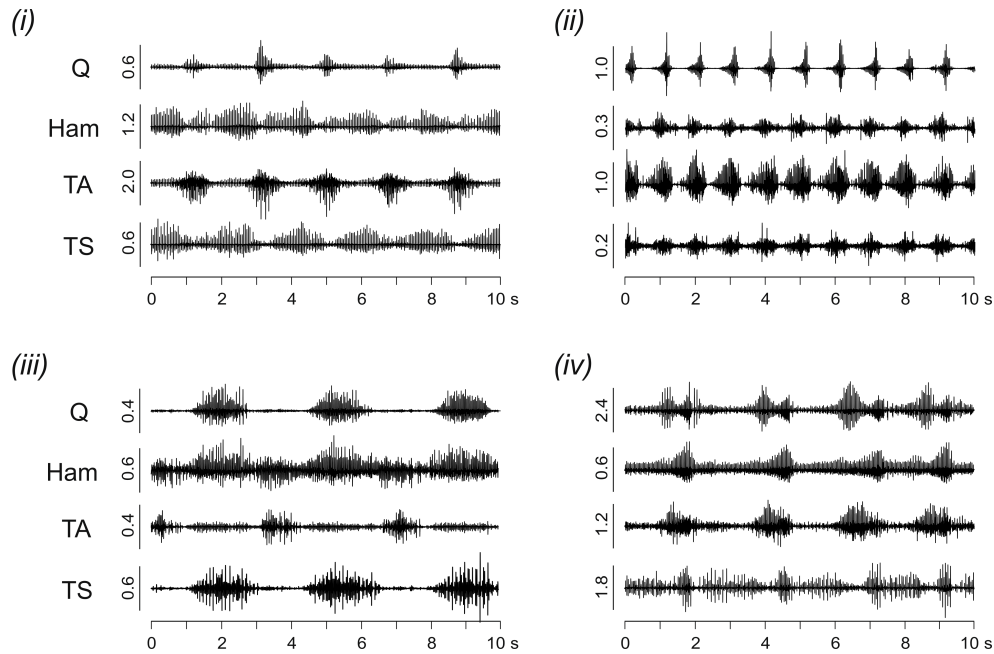


Figure 3.1: Ten seconds-EMG segments of rhythmic activity with stable pattern evoked by non-patterned epidural SCS in quadriceps (Q), hamstrings (Ham), tibialis anterior (TA), and triceps surae (TS). Exemplary results with a variety of rhythm frequencies and patterns, (i) subject 3, l, 0+3-, 10 V, 22.5 Hz (ii) subject 2, r, 0+1-, 7 V, 30.1 Hz; (iii) subject 4, l, 0+3-, 6 V, 31.5 Hz; (iv) subject 2, r, 1+3-, 10 V, 27.7 Hz. Vertical Scale bars are in mV.

$p < .001$ ). Thus both, the absolute flexion and extension phase duration became shorter with higher rhythm frequency, while relatively, there is a decrease in the extension phase duration.

All the observed rhythmic activity of each single muscle group was phase locked with any other rhythmically active muscle group. There were, however, various phase relations in-between the activities of different muscles. The most common occurrences of phase shifting were that one muscle group was either actively bursting at the same time when another muscle group was also bursting or was in its silent phases. The categorization of each 10-s segment based on the co-activities of every muscle group to tibialis anterior are listed in table 3.1. Three samples did not clearly follow this clear reciprocity. The most common pattern observed was the co-activation pattern with all ipsilateral muscle groups being activated in-phase (Pattern 1;  $n = 15$ ), while Pattern 5, with TA and Ham active in-phase with TA, and Q being active reciprocally, did not occur at all. The number of observations of the remaining patterns ranged from 2 to 5. Locomotor-like EMG activity with reciprocal activity in antagonistic muscles (Pattern 4) was observed 4

Table 3.2: NMF solutions

$k$	$R^2$	AIC	$\Delta$ AIC	$w$
1	.261	831.884	818.019	.000
2	.832	111.085	97.221	.000
3	.908	13.864	0.000	.998
4	.944	19.922	6.058	.002
5	.968	121.588	107.724	.000
6	.979	251.915	238.051	.000
7	.985	407.198	393.334	.000
8	.987	468.902	455.037	.000

NMF: non-negative matrix factorization

times in three subjects. In 27 cases quadriceps was co-active with tibialis anterior, hamstring in 14 cases and triceps surae in 15 cases. Using a logistic regression model, stimulation frequency did not predict whether quadriceps was co-active with tibialis anterior or not (constant:  $B=0.165$ ,  $SE=2.180$ ; frequency:  $B=0.022$ ,  $SE=0.073$ ,  $p=.765$ , Cox & Snell  $R^2=0.002$ ), similarly it did not significantly predict whether hamstrings (constant:  $B=-0.255$ ,  $SE=2.022$ ; frequency:  $B=0.17$ ,  $SE=0.068$ ,  $p=.797$ , Cox & Snell  $R^2=0.002$ ) or triceps surae were co-active with tibialis anterior (constant:  $B=-1.766$ ,  $SE=2.078$ ; frequency:  $B=0.065$ ,  $SE=0.070$ ,  $p=.351$ , Cox & Snell  $R^2=0.023$ ).

### 3.1 Identification of primitives

The NMF performed on the per recording and muscle group averaged lowpass filtered envelopes of the EMG activities ( $N=156$ ; i.e. 4 muscle groups x 39 recordings) yielded the results presented in figure 3.2 and table 3.2.

According to the Akaike weights  $w$  presented in table 3.2 a solution with 3 basic patterns was most likely. The second best solution was with  $k = 4$ , all other solutions, judged by the  $\Delta$ AIC and Akaike weights  $w$  were very unlikely. Nonetheless the two basic pattern solution already explained 83% of the total variance. As can be seen from figure 3.2 the two factor solution consisted of almost sinusoid factors with a period equal to that of the rhythmic cycle. Furthermore, one factor had the strongest contribution during the phase where tibialis anterior was active, the flexion phase, and the other one during the phase where tibialis anterior was not active, the extension phase. The three basic pattern solution pertained the factor mainly contributing to the extension phase but introducing two patterns that mainly contributed to the flexion phase, one with an early contribution (peak at 15% of the flexion



### 3.1. Identification of primitives

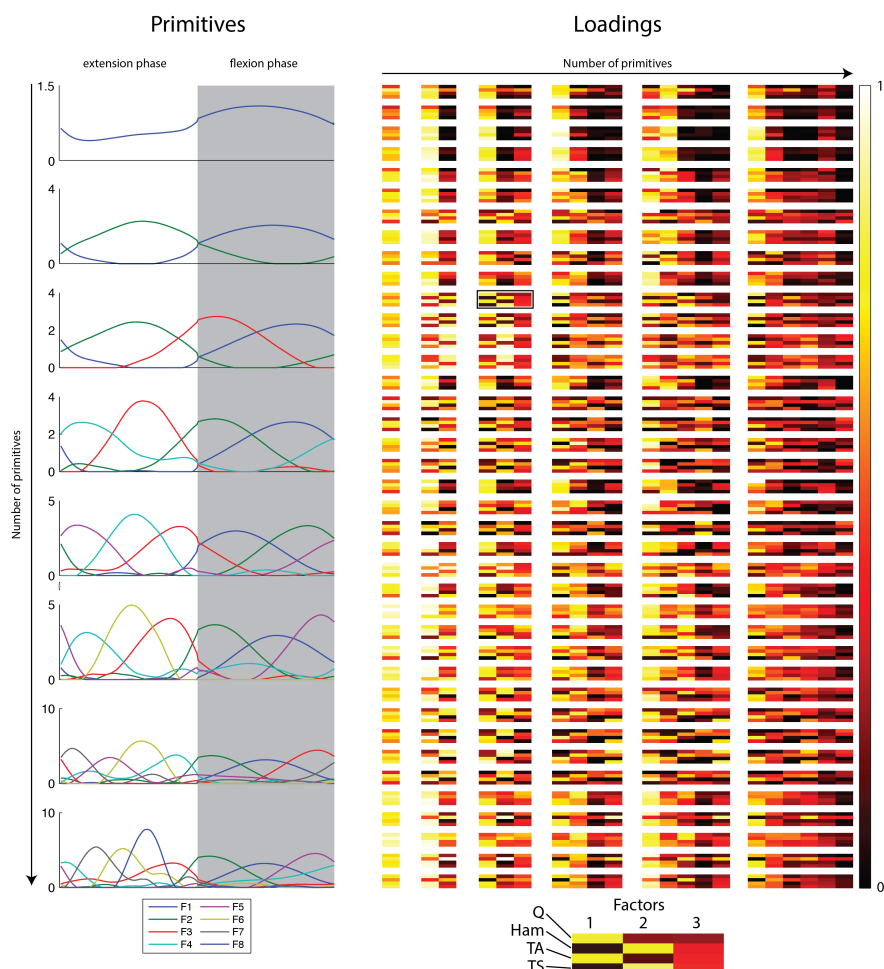


Figure 3.2: Presentation of the multiple solutions of the non-negative matrix factorization (NMF) performed on the per muscle group and sample averaged lowpass filtered posterior root-muscle reflex envelopes. *Left*: The primitives or basic patterns (F1–8) selected by the NMF depending on the specified  $k$ . Note that the three basic pattern (primitive) solution was the optimal one according to the Akaike information criterion. *Right*: Factor loading for all muscle groups and specified  $k$  (up to 6). The two-factor solution was characterized by almost sinusoid basic patterns, where one was predominately active during the flexion and the other one during the extension phase. Their loadings showed that when one of the patterns had a high loading that the loading of the other primitive was usually low. The three-factor solution introduced an early component in the flexion phase (red line) while still retaining the reciprocity between the first two factors (blue and green lines). Similarly, the four-factor solution splits the in the extension phase active component into two factors, one with an earlier and one with a later peak.

### 3. RESULTS

---

Table 3.3: Correlations between the different factor loadings (H)

		H 1	H 2	H 3	H 4
Two basic pattern solution	H1	1			
	H2	-.566***	1		
Three basic pattern solution	H1	1			
	H2	-.728***	1		
	H3	-.104	.146	1	
Four basic pattern solution	H1	1			
	H2	.062	1		
	H3	-.856***	-.024	1	
	H4	-.438***	.152	.473***	1

\*\*\* $p < .001$ , all values are Pearson's correlation coefficients

phase) and one with an late contribution (peak at 75% of the flexion phase) to the flexion phase. Similarly, the four basic pattern solution introduced a second factor in the extension phase. The first one peaked early (at about 17% of the extension phase) and the second one later (at 60% of the extension phase). The basic patterns contributing to the flexion phase were almost identically retained.

Table 3.4: Influence of muscle group, stimulation and burst frequency on the factor loadings and reconstruction error

		Stimulation Frequency			Burst frequency			$p$ post-hoc							
		B	$F_{1,150}$	$p$	$r$	B	$F_{1,150}$	$p$	Q-H	Q-TA	Q-TS	H-TA	H-TS	TA-TS	
H1 <sub>1F</sub>	.000	-0.001	9.371	.003	.059	0.020	44.330	.000	***	**	***	***	***	**	
H1 <sub>2F</sub>	.000	0.000	0.585	.446	.004	0.015	8.915	.003	***	***	***	***	***	***	
H2 <sub>2F</sub>	.000	-0.002	5.515	.020	.035	0.025	10.417	.002	***	**	***	***	***	***	
H1 <sub>3F</sub>	.000	0.000	0.114	.736	.001	0.007	1.221	.271	***	**	***	***	***	***	
H2 <sub>3F</sub>	.000	-0.002	5.510	.020	.035	0.020	5.615	.019	**	**	***	***	***	***	
H3 <sub>3F</sub>	.000	-0.001	1.135	.289	.008	0.032	24.502	.000	***	***	***	***	***	***	
H1 <sub>4F</sub>	.000	0.000	0.011	.917	.000	0.001	0.037	.848	***	***	***	***	***	***	
H2 <sub>4F</sub>	.000	-0.001	1.154	.284	.008	0.033	30.745	.000	***	***	***	***	***	***	
H3 <sub>4F</sub>	.000	-0.002	3.885	.051	.025	0.010	1.236	.268	*	**	***	***	***	***	
H4 <sub>4F</sub>	.000	-0.002	4.666	.032	.030	0.032	13.783	.000	**	**	***	***	***	*	
$d_{1F}$	.000	0.001	0.001	.978	.000	-0.711	9.759	.002	***	***	***	***	***	**	
$d_{2F}$	.000	0.004	0.177	.675	.001	-0.465	13.755	.000	***	***	***	***	***	***	
$d_{3F}$	.000	0.008	0.989	.322	.007	-0.618	43.544	.000	***	***	***	***	***	***	
$d_{4F}$	.000	0.012	3.956	.049	.026	-0.631	75.810	.000	***	***	***	***	***	***	
Muscle group - fixed effect															
		$F_{3,150}$	$p$	par	$\eta^2$	Q	H	TA	TS	Q-H	Q-TA	Q-TS	H-TA	H-TS	TA-TS
H1 <sub>1F</sub>	11.803	.000	.191		0.071 (0.023)	0.087 (0.012)	0.082 (0.010)	0.071 (0.020)	0.071 (0.020)	***	**	***	***	***	**
H1 <sub>2F</sub>	14.171	.000	.221		0.068 (0.033)	0.073 (0.022)	0.096 (0.005)	0.062 (0.032)	0.062 (0.032)	***	***	***	***	***	***
H2 <sub>2F</sub>	21.217	.000	.298		0.061 (0.042)	0.097 (0.042)	0.030 (0.024)	0.075 (0.046)	0.075 (0.046)	***	**	***	***	***	***
H1 <sub>3F</sub>	12.155	.000	.196		0.066 (0.038)	0.061 (0.031)	0.099 (0.005)	0.060 (0.043)	0.060 (0.043)	***	***	***	***	***	***
H2 <sub>3F</sub>	19.953	.000	.285		0.059 (0.047)	0.093 (0.047)	0.023 (0.024)	0.076 (0.048)	0.076 (0.048)	**	**	***	***	***	***
H3 <sub>3F</sub>	7.369	.000	.128		0.063 (0.044)	0.090 (0.033)	0.074 (0.012)	0.060 (0.038)	0.060 (0.038)	***	***	***	***	***	***
H1 <sub>4F</sub>	14.620	.000	.226		0.067 (0.039)	0.058 (0.033)	0.101 (0.008)	0.059 (0.040)	0.059 (0.040)	***	***	***	***	***	***
H2 <sub>4F</sub>	9.071	.000	.154		0.063 (0.043)	0.089 (0.029)	0.079 (0.012)	0.059 (0.035)	0.059 (0.035)	***	***	***	***	*	***
H3 <sub>4F</sub>	17.026	.000	.254		0.057 (0.050)	0.087 (0.047)	0.017 (0.019)	0.076 (0.061)	0.076 (0.061)	*	**	***	***	***	***
H4 <sub>4F</sub>	10.298	.000	.171		0.058 (0.047)	0.091 (0.048)	0.039 (0.032)	0.069 (0.049)	0.069 (0.049)	**	**	***	***	***	*
$d_{1F}$	3.529	.016	.066		2.966 (1.201)	2.971 (1.302)	2.490 (0.920)	3.322 (1.202)	3.322 (1.202)					**	**
$d_{2F}$	13.674	.000	.215		1.627 (0.705)	1.351 (0.625)	0.804 (0.406)	1.546 (0.797)	1.546 (0.797)		***	**	**	***	***
$d_{3F}$	6.158	.001	.110		1.081 (0.606)	0.894 (0.420)	0.762 (0.389)	1.177 (0.648)	1.177 (0.648)		*			***	***
$d_{4F}$	3.171	.026	.060		0.864 (0.504)	0.676 (0.396)	0.659 (0.407)	0.822 (0.450)	0.822 (0.450)					***	***

\*  $p < .05$ , \*\*  $p < .01$ , \*\*\*  $p < .001$ ,  $d$ : euclidian distance between original and reconstructed rhythmicity pattern, nF: n-pattern solution, par.  $\eta^2$ : partial  $\eta^2$

### 3. RESULTS

---

Table 3.3 shows the correlation coefficients of the factor loadings for the 2 to 4-factor solutions. The two basic patterns of the  $k = 2$  solution had a highly significant negative correlation, thus, when one factor had a strong contribution to the EMG pattern the other one usually had a minor contribution. This finding is in accordance with the aforementioned categorization in patterns depending on co-activation of the muscle groups with tibialis anterior. The same highly significant negative correlation between the loadings of the basic pattern contributing to extension phase and the late pattern contributing to flexion phase was evident in the three pattern solution. Interestingly, the loadings of the third one was not correlated with those of any of the others. Again the correlations with the loadings of the four pattern solution was similar (note that factor 2 and 3 are swapped), with highly significant correlations of the loadings of the two patterns occurring late during the extension and flexion phases, respectively. Additionally the fourth basic pattern (the one occurring early on in the extension phase) has a highly significant positive correlation with the basic pattern present later on in the extension phase and a highly significant negative correlation with the one present late in the flexion phase. The loadings of the early pattern in the flexion phase were not significantly correlated to any patterns' loadings.

Table 3.4 summarizes multiple analyses of covariances with factor loadings and the euclidian distances between original and reconstructed rhythmic patterns as dependent variables, the muscle group as a fixed factor independent variable and the burst and stimulation frequencies as covariates. Notable results are summarized in the following text. Increased stimulation frequency significantly reduces the factor loadings of the basic pattern of the  $k = 1$  solution, the second basic pattern of the two and three pattern solution and the fourth of the three pattern solution. Whereas, an increased burst frequency increases almost any factor loadings, but most notable the one of the 1 pattern solution, the third of the three pattern solution and the second of the four pattern solution. The latter two were the early responses in the flexion phase. For all factor loadings there were highly significant differences between the muscle groups. Most of them involve the tibialis anterior, which was the muscle group the categorization into the flexion and extension phases were based on and thus the burst were well aligned. The post-hoc test of the second basic pattern of the  $k = 1$  solution as well as the second and the third of the three and four basic pattern solutions, respectively, showed that hamstrings were more active during the extension phase than most other muscle groups. Furthermore, the hamstrings had heightened factor loadings in comparison to quadriceps and triceps surae for the early flexion phase factor loadings in the three and four factor solution.

The reconstruction error as measured by the euclidian distance between the reconstructed and original data was related to various parameters. There was no significant influence of the stimulation frequency on the reconstruction error for the one to three factor solution and a slight positive influence on the

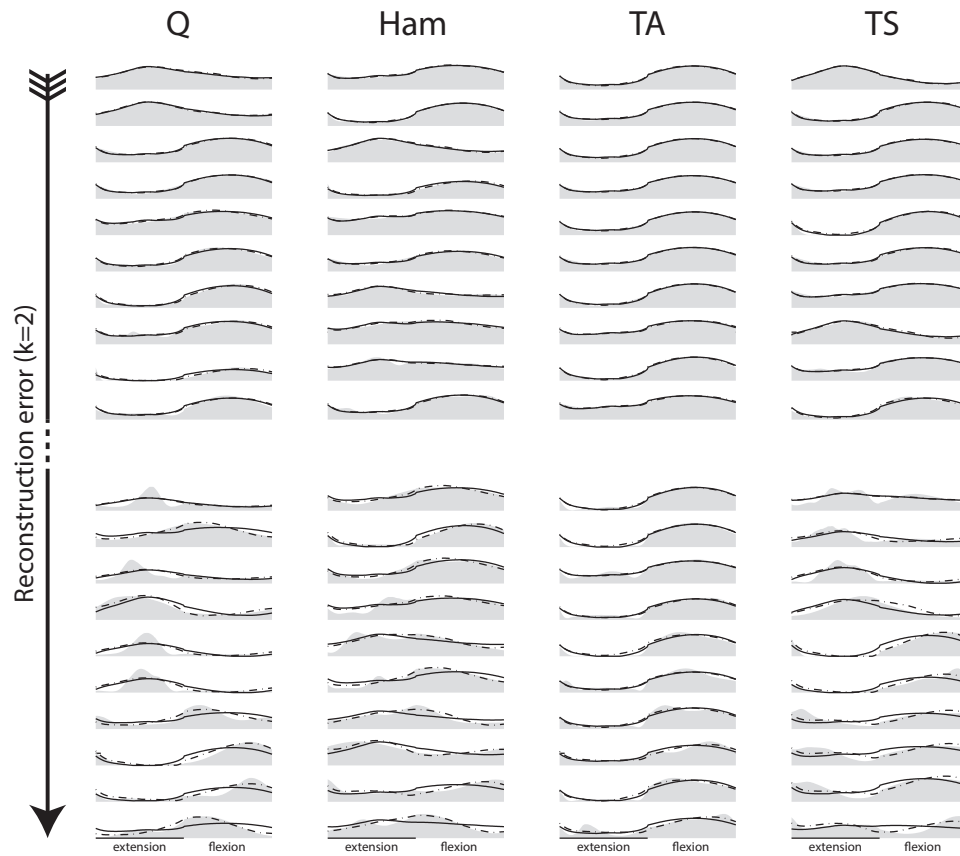


Figure 3.3: Reconstruction of signals with the two basic pattern model. The shaded gray area signifies the original data, the solid line the reconstruction with the two basic pattern model and the dashed line the reconstruction with the three basic pattern model. The top half shows ten rhythm cycles with the smallest reconstruction error with the model incorporating two basic patterns ( $d_{F2}$ ) of each muscle group and the bottom half shows the rhythm cycles with the biggest reconstruction error for each muscle group. The biggest deviations from the original data accumulated in the flexion phase and were somewhat better represented by the three factor model. Q: quadriceps, H: hamstrings, TA: tibialis anterior, TS: triceps surae.

### 3. RESULTS

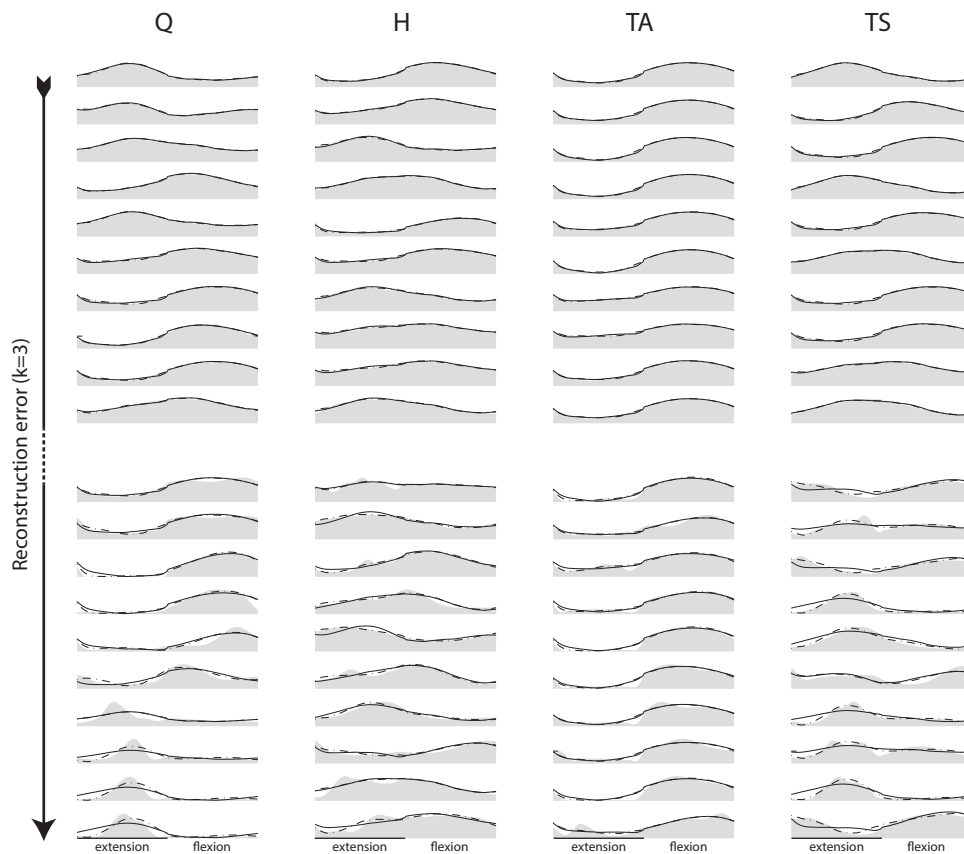


Figure 3.4: Reconstruction of signals with the three basic pattern model. The shaded gray area signifies the original data, the solid line the reconstruction with the three basic pattern model and the dashed line the reconstruction with the four basic pattern model. The top half shows ten rhythm cycles with the smallest reconstruction error with the model incorporating three basic patterns ( $d_{F3}$ ; based on the three factor model) of each muscle group and the bottom half shows the rhythm cycles with the biggest reconstruction error for each muscle group. The biggest deviations from the original data accumulated in the extension phase and are somewhat better represented by the four factor model. Q: quadriceps, H: hamstrings, TA: tibialis anterior, TS: triceps surae.

four factor solution, indicating a higher reconstruction error with higher stimulation frequencies. The burst frequency, on the other hand, was significantly negatively related with the reconstruction error of all investigated solutions (one to four factors). Thus, indicating that the envelopes of the rhythm cycles were better described when the burst rate was higher. The strength of this observed relation between reconstruction error and burst frequency increased with the number of factors in the model. The reconstruction error of tibialis anterior was always the smallest compared to the other muscle groups but only significant for the comparison with TS in the one factor solution, all muscle groups in the two factor solution, quadriceps and tibialis anterior in the three factor solution and not significant in the four factor solution, although there was a significant total effect.

Figures 3.3 and 3.4 shows the ten best and worst reconstructed envelopes of each muscle group with the two and three basic pattern models, respectively. For all examples the underlying data and the reconstruction with the model with one more basic patterns are shown. The comparison of the data and its reconstruction with the model consisting of two basic patterns showed that many distributions of EMG activity during the rhythm cycle in all muscle groups can be approximated well. The comparison with the model using three patterns showed that differently timed responses in the flexion phase were better reproduced. Furthermore, it can be seen that tibialis anterior had the smallest reconstruction errors. In the four patten model (figure 3.4) the majority of the deviation from original data happened in the extension phase. The additional basic pattern in the extension phase of the four pattern model helped to approximate most of the deviating data. Nonetheless, differently timed peaks remained that could not be described by the additional factor. On the other hand, it is noteworthy that all peaks clearly occur in either the flexion or extension phase and there were no peaks that were in the transition phase. Furthermore, in all investigated models, i.e.  $k = 1-8$ , there was no identified factor or primitive that peaked between the two phases (see figure 3.2).

## 3.2 Phase lags

The phase relation between two pairs of co-active muscle groups was calculated using cross-correlations. The phase lags to the maximal value of the cross-correlation normalized to the rhythm cycle duration are illustrated in figure 3.5. It can be seen that that most phase lags were close to zero. A total of 50% of all samples had a phase lag smaller or equal to 1.67% of the rhythm cycle. Similarly, 75%, 90% and 95% of all samples had a phase lag smaller or equal to 5.81%, 11.71% and 15.69% of the the rhythm cycle duration, respectively. The mean values of the phase lags for all muscle group pairs were close to zero and have similar standard deviations. Likewise, the median of the distributions

### 3. RESULTS

---

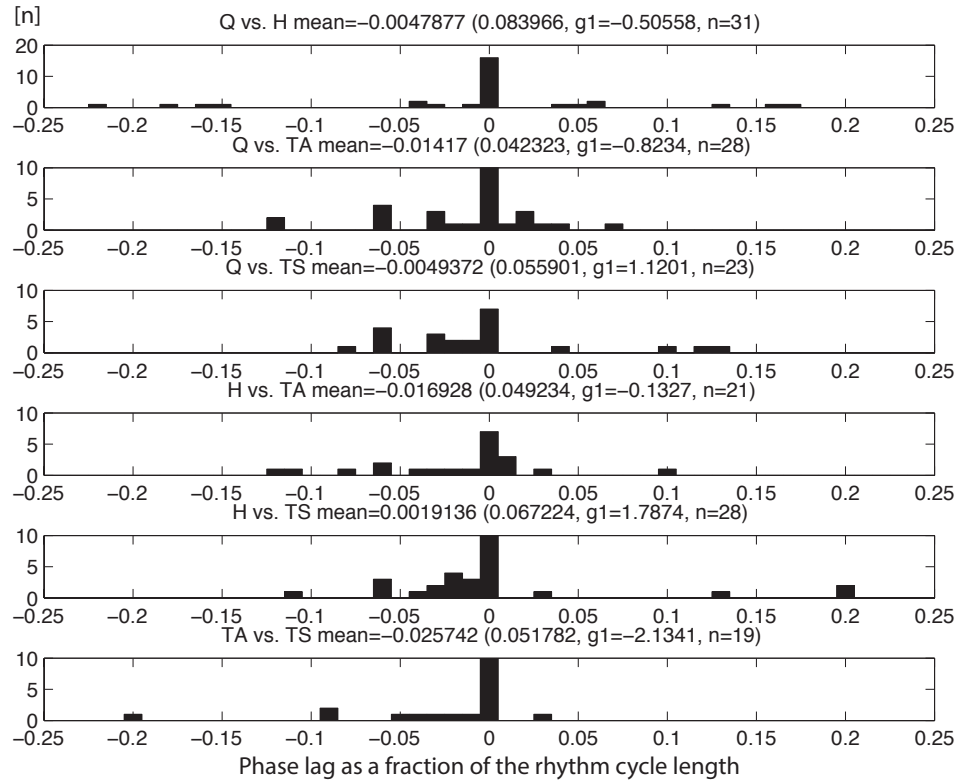


Figure 3.5: Histograms of the phase lags to the maximal cross-correlations. The phase lags are shown for pairs of co-active muscle groups on a per pair basis. The phase lag values were normalized to the duration of the rhythm cycle of the the corresponding sample. For all histograms the sample characteristics are depicted above, i.e. the mean value, followed by the standard deviation, the skewness ( $g_1$ ) and the sample size  $n$ . Q: quadriceps, H: hamstrings, TA: tibialis anterior, TS: triceps surae.



was zero for all pairs except for 'Q vs. TS' and 'H vs. TS' where the median was -1.17% and -0.44% of the rhythm cycle duration, respectively. The skewness ( $g_1$ ), on the other hand, differed in sign and magnitude between the muscle group pairs, indicating differences in the distribution of the phase lags.

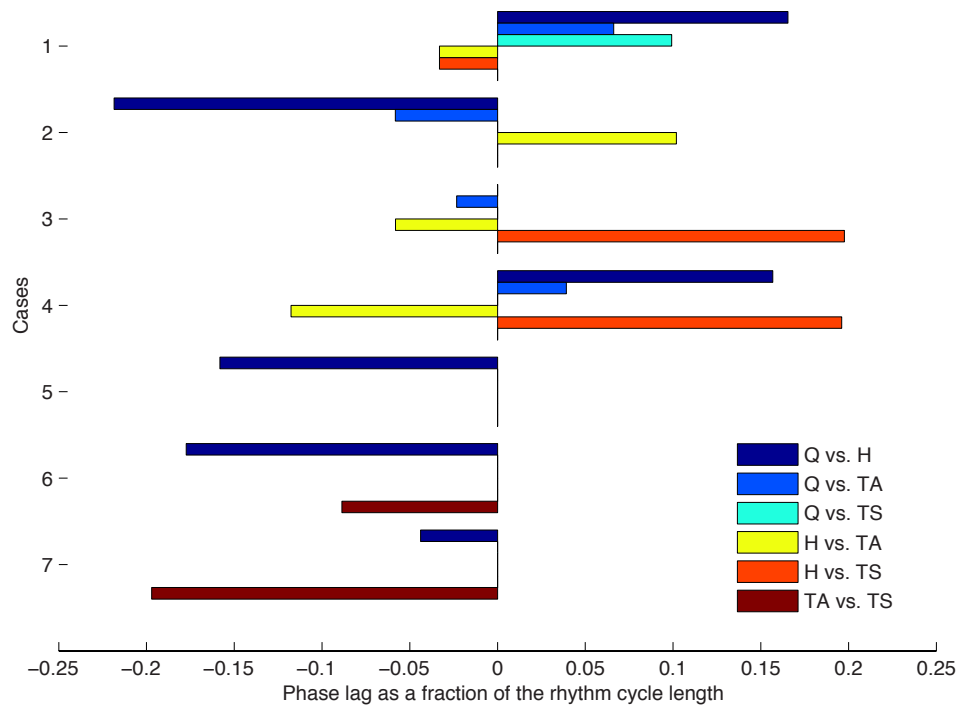


Figure 3.6: The relation of the phase lags between all co-active muscle groups of the samples with phase lag values above 15% of the rhythm cycle duration. Q: quadriceps, H: hamstrings, TA: tibialis anterior, TS: triceps surae.

Seven cases had phase lags that were larger than 15% of the rhythm cycle duration. For those samples phase lags for all muscle group pairs are depicted in figure 3.6. There the various phase lag distributions are illustrated.

There was a difference between the absolute values of the phase lag between the subjects (S1:  $M=0.029$ ,  $SD=0.037$ ; S2:  $M=0.046$ ,  $SD=0.055$ ; S3:  $M=0.008$ ,  $SD=0.019$ ; S4:  $M=0.023$ ,  $SD=0.038$ ; S5:  $M=0.064$ ,  $SD=0.059$ ; S6:  $M=0.086$ ,  $SD=0.074$ ; S7:  $M=0.086$ ,  $SD=0.074$ ;  $F(6,143)=5.520$ ,  $p<.001$ ). Bonferroni corrected post-hoc tests revealed that subject number 5 and 6 had larger phase lags than subjects 3, 4 and 7, and subject 6 additionally had larger phase lags than subject 1. All other post-hoc tests yielded not significant results. Furthermore, there was no significant differences between the muscle group pairs on the absolute values of the phase lag,  $F(5,155)=0.563$ ,  $p=.728$ . Finally, there was no correlation between the stimulation frequency

### 3. RESULTS

---

and the absolute value of phase lag ( $r=-.042$ ,  $p=.606$ ).

### 3.3 CMAP parameters

A total of 45,880 CMAPs were investigated, and of those onset latencies for 28,927 (63.1%) and centers of gravity ( $cg$ ) for 44,913 (97.9%) could be calculated. Eight-thousand-three-hundred-forty-four (60.1%) and 4,946 (66.8%) onset latencies corresponded to the extension and flexion phases, respectively. Similarly, 13,655 (98.3%) and 7,352 (99.2%) weighted latencies corresponded to the extension and flexion phases, respectively. A histogram of all onset latencies subtracted by the latencies of the respective controls are illustrated in figures 3.7 and 3.8. Note that due to the absence of some responses in the control recordings relative values of the latencies could not be calculated for all muscle groups in all recordings. There were 26,215 (90.6%) and 39,342 (87.6%) relatively adjusted onset latencies and centers of gravity, respectively.

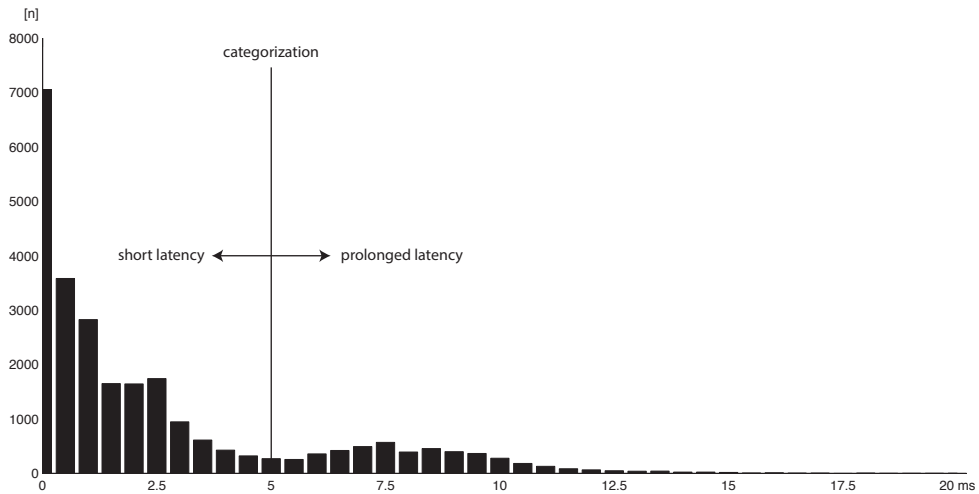


Figure 3.7: Histogram of the onset-latencies of all compound motor action potentials of all rhythmic samples that were classified as belonging to one of the phases, i.e. extension or flexion phase. The onset latencies were subtracted by the mean of the control latencies. Various degrees of prolonged latencies can be seen. The categorization threshold ( $\geq 5$  ms) for prolonged responses is illustrated.

There, were 7,332 (87.9% of the available onset latencies) and 4,498 (90.9%) validly assigned relative onset latency values for the extension and flexion phases, respectively. An independent-samples Mann-Whitney U test showed that the distributions of onset latencies differed between the phases with relatively longer latencies in the flexion phases; extension phase: mean rank=

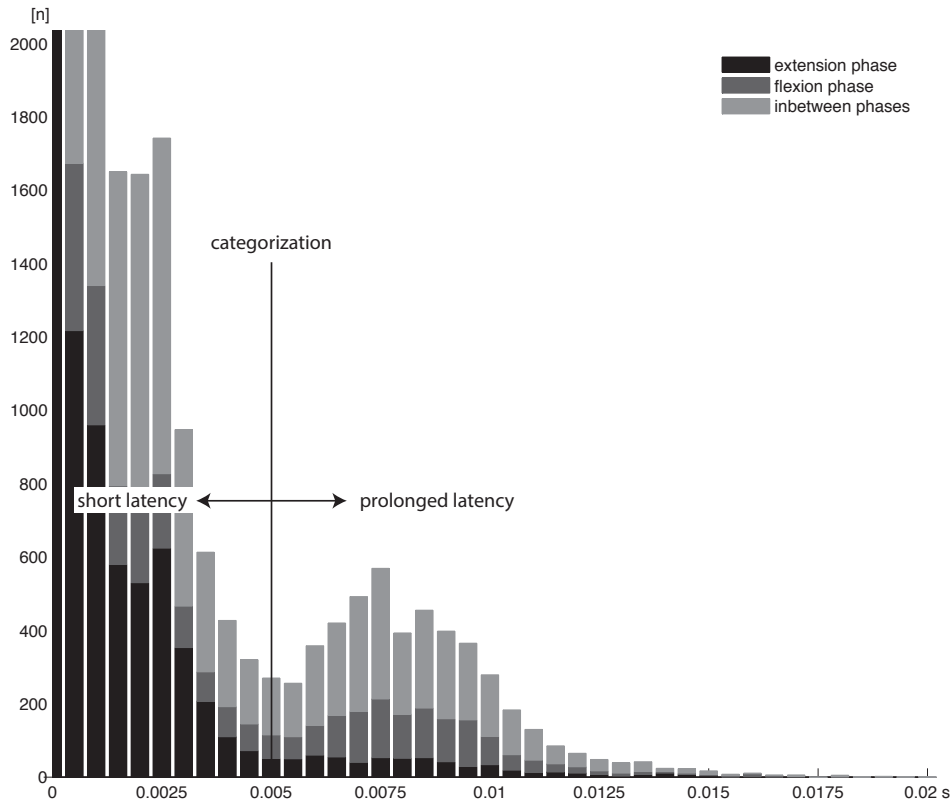


Figure 3.8: Histogram of the onset-latencies of all compound motor action potentials of all rhythmic samples split into their corresponding phases, i.e. extension or flexion phase. The onset latencies were subtracted by the mean of the control latencies. Various degrees of prolonged latencies can be seen. The categorization threshold ( $\geq 5$  ms) for prolonged responses is illustrated.

5,556.55; flexion phase: mean rank=6,500.61,  $U(11,830)=19,121,485$ ;  $z=14.596$ ;  $p < .001$ . A  $\chi^2$ -test confirmed that prolonged latencies ( $\geq 5$  ms prolonged in comparison to the onset latencies of the controls) occurred relatively more often during the flexion ( $N=1336$ , 29.7%) than during the extension phases ( $N=610$ , 8.3%,  $\chi^2(1)=927.393$ ,  $p < .001$ ,  $OR=4.667$ ).

Similarly, the centers of gravities were later in the flexion than in the extension phases; extension phase: mean rank=8,482.46; flexion phase: mean rank=10,507.61,  $U(18,408)=47,441,395.5$ ;  $z=24.769$ ;  $p < .001$ . A  $\chi^2$ -test also confirmed that prolonged centers of gravities occurred relatively more often during the flexion ( $N=2,086$ , 28.2%) than during the extension phases ( $N=1,394$ , 10.0%,  $\chi^2(1)=1161.117$ ,  $p < .001$ ,  $OR=3.535$ ).

Furthermore, prolonged onset latencies were strongly related to the muscle group (see figure 3.9;  $\chi^2(3)=1,124.522$ ,  $p < .001$ ). Tibialis anterior was most

### 3. RESULTS

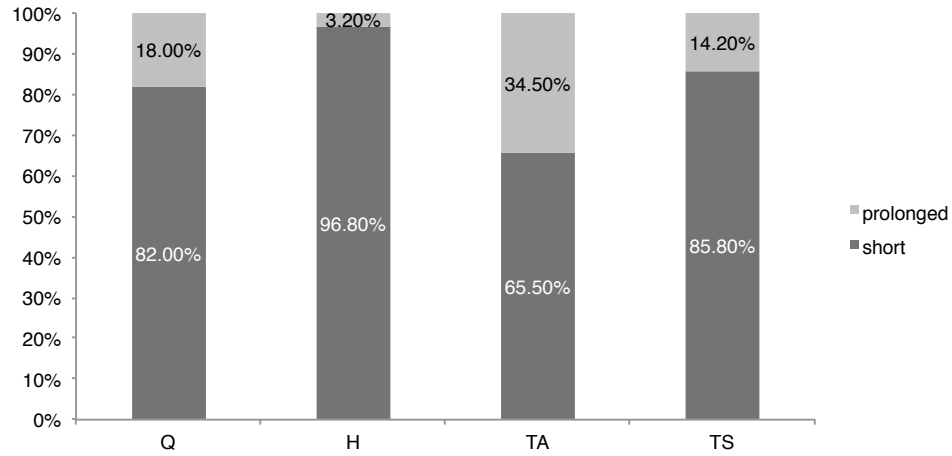


Figure 3.9: Relative frequencies of prolonged and short latencies depending on the muscle group. Q: quadriceps, H: hamstrings, TA: tibialis anterior, TS: triceps surae.

likely (N=942 of 2,731, 34.5%, Standardized Residual SRES=23.2) and hamstrings least likely (N=116 of 3,628, 3.2%, SRES=-19.7) to show prolonged latencies. Quadriceps (N=524 of 2,915, 18.0%, SRES=2.0) and triceps surae (N=364 of 2,556, 14.2%, SRES=-2.8) had relative frequencies of prolonged latencies around the grand mean (1,946 of 9,884, 16.4%). As for the case of prolonged centers of gravities more pronounced results could be observed,  $\chi^2(3)=9,537.660$ ,  $p < .001$ . Tibialis anterior was most likely (N=4,251 of 7,571, 53.0%, SRES=69.9) and hamstrings least likely (N=360 of 10,374, 3.5%, SRES=-38.2) to show prolonged latencies. Triceps surae (N=2,741 of 10,080, 27.2%, SRES=15.1) had relative frequencies of prolonged latencies slightly above the grand mean (8,023 of 39,342, 20.4%) and quadriceps showed relatively few prolonged centers of gravities (671 of 11,317, 5.9%, SRES=-34.1).

In mean the response amplitudes were  $50.4\% \pm 186\%$  of the amplitudes of the controls (note that in this section only the responses are described for which controls have a definite response). Depending on the muscle groups the mean varied substantially, Kruskal-Wallis  $H(3)=5,407.550$ ,  $p < .001$ . Quadriceps' ( $18.7\% \pm 41.3\%$ ) and hamstrings' ( $18.7\% \pm 21.3\%$ ) amplitudes were well below the grand mean whereas tibialis anterior ( $164.6\% \pm 278.3\%$ ) and triceps surae ( $109.1\% \pm 338.5\%$ ) had the highest relative response amplitudes. All pairwise post-hoc tests were highly significant. Judging from the standard deviations it can be seen that response amplitudes can be increased over the unconditioned controls.

Prolonged latency responses were more likely (N=626 of 4,875, 12.8%) than short latency responses (N=1242 of 21,340, 5.8%) to be subject to in-

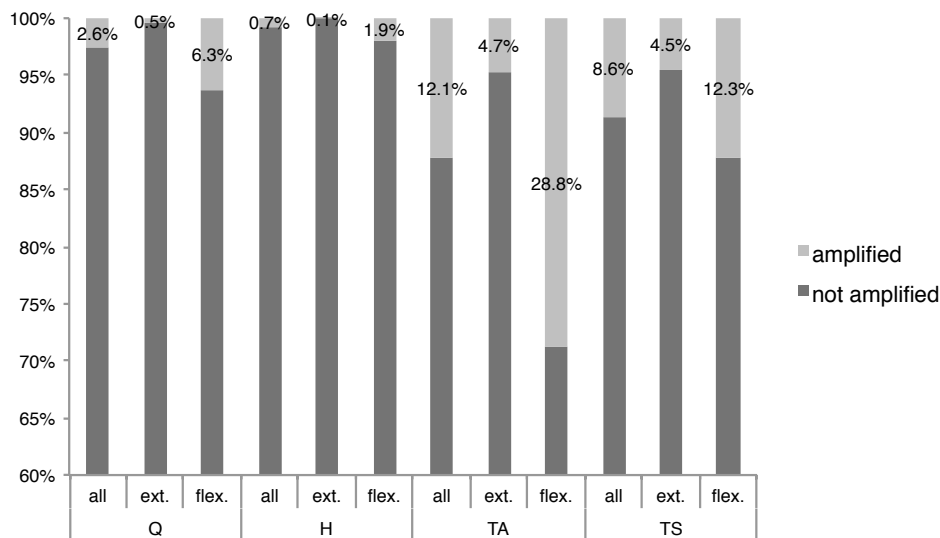


Figure 3.10: Increased response amplitude (amplitude  $>1.2$  times the control's amplitude) and its dependence from the muscle group. ext: extension phase, flex: flexion phase. Q: quadriceps, H: hamstrings, TA: tibialis anterior, TS: triceps surae.

creased amplitude in comparison to the controls ( $> 120\%$  of the control's mean amplitude) during rhythmically modulated output,  $\chi^2(1)=292.591$ ,  $p < .001$ ,  $OR=2.384$ . The occurrence of amplified response amplitudes depending from muscle group and phase is depicted in figure 3.10. It can be seen that in the flexion phase there were relatively more amplified responses (911, 12.3%) than in the extension phase (339, 2.4%),  $\chi^2(1)=849.833$ ,  $p < .001$ ,  $OR=5.704$ . Furthermore, tibialis anterior showed most frequently amplified responses, especially in the flexion phase (28.8%).

Moreover, prolonged onset latency responses occurred more often in the phases that constitute bursts (1,402, 72.1%) than those in silent periods (544, 13.7%) in the same muscle group. In the phases that showed relatively stronger EMG output the flexion phase (1,297, 38.2%) was more likely to show prolonged onset latencies than the extension phase (105, 7.5%,  $\chi^2(1)=1,280.408$ ,  $p < .001$ ,  $OR=7.624$ ). Conversely, when the phases were of relatively smaller amplitude the flexion phase (39, 3.5%) was less likely than the extension phase (505, 12.7%) to show prolonged onset latencies,  $\chi^2(1)=76.160$ ,  $p < .001$ ,  $OR=0.249$ .

Any recording of rhythmic activities in one muscle group can be grouped into four different cases depending on the phase relation of long latency responses. Only recordings with 10 and more relative onset latencies available

### 3. RESULTS

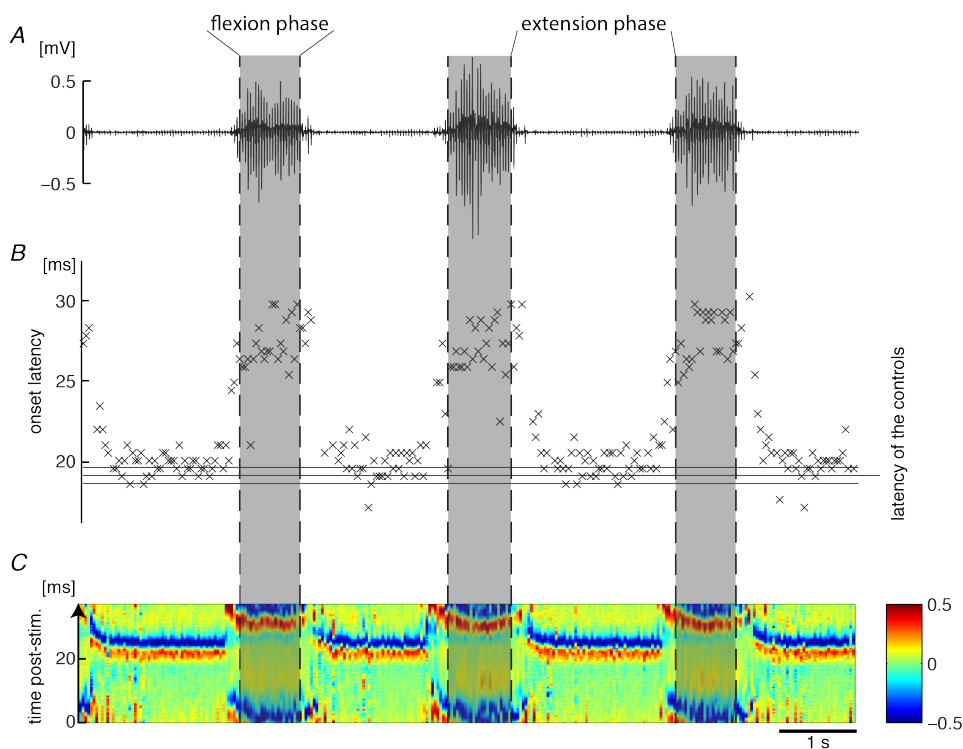


Figure 3.11: Example of rhythmically modulated onset latencies. *A*. Electromyographic activity in tibialis anterior of subject 4, recording 18. *B*. Onset latencies of the compound muscle action potentials (CMAPs) comprising the signal of *A*. It can be seen that during the bursts of high activity (flexion phases) the onset latencies of the reflexes was increased in comparison the controls (horizontal lines; mean and standard deviation) as well as to the phases with low activities (extension phases, cf. table A.1). The same is true for the centers of gravity (*cgs*; cf. table A.2). *C*. Stimulus triggered drawings of the CMAPs. Each row represents one CMAP and the normalized amplitudes are color coded.

for both the extension and flexion phase were included—in total 97 of 156 (62.2%). Following cases were identified: i) predominately long latencies in the flexion and ii) extension phase (defined by 0.2 greater relative frequency of long latency responses of one in comparison to the other phase). iii) neither phase was subject to long latency responses (i.e. relative frequency of long latency responses smaller than 0.2) or iv) both phases respond with long latency responses (i.e. relative frequency of long latency responses greater than 0.2). Twenty (20.6%) of the muscle groups showed predominantly long latency responses during the flexor phase (i), 2 (2.1%) during the extension phase (ii), 68 (70.1%) during neither (iii) and 7 (7.2%) during both phases (iv). In total there were 43 (36.1%) muscle group recordings that showed relative frequencies of long latency responses greater than 0.2 times in the flexion phase and 14 (12.8%) in the extension phase. Long latency responses in the flexion phase (again more than 20% of the respective phase) were most frequently recorded in tibialis anterior (20 of 29, 70.0%), followed by triceps surae (10 of 16, 38.5%), quadriceps (11 of 19, 36.7%) and hamstrings (2 of 34, 5.9%) with very few prolonged latency responses,  $\chi^2(3)=27.093$ ,  $p < .001$ . Similarly, in the extension phase tibialis anterior showed most long latencies (7 of 27, 25.9%) followed by quadriceps (5 of 25, 20.0%), triceps surae (2 of 25, 7.4%) and hamstrings (0 of 30, 0.0%,  $\chi^2(3)=10.405$ ,  $p = .015$ ). Examples of different cases of modulated latencies can be seen in figures 3.11, 3.12 and 3.13. Figure 3.11 shows phase-dependent rhythmic alternation of long and short latency responses, figure 3.12 shows constantly long but slightly rhythmically modulated responses and figure 3.13 shows rhythmic activity with only short monosynaptic onset latencies. Yet, in the latter example the centers of gravity were later for the flexion phase, indicating two components of responses, an early and late one, that were simultaneously present.

The grouping of the rhythmic activities of every single muscle group into the same four categories as in the above paragraph depending on the center of gravity  $cg$  instead of the onset latencies yielded following results. One-hundred-thirty-seven of the 156 samples (87.8%) were included due to the restraint that every phase of every sample needs to have at least 10 validly assigned values. Forty-four (32.1%) showed predominantly prolonged  $cg$  responses in the flexion phase (i), 5 (3.5%) cases had predominantly prolonged  $cg$  responses during the extension phase (ii), 75 (54.7%) samples had almost no prolonged  $cg$  in either phase (iii) and 13 (9.5%) cases had prolonged  $cgs$  in both phases (iv). Split up into the different muscle groups it can be seen that tibialis anterior (26 of 27, 96.3%) had most cases of prolonged  $cgs$  during flexion phase, followed by triceps surae (21 of 35, 60.0%), quadriceps (8 of 39, 20.5%) and hamstrings (2 of 36, 5.6%,  $\chi^2(3)=64.514$ ,  $p < .001$ ). Similarly, during extension phase tibialis anterior was subject to most prolonged responses (16 of 37, 59.3%), followed by triceps surae (8 of 35, 22.9%), quadriceps (4 of 39, 10.3%) and hamstrings (2 of 36, 5.6%,  $\chi^2(3)=30.768$ ,  $p < .001$ ).

Table A.1 shows for every subject, session and muscle group the mean

### 3. RESULTS

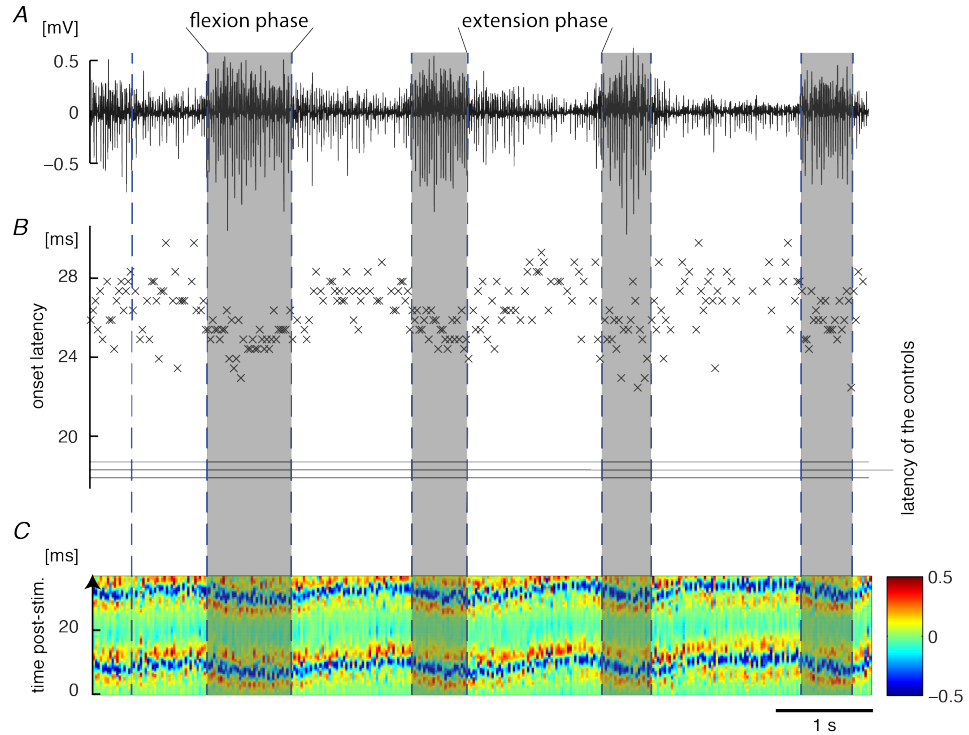


Figure 3.12: Example of tonically prolonged onset latencies with a slight rhythmic modulation. This sample shows the electromyographic activity, latencies and response shapes of subject 7, recording 39 in tibialis anterior. There was a significant difference between the onset latencies and the centers of gravity of the flexion (high activity) and extension (low activity) phases (cf. tables A.1 and A.2). For both measures the extension phase shows higher values. A–C. See figure 3.11 for the technical description of the figure.

values, standard deviations and counts of all validly assessed onset latencies as well as the significance level of the pairwise comparisons using Whitney-Mann-U tests. In summary, 88 (56.4%) samples showed a significant increase and 19 (12.2%) a significant decrease of the onset latency during the flexion phase. Eighty-two (52.6%) and 19 (12.2%) samples were subject to significantly increased and decreased onset latencies, respectively, during the extension phases. Furthermore, in 41 (26.3%) cases the flexion phase showed significantly longer onset latencies than the extension phase and in 42 (26.9%) cases the opposite was the case. The standard deviations of the onset latencies of the controls were in mean 0.37 ms, of those of the flexion phase 1.68 ms and of the extension phase 1.40 ms. Thus, a much greater variability of the responses is observed during rhythmic activity in comparison to unconditioned



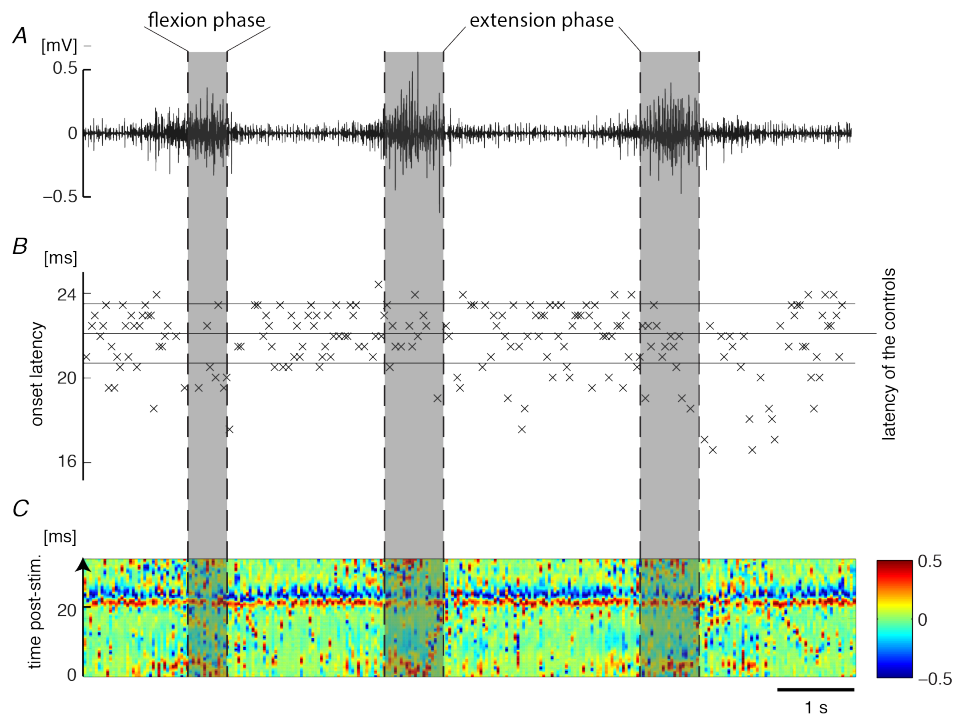


Figure 3.13: Example of tonically not-prolonged onset latencies with a slight rhythmic modulation. This sample shows the electromyographic activity, latencies and response shapes of subject 2, recording 8 in tibialis anterior. There was no significant difference between the onset latencies of the flexion (high activity) and extension (low activity) phases (cf. table A.1). When investigating the compound motor action potentials in *C* it becomes evident that during the flexion phase (high activity phase) later components existed that were not, or less often, present during the extension phase. The comparison of the centers of gravity (*cgs*) showed that they were indeed significantly prolonged in the flexion phase (in comparison to the controls as well as the responses in the extension phase; cf. table A.2). *A–C*. See figure 3.11 for the technical description of the figure.

### 3. RESULTS

---

responses. When the flexion phase was significantly prolonged in comparison to the controls the prolongation amounted in mean to  $4.5 \text{ ms} \pm 3.5 \text{ ms}$  (max=21.0 ms,  $g_1=3.7 \text{ ms}$ ). When the onset latencies of the extension phase was significantly later than those of the controls the prolongation was in mean  $3.0 \text{ ms} \pm 2.7 \text{ ms}$  (max=12.8 ms,  $g_1=1.7 \text{ ms}$ ). In case of significantly earlier onset latencies of the CMAPs comprising rhythmic activity the difference was  $0.8 \text{ ms} \pm 0.3 \text{ ms}$  (max=1.45 ms,  $g_1=1.2 \text{ ms}$ ) and  $0.9 \text{ ms} \pm 0.4 \text{ ms}$  (max=2.1 ms,  $g_1=0.7 \text{ ms}$ ) for the flexion and extension phases, respectively. For the direct comparison of the onset latencies of the CMAPs comprising the flexion and extension phases, the latencies of the flexion phase CMAPs were prolonged by  $3.6 \text{ ms} \pm 2.1 \text{ ms}$  (max=8.8 ms,  $g_1=-1.3$ ) in comparison to those of the extension phase if they are significantly later. Vice-versa the difference when the extension phase showed longer latencies than the flexion phase amounted to  $2.7 \text{ ms} \pm 1.9 \text{ ms}$  (max=8.8 ms,  $g_1=-4.3 \text{ ms}$ ). When just counting significant results where the difference of the means was larger than a certain threshold  $th$  following frequencies were obtained: 60 (68.2% of all significant results;  $th = 2 \text{ ms}$ ) and 34 (38.6%;  $th = 5 \text{ ms}$ ) cases showed an increased onset latency in the flexion phase in comparison to the controls, 24 (58.5%;  $th = 2 \text{ ms}$ ) and 15 (36.6%;  $th = 5 \text{ ms}$ ) cases showed increased latency during the flexion in comparison to the extension phase, in 41 (50%;  $th = 2 \text{ ms}$ ) and 15 (18.3%;  $th = 5 \text{ ms}$ ) cases the extension phase was subject to prolonged latencies in comparison to the controls, 21 (50%;  $th = 2 \text{ ms}$ ) and 6 (14.3%;  $th = 5 \text{ ms}$ ) times the extension phase had longer latency times than the flexion phase and in 1 (5.2%;  $th = 2 \text{ ms}$ ) and 0 (0%;  $th = 5 \text{ ms}$ ) case the latency times of the CMAPs in the extension phase were lower than those of the controls.

In the same way the center of gravity ( $cg$ ) values are listed for every subject, session and muscle group in table A.2. In summary, 75 (48.1%) cases showed significantly later centers of gravities during the flexion phase in comparison to the controls and in 32 (20.5%) cases the centers of gravities were significantly earlier. During the extension phase in 65 (41.7%) cases the centers of gravities were prolonged and in 52 (33.3%) cases they were significantly earlier in comparison to the controls. The comparison of the two phases showed that the flexion phase showed significantly later centers of gravities in 83 (53.2%) and significantly earlier ones in 43 (27.6%) than in the extension phase. The standard deviations of the  $cgs$  of the controls were in mean 0.92 ms, of those of the flexion phase 2.15 ms and of the extension phase 2.07 ms. For the above listed 6 cases of significant results descriptive parameters of the relative changes of the centers of gravity were calculated. When the  $cgs$  were significantly later in the flexion phase in comparison to the controls the mean increase was  $5.5 \text{ ms} \pm 3.5 \text{ ms}$  (max=12.9 ms,  $g_1=-0.8 \text{ ms}$ ). In the case of significantly earlier latencies the  $cgs$  were lower by  $2.6 \text{ ms} \pm 1.4 \text{ ms}$  (max=9.7,  $g_1=-3.3 \text{ ms}$ ). The increased  $cgs$  of the extension phase were in mean  $3.4 \text{ ms} \pm 2.6 \text{ ms}$  (max=12.3 ms,  $g_1=0.9 \text{ ms}$ ) later than those of the controls and the

earlier responses in the extension phase had *cgs* that were smaller by  $2.1 \text{ ms} \pm 1.3 \text{ ms}$  (max=-5.9 ms,  $g_1=0.2 \text{ ms}$ ). Furthermore, if the flexion phase had significantly later *cgs* than the extension phase, the difference was  $4.4 \text{ ms} \pm 2.9 \text{ ms}$  (max=10.8 ms,  $g_1=-0.7 \text{ ms}$ ) and if the extension phase's *cgs* were later the difference amounted to  $2.7 \text{ ms} \pm 1.6 \text{ ms}$  (max=8.4 ms,  $g_1=-0.6 \text{ ms}$ ). When counting all significant differences that exceeded a certain threshold (*th*) following results were found: the flexion phase was subject to later than the controls *cgs* than the controls in 64 (85.3% of all significant differences) and 42 (56.0%) cases by  $th = 2 \text{ ms}$  and  $th = 5 \text{ ms}$ , respectively. In 14 (43.8%) and 3 (9.4%) cases the significant differences between flexion phase and control were in mean smaller by 2 ms and 5 ms (*th*). For the comparison between the flexion and extension phases in 61 (73.5%) and 34 (41.0%) cases the *cgs* in the flexion phase were later than in the extension phase by 2 ms and 5 ms, respectively and in 19 (44.2%) and 7 (16.3%) cases the extension phase had longer *cgs* than the flexion phase by 2 ms and 5 ms, respectively. In 38 (58.5%) and 14 (21.5%) cases the extension phase was later than the controls by 2 ms and 5 ms, respectively, and in 21 (40.4%) and 2 (3.8%)t he extension phase was earlier than the controls by 2 ms and 5 ms, respectively.



## Chapter Four

---

### *Discussion*

The human lumbosacral spinal cord isolated from descending modulations can generate a variety of stable rhythmic EMG patterns in the lower limbs in response to non-patterned, tonic posterior root stimulation. Dimensionality reduction by non-negative matrix factorization of the EMG activities across muscles and subjects revealed that the rich repertoire of rhythmic behavior could be explained by the combination of a small set of common stereotyped rhythmic activation patterns. The EMG profiles across all analyzed segments of rhythmic activity were best reproduced by a linear combination of 3 to 4 simple basic patterns. Even a two factor model with two sinusoidal-like basic activation patterns with a reciprocal relation of their temporal structure could explain a substantial amount of the total variance of the EMG data. The basic activation patterns peaked during either of two alternating phases of the rhythm cycle resembling extension and flexion phases. The third and fourth pattern would split the flexion and extension phases, respectively, into two basic patterns. Differences in the neural control of the flexion and extension phases comprising rhythmic activity was found by the second step of analysis, that was made possible due to the characteristic stimulus-triggered mechanisms of motor output generation. Analysis of latencies of series of stimulus-time related CMAPs constituting the rhythmic EMG activities demonstrated that the central spinal processing of the input signals provided by SCS were statistically associated with a longer delay during the flexion than the extension phases.

The research model was the human lumbosacral spinal cord chronically isolated from volitional motor control by traumatic spinal cord injury. Clinical and neurophysiological assessments were conducted to identify and characterize potential supraspinal contribution to the central state of excitability of lumbosacral spinal cord circuitries. None of the subjects demonstrated clinically evident voluntary muscle contractions below the lesion level and none of them had the ability to volitionally induce task-appropriate EMG activity by the volitional attempt of performing single-joint motor tasks. In 4 of the 7 subjects that showed rhythmic EMG activities for 10 seconds or longer in 4 ipsilateral muscle groups there was detectable EMG activity below the level of lesion in response to reinforcement maneuvers (Sherwood, Dimitrijevic, & McKay, 1992; Sherwood, McKay, & Dimitrijevic, 1996), the other 3 did not respond with EMG activity in the lower limbs to reinforcement maneuvers.

Thus, the sample includes also neurophysiologically motor complete SCI subjects. This means that it is not necessary that supraspinal influence is present for the lumbar spinal cord to respond with rhythmic EMG activity to posterior root stimulation.

### 4.1 Rhythms and patterns

In this first part it was shown that the human lumbar spinal cord can generate a variety of rhythms and patterns of motor outputs to the otherwise paralyzed lower limbs. The rhythm frequencies were identical across all muscle groups in a given EMG segment. Locomotor-like patterns defined by reciprocal relation between agonists and antagonists were rare, while co-activation between all muscle groups occurred most frequently. Different mixed-synergy patterns made up the remaining cases. The variety of rhythmic patterns could be reproduced by a linear combination of 3–4 basic components with appropriate weights. The model with 2 reciprocal sinusoidal-like components, one peaking in the extension and one in the flexion phase, accounted for 83.2% of variance across all muscles and EMG samples. Three basic components, one in the extension, and two in the flexion phase (peaking at 15% and 75% of the flexion phase, respectively) explained 90.8% of the variance and were favored by the Akaike Information Criterion. A 4-component solution introduced a similar decomposition of the extension-phase activity, accounted for 94.4% of variance.

Rhythmic involuntary contractions of multiple lower limb muscles bilaterally called spinal myoclonus can occur in a very small number of people with traumatic chronic SCI under certain conditions (Calancie et al., 1994; Calancie, 2006). The patterns are characterized by individually highly reproducible period and rate of rhythmicity (very stereotyped). The contraction rates are between 0.3 Hz–0.5 Hz. Involuntary contractions with reciprocity between agonists and antagonists have been observed only in motor incomplete spinal cord injured subjects, while co-activations dominated also in these subjects. The involuntary activities were initiated by extending the hips of the subjects in a supine position and were thus triggered by ‘externally induced’ peripheral input. They all had injuries to the cervical spinal cord and nociceptor input to the lumbosacral enlargement due to some other pathology, most probably increasing spinal cord excitability. Here we have shown that the lumbar spinal cord networks, when activated by SCS, can produce co-activation patterns as well as a variety of patterns with reciprocity between pairs of muscles in motor complete SCI people. Slow (2.6 km/h) and fast (6.0 km/h) gate of adults with intact CNS involve rhythm cycle frequencies of 0.77 Hz to 1.31 Hz (1.54 to 2.61 steps per second; Oberg, Karsznia, & Oberg, 1993). All the analyzed data fall into these rhythm cycle ranges.

The constant phase relation of rhythmic outputs to one lower limb sug-

gests a common, plurisegmental rhythm generator, and the various EMG patterns indicate separate stereotypic pattern formation modules. These neural circuitries possess many of the necessary components to generate functional locomotor activity (Grillner, 2011). A similar method for the decomposition of rhythmic activities was applied to EMG patterns generated during walking of humans of different ages (Dominici et al., 2011). They identified 2 basic patterns that explained neonatal stepping (when an infant is held upright, coordinated walking movements are elicited by tactile stimuli to the plantar surface; McGraw, 1940; Zelazo, Zelazo, & Kolb, 1972; Okamoto, Okamoto, & Andrew, 2001). These two basic patterns are arguably similar to the here presented two pattern model. From toddler up to adult human walking, four basic patterns were needed to explain the resulting EMG patterns (Dominici et al., 2011). The peaks of the basic patterns are similarly distributed as in the here presented four factor model. The basic patterns of the adult human have specific shapes that were not observed in rhythmic activities of motor complete spinal cord injury subjects under epidural posterior root stimulation. Thus, it might be hypothesized that the lumbar spinal cord disconnected from suprasegmental (brain, brainstem, cervical lumbar cord) input possesses similar capabilities to express motor patterns as toddlers (the patterns of the toddlers were shown to be similar to those of monkeys, cats and rats). Yet, there is a lack of coordination between the muscles. Numerous counts of co-activation of flexor and extensor muscles were observed as well as expressions of rather ‘unphysiological’ combination of patterns. Such coordination may require inputs from supraspinal centers as well as movement related feedback from periphery.

## 4.2 Reflex latencies

PRM reflexes that constituted locomotor-like lower limb muscle activity generated by sustained SCS in motor complete (ASIA A and B) SCI subjects have been explored. The motor patterns were shaped by amplitude modulations of the successive PRM reflexes, i.e., by rhythmic variations of the size of motoneuron populations responding to the invariant stimulation. Bursts of short-latency PRM reflexes characterized extension-like phases. During flexion-like phases of rhythmic activities, the short-latency PRM reflexes were replaced by PRM reflexes with increased latency that were otherwise not present. Similar prolonged latencies were also observed during the extension phase but less frequently.

Previously, it has been shown that epidural stimulation of the lumbar spinal cord with low stimulation frequencies (2 Hz–5 Hz) evokes monosynaptic PRM reflexes in the lower limb muscle groups of SCI subjects (Rattay et al., 2000; Minassian, Jilge, et al., 2004; Minassian, Persy, Rattay, Pinter, et al., 2007). The same posterior root afferents are also directly activated with

higher stimulation frequencies (10 Hz and higher), although the CMAPs of the responses are modulated in their amplitude, shape and/or latency. This modulation is caused by neural networks, transynaptically activated by the posterior root stimulation. Two different types of functional motor outputs were observed that were dependent on the stimulation frequency. Stimulation of 5 Hz–16 Hz produced a bilateral extension movement with a characteristic motor patterns (Jilge, Minassian, Rattay, & Dimitrijevic, 2004). The PRM reflexes constituting the extension like patterns were amplitude-modulated and of short latency, comparable with latencies of PRM reflexes in response to 2 Hz stimulation. The width of the CMAPs was reduced. With higher stimulation frequencies of 20 Hz and more reciprocal, rhythmic activation of lower limb muscle groups, i.e. locomotor like activity, can be observed (Dimitrijevic et al., 1998b; Minassian, Jilge, et al., 2004). It has been reported that during rhythmic locomotor like activity the tibialis anterior muscle group can exhibit prolonged latency responses (Minassian, Jilge, et al., 2004; Minassian, Persy, Rattay, Pinter, et al., 2007). Furthermore, Gerasimenko, Daniel, et al. (2001) described a similar finding in tibialis anterior, when eliciting rhythmic activity of ankle flexors and extensors in chronic paraplegic persons by SCS with 25 Hz–40 Hz. Recent studies investigated SCS-facilitated locomotion on a moving treadmill in spinal rats (Gerasimenko, Ichiyama, et al., 2007; Gerasimenko, Roy, & Edgerton, 2008; Lavrov et al., 2008). These experiments revealed differences in the EMG characteristics between the medial gastrocnemius and TA during stepping. Monosynaptic responses were prominent in medial gastrocnemius, whereas the TA motor pools were activated predominantly polysynaptically in response to epidural SCS. Moreover, when the semitendinosus muscle was bifunctionally activated in the spinal rat, the extensor bursts during stepping were composed of monosynaptic responses to SCS, while the flexor bursts of the same muscle were associated with a predominance of polysynaptically evoked responses (Gerasimenko, Roy, & Edgerton, 2008). These results demonstrate a striking similarity to the data presented here. Lavrov et al. (2008) suggested that the delayed responses to SCS reflected synaptic events of spinal locomotor networks.

Here, all identifiable latencies of CMAP responses constituting the bursts as well as occurring in-between the bursts of all muscle groups were analyzed. Prolonged latency CMAP responses occurred most frequently during the flexion phase across all muscles. Tibialis anterior had the highest number of prolonged responses whereas there were very few occurrences of prolonged latencies in the hamstring muscle group.

The occurrence of these reflexes has to be due to the reorganization of reflex systems during rhythmicity, since the stimulation site and intensity was kept constant, the stimulated structures and amount of input was invariable. This reorganization involves several mechanisms including the emergence of phase-dependent polysynaptic excitation of flexor motoneurons and concomitant phase-dependent suppression of short-latency reflex pathways.



Candidate interneurons for mediating these effects are chains of excitatory interneurons interposed between the directly, electrically stimulated afferents and the motoneurons, and interneurons mediating presynaptic inhibition of group I afferents, respectively. Both types of interneuronal populations are activated in phase mainly during the flexor-mode of lumbar cord network oscillations. According to Jankowska (2001), their activation in a specific phase of the rhythmic cycle distinguishes them as locomotion-related neurons.

The patterned amplitude modulations of the PRM reflexes that resulted in the burst-like shapes of the EMG activity alternating with phases of low activity or silent periods were discussed previously (Minassian, Gilge, et al., 2004; Minassian, Persy, Rattay, Pinter, et al., 2007). A postsynaptic inhibitory mechanism could account for such modulations of the overall motoneuron excitability thereby sculpting their firing patterns. Candidate last-order interneurons that can provide the rhythmic inhibition of individual motoneuron populations during the inactive phase of rhythmicity are Ia inhibitory interneurons (Jankowska, 2001; Rybak, Shevtsova, Lafreniere-Roula, & McCrea, 2006). However, inhibitory mechanisms alone can not account for the formation of the patterns, since PRM reflexes within bursts could attain larger amplitudes than the unconditioned control response to the first stimulus of the tonic train of stimuli. The controls were monosynaptic PRM reflexes with their amplitudes depending on the applied stimulus intensity determining the population size of depolarized Ia afferents (Lloyd, 1943; Minassian, Gilge, et al., 2004). PRM reflexes with amplitudes larger than these controls must have been subject to some additional excitatory sources that provided rhythmic drive to the motoneurons.

Single elements of the potential mechanisms controlling the state and phase dependent reorganization of reflex systems as well as the motoneurone excitability can be in principle explained by segmental effects at multiple levels of the lumbosacral cord. On the other hand, the observation that EMG bursts of all muscles occurred with the same rhythm within a given pattern, independently whether the pattern was locomotor or non-locomotor-like, clearly suggests a plurisegmental control mechanism. It was previously documented that the oscillating lumbar cord networks have the capacity of generating a variety of cycle frequencies (Dimitrijevic et al., 1998b). The same finding was reproduced here. Despite of this, the different muscle groups did not show independent cycle periods during a given rhythmic pattern. Neurons projecting over several segments like propriospinal tract neurons could account for coordinating activity at different levels of the lumbosacral cord.

### 4.3 Clues to the human locomotor networks

The question arises of what functional structures control the reorganization of reflex systems, sculpt the motoneuron firing patterns, and provide coordi-

nation at different segmental levels to generate complex rhythmic motor patterns. A consideration of the above mentioned characteristics of the putative functional control structures leads to suggest the activation of pattern generating locomotor-related neural circuits intrinsic to the human lumbar cord. These putative functional circuits were termed the lumbar locomotor pattern generator (LLPG) in previous work (Minassian, Gilge, et al., 2004; Minassian, Persy, Rattay, Pinter, et al., 2007). The LLPG must have been activated by relatively simple tonic signals initiated in large diameter afferents, probably of group I and II large diameter afferents within the posterior roots. Thus, one pre-condition of the hypothesis is that group I and II afferents have access to the locomotor-related interneuronal structures and can activate them.

Group I and II afferents make direct synaptic contacts with a variety of functionally identified and recognizable spinal interneurons, like inhibitory interneurons, interneurons within di-, oligo-, and polysynaptic excitatory pathways, as well as with interneurons mediating presynaptic inhibition (Jankowska, 1992; Jankowska, 2001; Jankowska & Hammar, 2002). Thereby, nerve impulses from a given fiber type reach interneurons of several pathways, and several types of fibers co-excite common interneurons (Jankowska, 1992). It can be expected that excitation of the various afferents by spinal cord stimulation can—due to the axonal projections and connectivity—exert excitatory action on these spinal interneurons by synaptically evoked depolarization (Guru, Mailis, Ashby, & Vanderlinden, 1987; Hunter & Ashby, 1994). During 2 Hz-stimulation, the low rate of synchronized afferent input was probably not efficient to trans-synaptically depolarize neurons other than motoneurons. Another explanation of the detection of a resting state of the central lumbar structures at 2 Hz might be the long inter-stimulus interval, with most of the effects of a preceding stimulus decayed entirely. When the stimulation frequency is increased, the effectiveness of elicited nerve impulses from afferents to activate interneurons increases due to temporal summation, especially when they act together with delayed nerve impulses from various longer central spinal pathways that co-excite common interneurons.

A well established evidence demonstrating that afferents are projecting to spinal locomotor networks comes from an experimental paradigm investigating the ability of afferents to perturb (reset) the locomotor cycle during induced fictive locomotion. In these experiments, locomotion is generated either by intravenous administration of L-dopa to the acute spinal cat or by stimulation of the mesencephalic locomotor region in the decerebrate cat (Hultborn, Conway, et al., 1998). At specific times of the locomotor cycle, brief stimulus trains are delivered to a peripheral nerve. If a stimulus leads to an interruption of the regular locomotor rhythm that subsequently restarts in a coordinated fashion, then the activated afferents must have access to the locomotor networks. The ability of afferents within a given peripheral nerve to affect flexor and extensor activity throughout the limb and to influence the locomotor cycle timing is strong evidence for afferent actions exerted through a common

network (Rybak, Stecina, Shevtsova, & McCrea, 2006). Based on this experimental paradigm of resetting, various afferent systems like group I and group II muscle afferents and cutaneous afferents from extensor and flexor muscles have been shown to have direct access to the spinal rhythm-generating circuitry (Rybak, Stecina, et al., 2006). Effective locomotor behavior requires sensory feedback from the moving limb to adapt to the environment. The interaction of sensory input with human spinal networks in the generation of locomotor patterns was studied in clinically complete and incomplete spinal cord injured subjects during supported treadmill stepping. It was shown that locomotor-related spinal neural circuits exhibit adaptive capacities by utilizing input from load receptors as well as from velocity-dependent afferents during stepping (Harkema et al., 1997; Beres-Jones & Harkema, 2004).

It can be concluded that there is evidence in the experimental animal that large-diameter afferents from extensors and flexors project to the spinal central pattern generator for locomotion. One might assume that also in humans, afferent systems and spinal rhythm-generating networks are integrated within the lumbar cord and can influence and modify the performance of each other (Hultborn & Nielsen, 2007).

To interpret this fact in the context of the present study, it can be suggested that the large-diameter afferents within the lumbar posterior roots depolarized by the tonic spinal cord stimulation do have access to the LLPG. Assuming a half-center architecture of the LLPG, such stimulation would provide a common excitatory tonic drive to the flexor and extensor half centers, due to the axonal projections and connectivity of the various afferents of multiple cord segments coming from flexors and extensors. There is a general agreement that such relatively simple tonic signals can activate the central pattern generator for locomotion (Pearson & Gordon, 2000; Parker, 2009). The input provided to the different half-centers and levels of the LLPG will be a rather synchronized tonic input with frequencies corresponding to the spinal cord stimulation frequencies. All rhythmic activities analyzed in the present study were elicited with frequencies of  $< 42.5$  Hz. These frequencies are in a similar range as shown for descending drive signals from suraspinal motor structures which can act to initiate stepping by exerting an energizing action on the relevant spinal circuits (Armstrong, 1988).

The assumption of a half-center architecture of the LLPG helps to explain the asymmetrical organization of central spinal pathways mediating the rhythmic activity in the extensor and flexor muscles as described in the present manuscript. The extensor mode of the oscillating state of lumbar cord networks based on the direct, most probably monosynaptic, drive from afferents to extensor motoneurons. The firing patterns were sculpted by additional inhibitory and excitatory influence governed by the LLPG and converging on the extensor motoneurons. Thereby, the LLPG was activated by axonal collaterals of the afferents providing the direct drive to the motoneurons, or of concomitantly stimulated fibers of other afferents types.

The flexor mode was characterized by a polysynaptic drive of the flexor motoneurons, that was accompanied by presynaptic inhibition acting on the axonal branches of group-Ia afferents directly synapsing on flexor motoneurons. There are two hypothetical excitatory interneurone populations that could have mediated the polysynaptic drive. The mediating interneurons could be part of polysynaptic reflexes outside of the LLPG that were disinhibited/facilitated by the flexor half center. In this case, such reflex pathways should exist for each of the studied muscles and they must have been simultaneously opened during the flexor mode for all muscles being active. Another possible explanation for the polysynaptic drive is that the delayed afferent-evoked excitation of flexor motoneurons was mediated by the flexor half center of the LLPG. The stimulated afferents were thus acting on flexor motoneurons through the human spinal rhythm generators. A similar explanation was suggested for the reflex actions of extensor group I afferents during induced locomotion in cat preparations. Stimulation of these afferents can evoke extension enhancement during locomotion via at least two types of excitatory reflex pathways that cannot be detected in the absence of locomotion. In addition to a disynaptic excitation, extensor group I afferents also evoke a longer latency depolarization of extensor motoneurons. This delayed excitation is transmitted through the spinal rhythm generator and more particularly, through the extensor half-center (Gossard, Brownstone, Barajon, & Hultborn, 1994; Hultborn, Conway, et al., 1998; McCrea, 1998, 2001; Hultborn & Nielsen, 2007). One should consider that the latter cited results were obtained in experimental animal models utilizing different methods and paradigms than in the present manuscript. Actually, these studies revealed reflex pathways through the the extensor half-center of the CPG, while it is suggested that the polysynaptic PRM reflexes were mediated via the flexor half-center of the LLPG. However, these experimental studies stress that it is plausible to assume the direct involvement of locomotor pattern generating networks in afferent-evoked responses under appropriate conditions.

The human LLPG activated by tonic spinal cord stimulation exhibits differences in the organizations of the putative extensor and flexor half centers. Analogous differences in the circuitry that generates extension and flexion during spinal cord stimulation-induced locomotion were found in spinal rat. It was suggested that this system is based on the direct driving of the extensor motoneurons, while for driving the flexors the activation of polysynaptic networks is necessary (Gerasimenko, Ichiyama, et al., 2007; Gerasimenko, Roy, & Edgerton, 2008).

### 4.4 Significance

During spinal cord stimulation-induced rhythmic activity, locomotor-related polysynaptic PRM reflexes were identified that could not be detected in a

resting state of the lumbar cord networks. It can be suggested that their occurrence was due to the reorganization of reflex systems, including phase-dependent opening of new reflex pathways and suppression of reflexes operating at rest. During the induced rhythmic activities, a plurisegmental control mechanism for coordinating activity at different levels of the lumbosacral cord was proposed. These modifications hint on the existence and the activity of pattern generating locomotor-related neural circuits intrinsic to the human lumbar cord. In the attempt to understand the origin of the PRM reflexes, some insight could be gained into internal organization of the human locomotor circuitries. The polysynaptic PRM reflexes could have been mediated through or controlled by the flexor half center of the pattern formation networks, thus the interneurons interposed in these reflex pathways might be part of the human locomotor circuits. The relatively short latency of these reflexes might facilitate the identification of the responsible interneurons in future studies. The change of the central lumbar cord function from a resting to a rhythmic state required the increase of stimulation frequency. Furthermore, the identification of basic patterns that can reproduce the EMG patterns of all muscle groups, in combination with equal rhythm frequencies over all muscle groups hint at a organization with a common rhythm generating network, at least per leg, and multiple pattern formation networks. It can be hypothesized that the human lumbar spinal cord possesses many capabilities, beyond rhythm generation, necessary for walking, but lacks the ability to coordinate them. In order to achieve functional recovery of locomotion by biological repair, knowledge on the function of lumbar cord networks is essential, since they processes arriving excitation into motor unit firing. It is conceivable that this methodology will not only help to understand how the human spinal machinery functions, but could be crucially important to determine how to design interventions that may help restore function. Furthermore, the fact that the EMG activities can be reproduced by a set of rhythmically activated basic patterns that are similar (at the very least in their amount) to those comprising EMG activities of gait in healthy people suggests that the lumbar spinal cord harbors circuitries that are capable of generating movements beyond those ascribed to a CPG. Thus, there is additional evidence that the lumbar cord is a viable target for SCI rehabilitation, which with recent methods can be accessed transcutaneously (Minassian, Persy, Rattay, Dimitrijevic, et al., 2007; Danner, Hofstoetter, Ladenbauer, Rattay, & Minassian, 2011; Minassian, Hofstoetter, Tansey, & Mayr, 2012; Danner, Hofstoetter, & Minassian, in-press).



**Part II**

**Computer simulation**





## Chapter Five

---

### *Introduction*

Spinal interneurons provide the large majority of inputs to motoneurons (Edgley, 2001). They process the neural signals arriving from brain structures to the spinal cord, and integrate sensory feedback information when motor outputs are generated. To reveal intrinsic functional capacities of interneuronal systems, they can be isolated from supraspinal and peripheral inputs under experimental conditions in animals. They are then artificially activated by simple tonic, i.e. non-oscillating, electric or pharmacological stimulation to form functional circuitries. Organizations of neuronal populations with sophisticated locomotor control capacities have been demonstrated under such conditions. These central pattern generators (CPGs) can produce rhythmic alternating flexion and extension between the different muscles of a limb to generate locomotion, even if the spinal cord is disconnected from the brain as well as isolated from sensory feedback (Grillner, 1981; Guertin, 2009, 2013).

Spinal locomotor CPGs have been identified in a large number of species including invertebrates (Marder & Calabrese, 1996), primitive vertebrates (Roberts, Soffe, Wolf, Yoshida, & Zhao, 1998; Grillner, 2003), mammals like cats (Grillner, 1981; Rossignol, 1996), as well as nonhuman primates (Hultborn, Petersen, Prownstone, & Nielsen, 1993; Fedirchuk, Nielsen, Petersen, & Hultborn, 1998; Vilensky & O'Connor, 1998).

The locomotor networks in invertebrates and primitive vertebrates have been revealed in detail through systematic studies, due to the relatively low complexity of the model's nervous system. In the lamprey, the neurons comprising the locomotor CPG as well as their synaptic interactions have been identified, and the involved transmitters and receptors, membrane properties and different types of ion channels have been analyzed (Grillner, 2003). In this prototypical vertebrate model system it is possible to understand CPG mechanisms from the cellular basis to the network level. In higher vertebrates, classical anatomical and electrophysiological techniques and systematic recordings of identified interneurons and their target neurons become increasingly complex. In mammals, many details of the basic structure of spinal CPGs, the interneurons constituting the networks as well as the interactions between these neuronal populations, are thus not known (Hultborn, Conway, et al., 1998; Kiehn, 2006). The understanding of the mammalian CPG is rather based on conceptual schemes. These models reproduce observed experimental phenomena and give explanations for some CPG features. The

half-center model was proposed by Brown (1914) following the early finding that the isolated cat spinal cord can generate rhythmic bursts of reciprocal activity in flexor and extensor motoneurons of the hind limb (Brown, 1911). The half-center model assumes an intrinsic organization of two populations of excitatory interneurons, an extensor and a flexor half-center, with mutual inhibition between them. Alternating activity in the half-center populations of interneurons results in respective activity in flexor and extensor motoneurons through direct projections (Rybak, Shevtsova, et al., 2006; McCrea & Rybak, 2008).

An indirect approach to investigate the intrinsic organization of the mammalian CPG relies on the fact that stimulation of a number of sensory pathways influence ('reset') the locomotor cycle during induced fictive locomotion (Hultborn, Conway, et al., 1998). Locomotor CPGs and reflex circuits appear to be closely integrated within the spinal cord and can modify the operation of each other (McCrea, 2001). In fact, there is a reorganization of spinal reflexes during locomotion in animal preparations. These changes involve the suppression of reflex pathways that are active at a resting, non-locomotor state of spinal cord circuits and the recruitment of otherwise inactive, polysynaptic spinal reflexes that are directly linked to the operation of the locomotor CPG (Gossard et al., 1994; Hultborn, Conway, et al., 1998). Insight from the effects of afferent stimulation together with the alteration of spinal reflexes can thus contribute to the understanding of the mammalian locomotor CPG (Rybak, Shevtsova, et al., 2006; Rybak, Stecina, et al., 2006; McCrea & Rybak, 2008).

In humans, the existence of spinal locomotor CPGs cannot be demonstrated with the same clarity as in animal experiments. The human spinal cord cannot be studied in complete isolation from descending as well as from afferent feedback input. Yet, some elements of locomotor pattern generating circuits in the human spinal cord have been identified (Roby-Brami & Bussel, 1987; Bussel et al., 1988; Calancie et al., 1994; Calancie, 2006).

When epidural spinal cord stimulation (SCS) became a clinical method for the control of spasticity in the lower limbs of spinal cord injured individuals (Dimitrijevic, Gerasimenko, & Pinter, 1998a; Pinter et al., 2000), it provided a means of applying continuous stimulation of the posterior structures of the upper lumbar cord segments (Rattay et al., 2000). These spinal levels correspond to the respective lumbar segments in the rat (Gerasimenko, Roy, & Edgerton, 2008) and cat spinal cord (Barthélemy, Leblond, & Rossignol, 2007), which are critical for hind limb locomotion. Indeed when tonic epidural stimulation was applied to the lumbar spinal cord in humans with complete spinal cord injury, stepping-like activity could be generated in the paralyzed lower limbs (Dimitrijevic et al., 1998b). The characteristic feature of a pattern generator was thus demonstrated in the human lumbar spinal cord—the processing of tonic neural signals into coordinated oscillating motor outputs (Pearson & Gordon, 2000).

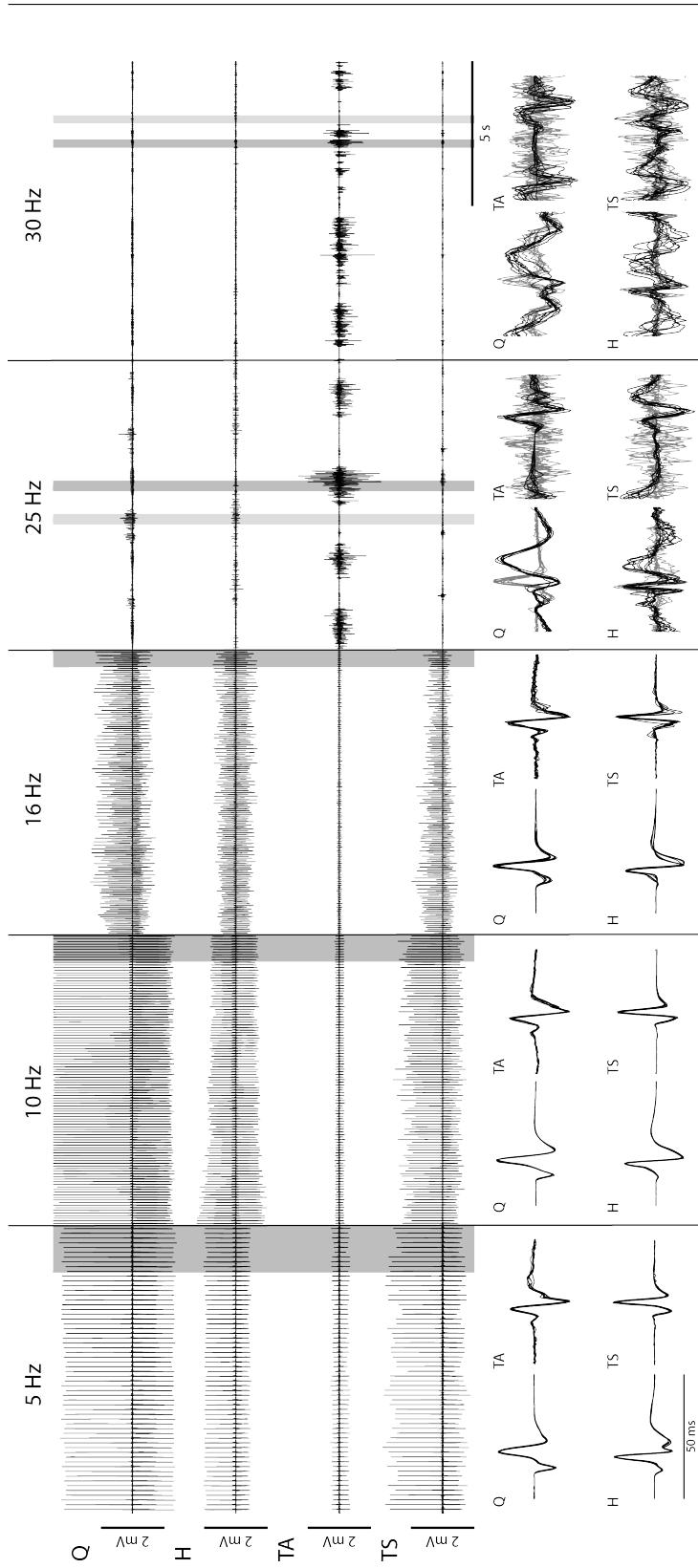


Figure 5.1: Surface EMG recordings from the right quadriceps (Q), hamstrings (H), tibialis anterior (TA), and triceps surae (TS) derived from a complete spinal cord injured person demonstrating tonic and rhythmic motor output, depending on the stimulation frequency (constant stimulation intensity of 6 V). Below are 10 compound muscle action potentials (CMAPs) of all four muscle groups illustrated as a superposition of the CMAPs normalized to the peak-to-peak amplitude. The CMAPs correspond to the shaded area of the traces above. For 25 and 30 Hz CMAPs are extracted from both burst phases, the grey and the black superposition correspond to the light and dark grey areas of the above traces, respectively. All CMAPs are stimulus time-locked (adapted from Danner, Rattay, et al., 2011; Danner, Hofstoetter, Minassian, et al., 2012).

Subsequent studies showed that the locomotor-like EMG activities induced by SCS were composed of series of compound muscle action potentials (CMAPs; Minassian, Gilge, et al., 2004). To be clearer, within the EMG activity induced by SCS, individual synchronous events can be clearly distinguished and can be unequivocally related to stimulus that triggered them (see figure 5.1). In the intact nervous system on the other hand, volitionally induced motor-outputs recorded from the muscles, display a so-called interference pattern reflecting various overlapping frequency components. The single responses within the locomotor-like EMG activities induced by SCS were identified as posterior root-muscle (PRM) reflexes—responses elicited in large-diameter posterior root afferents and detected from the muscles to which the responses were directed (Minassian, Gilge, et al., 2004; Minassian, Persy, Rattay, Pinter, et al., 2007). Series of PRM reflexes were subject to rhythmic modulation processes in response to the constant stimulus trains.

It is hypothesized that the repetitive, electrically induced, inputs via multiple posterior roots evokes PRM reflexes and concomitantly activated lumbar locomotor circuits via collateral branchings of the stimulated afferents. When set into action, the locomotor networks in turn modify the PRM reflex activity. With other words, the variation in CMAP shape, amplitude and latency of successively elicited PRM reflexes in response to the constant input train, reflects the influence of interneuronal systems with intrinsic locomotor capacities.

EMG recordings induced by spinal cord stimulation help to deduce structural as well as functional information of locomotion pattern generation system in the human (see figure 5.1). Rhythmic activities of motorpools, resulting from a direct drive of a pattern generator should include firing frequencies that depend on the system properties of the oscillating interneuronal populations. Within the data of rhythmic activities, the motor outputs instead reflect the externally imposed frequencies of the spinal cord stimulation (by the rate of successively elicited CMAPs). An interpretation of this fact can be that the excitatory actions of the CPG are at a subliminal level. CPG-excitatory actions might periodically increase the excitability of the immediate target neurons without bringing them to firing threshold level. These neurons in the subliminal fringe are then forced to discharge by the action of the electrically stimulated afferents due to spatial facilitation. This assumption is illustrated in figure 5.2.

It is proposed that the pattern generator in humans, activated by spinal cord stimulation, modulates the PRM-reflex pathway and produces sub-threshold postsynaptic potentials, instead of generating motor output by itself like in the classical ‘half center’ model. Such a mechanism has also been shown in animals (Degtyarenko, Simon, & Burke, 1998). With intracellular recordings Kinoshita and Yamaguchi (2001) showed time-locked, spike like activity of motoneurons that were rhythmically modulated in decerebrated cats during fictive locomotion. Intracellular recordings during stimulation of the mesen-

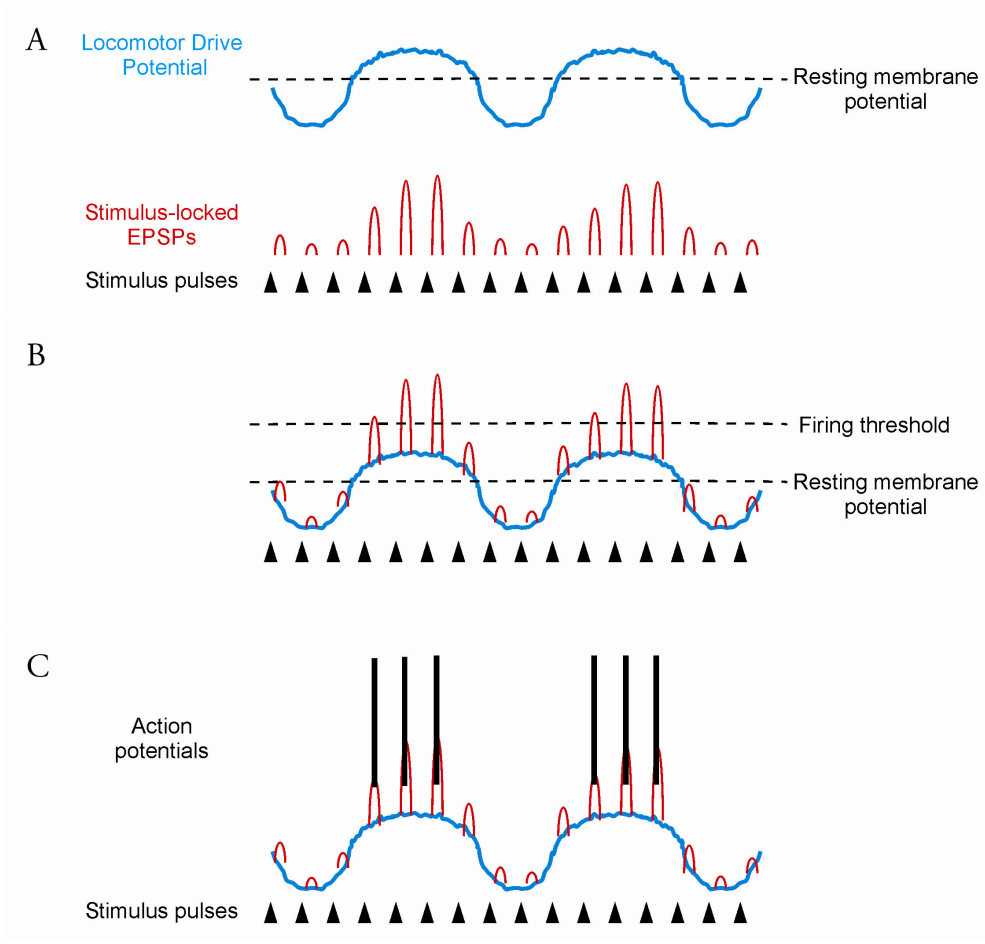


Figure 5.2: Illustration of the assumed effects of the operation of the pattern generator. A: two separate effects are proposed to be involved: (blue) resting membrane potential oscillations of the motoneurons, due to the excitatory and inhibitory influence of a various last-order interneurons driven rhythmically by the CPG or by direct CPG influence and (red) concomitant modulation of the stimulus locked excitatory post synaptic potentials (EPSPs) produced by the incoming volleys via posterior root afferents. B and C show how those to influences sum up at the motoneuronal level and produce stimulus locked action potentials only during one phase of the oscillations.

cephalic locomotor region (MLR) of the decerebrated cat showed that the motoneurons are rhythmically depolarized and hyperpolarized due to excitatory and inhibitory input during the step cycle (Noga, Kriellaars, Brownstone, & Jordan, 2003). During the depolarization phase action potentials were recorded after every MLR-stimulation pulse. Hyperpolarization mostly inhibited the action potential generation. Thus the excitatory postsynaptic potentials, produced by tonic MLR-stimulation, are stimulus locked responses that are rhythmically modulated in amplitude.

Independently, it is well described that with the onset of fictive locomotion in cats there is a presynaptic suppression of excitatory postsynaptic potentials produced by primary afferents (Gosgnach, Quevedo, Fedirchuk, & McCrea, 2000). Particularly a tonic excitatory postsynaptic potentials suppression (generating decreased efficacy) as well as phasic modulation (generating rhythmicity) has been observed. Further presynaptic mechanisms, which influence synaptic transmission from primary afferent neurons, have been shown to influence various voluntary and reflex movement tasks (Nusbaum, El Manira, Gossard, & Rossignol, 1999; Rudomin & Schmidt, 1999). Such mechanisms of presynaptic inhibition are most likely to account for the decrease of amplitude in the single responses when the pattern generator is active.

Another distinct feature of the pattern recorded with the EMG is that once the pattern generator is active the latency of the flexor PRM-reflexes increases up to 10 ms whereas the latency of the extensor muscle stays the same (part I; Minassian, Jilge, et al., 2004; Minassian, Persy, Rattay, Pinter, et al., 2007). The data suggest an asymmetrical circuitry with the flexor side being more complex and including the facilitation/disinhibition of alternative polysynaptic PRM reflex pathways.

According to De Schutter, Ekeberg, Kotaleski, Achard, and Lansner (2005) the central role of modeling small neural structures with biologically based models is to promote synthesis of experimental data from different sources into a coherent picture of the system under study. The resulting model can then, for instance, demonstrate how seemingly unexplained phenomena are in fact a consequence of what is already known. Further the exploration of the model can lead to unexpected findings and thus can provide important input for further experiments. Therefore, modeling is an important method for extracting knowledge from existing data and helps to find the most promising way for further research (Calabrese & Prinz, 2010).

Simulations are ultimately essential to explore whether a given set of data actually can account for a given function (De Schutter et al., 2005; Grillner, Markram, De Schutter, Silberberg, & LeBeau, 2005; Calabrese & Prinz, 2010). This leads to the necessity of a computer model of the neural structure of the locomotor pattern generator in humans that incorporates the newly available data.

Furthermore, the aforementioned human EMG data is ideal for creating a computer model. It supplies information on the operation of neural cir-

uits within the lower spinal cord in isolation from more complex, brain and brainstem originated signals. Especially the artificial synchronous pulses and the respective discrete responses grant insight into the workings of the neural system in between. With pharmacological or more natural activation of spinal cord structures as on a moving treadmill, only the output is specified and the input is complex, but with artificial stimulation of the afferent fibers the input can be tightly controlled. It should be noted that the proposed modeling is not a “black box” approach, since there is extensive information of structures and function, responsible for the observed behavior that were thoroughly investigated in animals.

## 5.1 Aims

The main goal of this part is to gain insight into the motor repertoire of the human lumbar cord independent from brain control. This shall be done using computer modeling to simulate the neural circuits of the locomotion pattern generator activated by spinal cord stimulation. The model shall test the hypotheses on the function and structure of the pattern generating circuits described above.

The complete network model shall contain interconnected neuronal populations, each simulated with Hodgkin and Huxley (1952)-like formulations and including realistic firing properties and spike conduction delays. The system shall be set into action by specific sequences of action potentials transmitted via afferent pathways, representing epidural electrical stimulation. The time-dependent model behavior shall provide insight into the population sizes of active neurons in every pool. The system output shall mimic the measured multichannel electromyographic activity. The model shall test general principles of formation of interneuronal systems in the isolated spinal cord and characterize similarities and differences of these principles in human and animal models.

The specific features that the model should be able to reproduce are the following:

1. The motor output consists of stimulus triggered responses.
2. Repetitive afferent input produced by SCS at frequency ranges from 20 to 50 Hz evoke rhythmic activity within the motor pools with two alternating phases (‘flexion’ and ‘extension’; part I; Dimitrijevic et al., 1998b; Minassian, Jilge, et al., 2004).
3. Frequency ranges from 5 to 15 Hz induce a sustained extension of the lower limbs, i.e. tonic motor output (Jilge, Minassian, Rattay, Pinter, et al., 2004).

4. Single stimuli and frequencies below 5 Hz do not activate the pattern generator in a manner that it generates rhythmic activity and solely result in activation of monosynaptic PRM-reflexes (Minassian, Gilge, et al., 2004; Danner, Rattay, et al., 2011).
5. The model replicates the mechanisms of sub-threshold modification of the postsynaptic potentials of the motoneurons in cats to test whether this can also account for the locomotor pattern generation in humans and what modifications from the classical ‘half center’ model are needed to reproduce the behavior seen in human studies.
6. The model reproduces the selection of alternative pathways of PRM reflexes of flexor motoneurons during the locomotor state of the spinal circuits, i.e. when the pattern generator network is active. It should give insight in the complexity and properties of the additional pathways. When the alternative pathway is activated, the flexor side exhibits a prolongation of the response latencies.

A model shall be developed that captures a description that can be used to generate experimentally testable hypotheses about the network and not a model that represents the optimal description of the living network; indeed such a single description may not exist (Calabrese & Prinz, 2010).



---

*Methods*

The design of the network model is similar to the modeling of spinal circuitry involved in mammalian locomotor pattern generation from the Rybak and McCrea group (Rybak, Shevtsova, et al., 2006; Rybak, Stecina, et al., 2006). The network model is implemented using Brian, a simulator for spiking neural networks based on python (Goodman & Brette, 2008, 2009) and uses conductance based models of individual neurons grouped into populations. Small networks of neurons are attractive objects for modeling using such conductance based neuron models (De Schutter et al., 2005; Grillner et al., 2005; Marder, Bucher, Schulz, & Taylor, 2005; Calabrese & Prinz, 2010). Additional circuits are added to account for the observation in human studies (see part I). The code used to simulate all models can be found in the appendix.

## 6.1 Neuron models

Here the models of single neurons are described. All neurons are modeled using Hodgkin and Huxley (1952)-like formulations for ion channel dynamics. Each of the interneurons consisted of a single compartment. Motoneurons include two compartments, one for the soma and one for the dendrite. The actual surface area of the cells are neglected, thus all conductances are actually calculated as electrical conductances per area with the unit of siemens per square meter, currents are calculated as currents per area with the units ampere per square meter and the capacitance is also given per meter. Due to the similarity with the Rybak, Shevtsova, et al. (2006)-model the same nomenclature/model description is used. The motoneurons are modeled after Booth, Rinzel, and Kiehn (1997). Accordingly, following ionic currents were incorporated:

1. fast sodium (current:  $I_{Na}$ , maximal conductance:  $\bar{g}_{Na}$ ),
2. slowly inactivating (persistent) sodium (current:  $I_{NaP}$ , maximal conductance:  $\bar{g}_{NaP}$ ),
3. delayed-rectifier potassium (current:  $I_K$ , maximal conductance:  $\bar{g}_K$ ),
4. calcium-N (current:  $I_{CaN}$ , maximal conductance:  $\bar{g}_{CaN}$ ),
5. calcium-L (current:  $I_{CaL}$ , maximal conductance:  $\bar{g}_{CaL}$ ),

## 6. METHODS

---

6. calcium-dependent potassium (current:  $I_{K,Ca}$ , maximal conductance:  $\bar{g}_{K,Ca}$ ) and

7. leakage (current:  $I_L$ , constant conductance:  $\bar{g}_K$ ).

The above listed currents were modeled using following equations:

$$I_{Na} = \bar{g}_{Na} \cdot m_{Na}^3 \cdot h_{Na} \cdot (V - E_{Na}), \quad (6.1)$$

$$I_{NaP} = \bar{g}_{NaP} \cdot m_{NaP} \cdot h_{NaP} \cdot (V - E_{Na}), \quad (6.2)$$

$$I_K = \bar{g}_K \cdot m_K^4 \cdot (V - E_K), \quad (6.3)$$

$$I_{CaN} = \bar{g}_{CaN} \cdot m_{CaN}^2 \cdot h_{CaN} \cdot (V - E_{Ca}), \quad (6.4)$$

$$I_{CaL} = \bar{g}_{CaL} \cdot m_{CaL} \cdot (V - E_{Ca}), \quad (6.5)$$

$$I_{K,Ca} = \bar{g}_{K,Ca} \cdot m_{K,Ca} \cdot (V - E_K), \quad (6.6)$$

$$I_L = g_L \cdot (V - E_L), \quad (6.7)$$

where  $E_x$  is the reversal potential of ionic currents  $x$  (i.e.  $Na$  sodium,  $K$  potassium,  $Ca$  calcium,  $L$  leakage),  $V$  the membrane potential of the respective compartment (subscripts “(S)” and “(D)” will be used to denote the soma and dendrite, respectively) and  $m$  and  $h$  with the respective indices corresponding to the ion channel, are the corresponding activation and inactivation variables.

The currents coupling the soma and dendrite compartments of the Booth et al. (1997)-motoneuron model for the soma ( $I_{C(S)}$ ) and dendrite ( $I_{C(D)}$ ) are given by:

$$I_{C(S)} = \frac{g_C}{p} \cdot (V_{(S)} - V_{(D)}), \quad (6.8)$$

$$I_{C(D)} = \frac{g_C}{1-p} \cdot (V_{(D)} - V_{(S)}), \quad (6.9)$$

where  $g_C$  is the coupling conductance and  $p$  a parameter defining the ratio of somatic to total surface area.

To model network activity excitatory and inhibitory synaptic currents were also included into the model with following equations:

$$I_{SynE} = g_{SynE} \cdot (V - E_{SynE}), \quad (6.10)$$

$$I_{SynI} = g_{SynI} \cdot (V - E_{SynI}), \quad (6.11)$$

where  $E_{SynE/-I}$  are the reversal potentials  $I_{SynE/-I}$  the currents and  $g_{SynE/-I}$  the conductances of the excitatory and inhibitory synapses, respectively.

The Booth et al. (1997)-motoneuron model includes intracellular  $Ca^{2+}$  kinetics that are described for every compartment separately and are modeled by following differential equation:

$$\frac{dCa}{dt} = f \cdot (-\alpha \cdot I_{Ca} - k_{Ca} \cdot Ca), \quad (6.12)$$

where  $Ca$  is the intracellular  $Ca^{2+}$  concentration,  $f$  is the fraction of free (to total)  $Ca^{2+}$ ,  $\alpha$  is a constant that converts the  $Ca^{2+}$  current,  $I_{Ca}$ , to a  $Ca^{2+}$  concentration,  $k_{Ca}$  is the the  $Ca^{2+}$  removal rate and  $t$  the time.

Rybak, Shevtsova, et al. (2006) added the slowly inactivating, persistent sodium current ( $I_{NaP}$ ) to the motoneuron's dendrite. This addition to the Booth et al. (1997)-motoneuron model was also included in the present model. Thus, the differential equations for the membrane potentials of the soma ( $V_{(S)}$ ) and of the dendrite ( $V_{(D)}$ ) read as follows:

$$\frac{dV_{(S)}}{dt} = - (I_{Na(S)} + I_{K(S)} + I_{CaN(S)} + I_{K,Ca(S)} + I_{L(S)} + I_{C(S)})/C, \quad (6.13)$$

$$\frac{dV_{(D)}}{dt} = - (I_{NaP(D)} + I_{CaN(D)} + I_{CaL(D)} + I_{K,Ca(D)} + I_{L(D)} + I_{C(D)} + I_{SynE} + I_{SynI})/C, \quad (6.14)$$

where  $C$  is the membrane capacitance.

All interneurons except the excitatory interneurons of the rhythm generation and pattern formation networks (i.e. RG and PF neuron populations, respectively) were modeled with only sodium and potassium currents. Thus, their membrane potentials are described by following differential equation:

$$\frac{dV}{dt} = - (I_{Na} + I_{K} + I_{L} + I_{SynE} + I_{SynI})/C. \quad (6.15)$$

The RG and PF neuron population of the CPG are equal to the other neurons except the addition of the persistent (slowly inactivating) sodium current ( $I_{NaP}$ ). This current is an integral part for rhythm genesis in the model (Rybak, Shevtsova, et al., 2006). The membrane potential is characterized by following differential equation:

$$\frac{dV}{dt} = - (I_{Na} + I_{NaP} + I_{K} + I_{L} + I_{SynE} + I_{SynI})/C. \quad (6.16)$$

Injection of current is simulated by adding

$$I_{app}/C \quad (6.17)$$

to the right side of equations 6.13, 6.15 or 6.16, where  $I_{app}$  is a time dependent function of the injected current density (unit  $\mu A \text{ cm}^{-2}$ ).

The activation ( $m$ ) and inactivation ( $h$ ) variables of the voltage-dependent ion channels are given by the following differential equations:

$$\frac{dm_x}{dt} = (m_{\infty,x}(V) - m_x)/\tau_{m,x}(V), \quad (6.18)$$

$$\frac{dh_x}{dt} = (m_{\infty,x}(V) - h_x)/\tau_{h,x}(V), \quad (6.19)$$

## 6. METHODS

---

where  $i$  denotes the ion channel name,  $m_{\infty,x}(V)$  and  $h_{\infty,x}(V)$  are the voltage-dependent steady-states of the respective variable and  $\tau_{m,x}(V)$  and  $\tau_{h,x}(V)$  are the voltage dependent time constants of the respective activation and inactivation variables. Both  $\tau_{m/h,x}(V)$  and  $m/h_{\infty,x}(V)$  can be written as a function of the transition rates of the gates of the ion channels  $\alpha(V)$  and  $\beta(V)$ , with following relations:

$$\tau_{m/h,x}(V) = \frac{1}{\alpha_{m/h,x}(V) + \beta_{m/h,x}(V)}, \quad (6.20)$$

$$m/h_{\infty,x}(V) = \frac{\alpha_{m/h,x}(V)}{\alpha_{m/h,x}(V) + \beta_{m/h,x}(V)}. \quad (6.21)$$

The activation of the two sodium channels is instantaneous, i.e.  $\tau_{m,Na} = 0$  and  $\tau_{m,NaP} = 0$ . This reduces 6.18 to:

$$m_x = m_{\infty,x}(V), \quad (6.22)$$

where  $x$  is Na or NaP. As a side-note, due to specifics of the integration mechanism and simulation software used equation 6.18 with  $\tau_{m,Na} = \tau_{m,NaP} = 0.001$  ms was used for the actual calculation. Furthermore, the activation of the  $Ca^{2+}$ -dependent potassium channels ( $I_{K,Ca}$ ) is also instantaneous and depends from the  $Ca^{2+}$  concentration  $Ca$  of the corresponding compartment:

$$m_{K,Ca} = \frac{Ca}{Ca + K_d}, \quad (6.23)$$

where  $K_d$  is the half-saturation level of the very conductance.

The post-synaptic potentials, as modeled by exponential synapses (for the verification of the model implementation) and alpha synapses (in the final model, for everything except the afferent inputs to the motoneurons, which are modeled as exponential synapses). The conductances of the excitatory and inhibitory synapses in case of exponential synapses are given by following differential equations:

$$\frac{dg_{SynE}}{dt} = -g_{SynE}/\tau_{SynE} \quad (6.24)$$

$$\frac{dg_{SynI}}{dt} = -g_{SynI}/\tau_{SynI}, \quad (6.25)$$

where  $g_{SynE}$  and  $g_{SynI}$  are increased by  $\bar{g}_E \cdot w_{i,j}$  and  $\bar{g}_I \cdot w_{i,j}$ , respectively, every time, when a presynaptic spike is arriving at the synapse, where  $\bar{g}_E/\bar{g}_I$  are conductances that are the same over all connections and  $w_{i,j}$  is a specific, dimensionless weight specific to the connection of the  $i$ -th to the  $j$ -th neuron.

For the alpha synapses an additional helper variable is introduced for each type of synapse  $g_{hE}$  and  $g_{hI}$ . Following differential equations describe the

alpha synapses:

$$\frac{dg_{SynE}}{dt} = -g_{SynE} * 1/\tau_{SynE}, \quad (6.26)$$

$$\frac{dg_{SynI}}{dt} = -g_{SynI} * 1/\tau_{SynI}, \quad (6.27)$$

$$\frac{dg_{hE}}{dt} = (g_{SynE} - g_{hE}) * 1/\tau_{SynE}, \quad (6.28)$$

$$\frac{dg_{hI}}{dt} = (g_{SynI} - g_{hI}) * 1/\tau_{SynE}. \quad (6.29)$$

This time  $g_{hE}$  and  $g_{hI}$  are increased with the same value when a presynaptic spike arrives.

In addition, to model the constant drive from the brainstem to the CPG as described in the model of Rybak, Shevtsova, et al. (2006) equations 6.10 and 6.11 are extended to incorporate an additional constant conductance as follows:

$$I_{SynE} = (g_{SynE} + g_{driveE}) \cdot (V - E_{SynE}), \quad (6.30)$$

$$I_{SynI} = (g_{SynI} + g_{driveI}) \cdot (V - E_{SynI}), \quad (6.31)$$

where

$$g_{driveE} = \bar{g}_{Ed} \cdot S(w_{dmi}) \cdot d_{mi} \quad (6.32)$$

$$g_{driveI} = \bar{g}_{Ed} \cdot S(-w_{dmi}) \cdot d_{mi} \quad (6.33)$$

and

$$S(x) = \begin{cases} x, & \text{if } x \geq 0. \\ 0, & \text{otherwise} \end{cases} \quad (6.34)$$

where  $\bar{g}_{Ed}$  and  $\bar{g}_{Id}$  are the parameters that define the increase of excitatory or inhibitory synaptic conductances, respectively,  $d_{mi}$  the external input drive and  $w_{dmi}$  its weight.

Presynaptic inhibition is modeled similar to normal exponential synapses but with additional non-linearity that scales the sum of the synaptic weights of the synapses influenced by presynaptic inhibition. For every presynaptic spike that acts on the axons as presynaptic inhibition a helper variable  $x_{pre}$  is increased by a given factor  $w_{prei,j}$  and follows following differential equation:

$$\frac{dx_{pre}}{dt} = -x_{pre}/\tau_{pre} \quad (6.35)$$

the non-linearity  $P_{pre}(x_{pre})$  transform  $x$  into the into the interval  $[0, 1]$  with following equation:

$$P_{pre}(x_{pre}) = \frac{1}{1 + e^{6-x_{pre}}}. \quad (6.36)$$

Due to the inability of the used simulation software to calculate this equation it is rewritten as following differential equation:

$$\frac{dP_{pre}(x_{pre})}{dt} = \left( \frac{1}{1 + e^{6-x_{pre}}} - P_{pre}(x_{pre}) \right) / \tau_{Pre} \quad (6.37)$$

with a small  $\tau_{Pre}$  (0.01 ms). Now the total current of the excitatory synapses (eq. 6.30) can be written as

$$I_{SynE} = (g_{SynE} + g_{driveE} + g_{SynEPreI} * (1 - P_{pre} * \bar{f}_{pre})) * (V - E_{SynE}), \quad (6.38)$$

where  $g_{SynEPreI}$  is the the same as  $g_{SynE}$  but only of the synapses under influence of presynaptic inhibition, while  $g_{SynE}$  summarizes all synapses not influences by the presynaptic inhibition and  $\bar{f}_{pre}$  is a factor indicating the maximal influence of the presynaptic inhibition on the postsynaptic excitatory potentials.

## 6.2 Population and network model

Every type of neuron depicted in figure 6.1 is modeled as group of 20 neurons. Connections between two neuron groups were established in a manner that if group  $A$  has an excitatory or inhibitory connection to group  $B$  all neurons from group  $A$  have synaptic connections to all neurons in group  $B$ . Two cases of connections were implemented: *i*) instantaneous connection, i.e. if a spike is generated in neuron  $A_i$  post synaptic potentials are generated in all neurons of group  $B$  in the next integration step. This was done in order to be consistent with the model of Rybak, Shevtsova, et al. (2006) and to prove the correctness of the implementation. *ii*) an conduction delay ( $t_{cdi,j}$ ) was added to all connections from neuron  $i$  to  $j$ . The conduction delay  $t_{cdi,j}$  was defined for every run by a random gaussian distribution with a defined mean value and standard deviation as well as cutoffs for minimum (0 ms) and maximum (10 ms) values. The heterogeneity of the population was modeled by randomizing the leakage reversal potential ( $E_L$ ) of the individual neuron groups, again with a gaussian distribution defined by a mean and a standard deviation. Furthermore, every group of neurons was defined by its individual set of parameters.

The central part of the model were two half centers (see Brown, 1911, 1914) that generate the rhythmic pattern. Two populations of interneuron (RG-E for the extensor muscle and RG-F for the flexor muscle) have excitatory connections to themselves and reciprocally inhibit each other through the path of inhibitory interneurons (InRG-E and InRG-F). The neurons from the RG-E/F populations include a slowly inactivating, persistent sodium current that inhibits the bursting behavior of the neurons after some time and thus the

other population starts to burst (due to the missing inhibition), resulting in a rhythmic, alternating bursting behavior of RG-E and RG-F. The RG half center level is connected to the pattern formation (PF) layer that is similarly structured but is strongly influence, through excitation and inhibition by the RG layer and if not otherwise disturbed (externally stimulated, i.e. due to afferent stimulation or different intensities of MLR drive) the PF layer follows the rhythm of the RG layer.

The PF populations transmit alternating rhythmic activation to extensor (Mn-E) and flexor (Mn-F) motoneurons and to inhibitory extensor (Ia-E) and flexor (Ia-F) interneurons. These Ia populations form the second level of reciprocal inhibition in the system. They provide the rhythmic inhibition of motoneuron populations during the inactive phase of the step cycle (McCrea, Pratt, & Jordan, 1980). Further the model also includes extensor (R-E) and flexor (R-F) Renshaw cells, which receive collateral excitatory input from the corresponding motoneuron populations and provide feedback inhibition to the homonymous motoneurons (McCrea, Pratt, & Jordan, 1980; Rybak, Shevtsova, et al., 2006). The structure of the Renshaw cells (R-E and R-F), the motoneurons (Mn-E and Mn-F) and the inhibiting interneurons (Ia-E and Ia-F) are in accordance with extensive work done in anesthetized preparations (Jankowska, 1992; Rybak, Shevtsova, et al., 2006).

For monitoring of the modulation of the membrane potentials of the motoneurons one additional motoneuron has been introduced in each of the motoneuron groups. This additional motoneuron is equivalent to the others with the exception that the influence of all ionic currents were neglected. This was modeled by setting all maximal conductances of the ionic currents to 0. Thus only leakage and synaptic currents remain.

Afferent input is modeled by 20 metronomes that generate a spike with a constant frequency ( $f_q$ ). The offset ( $off$ ) is modeled by a random gaussian distribution with a mean and a standard deviation.

The drive to the InPath neuron group is modeled as a group of neurons that generate independent Poisson spike trains with a frequency of  $f_{pois}$ .

Spikes were detected when the membrane potential  $V$  or  $V_{(S)}$  reached a threshold value of 0 mV (for the reproduction of the Rybak, Shevtsova, et al., 2006-model with -20 mV). After the detection of a spike new spikes were only detected if the threshold is exceeded more then 3 milliseconds later<sup>1</sup>.

Model stability was tested by randomizing initial conditions and repeating the simulation several times. Stability was judged if in every run, after an allowed setting period of 20s, the results were qualitatively similar.

---

<sup>1</sup>This value was independently assumed since it is not specified in Rybak, Shevtsova, et al. (2006).

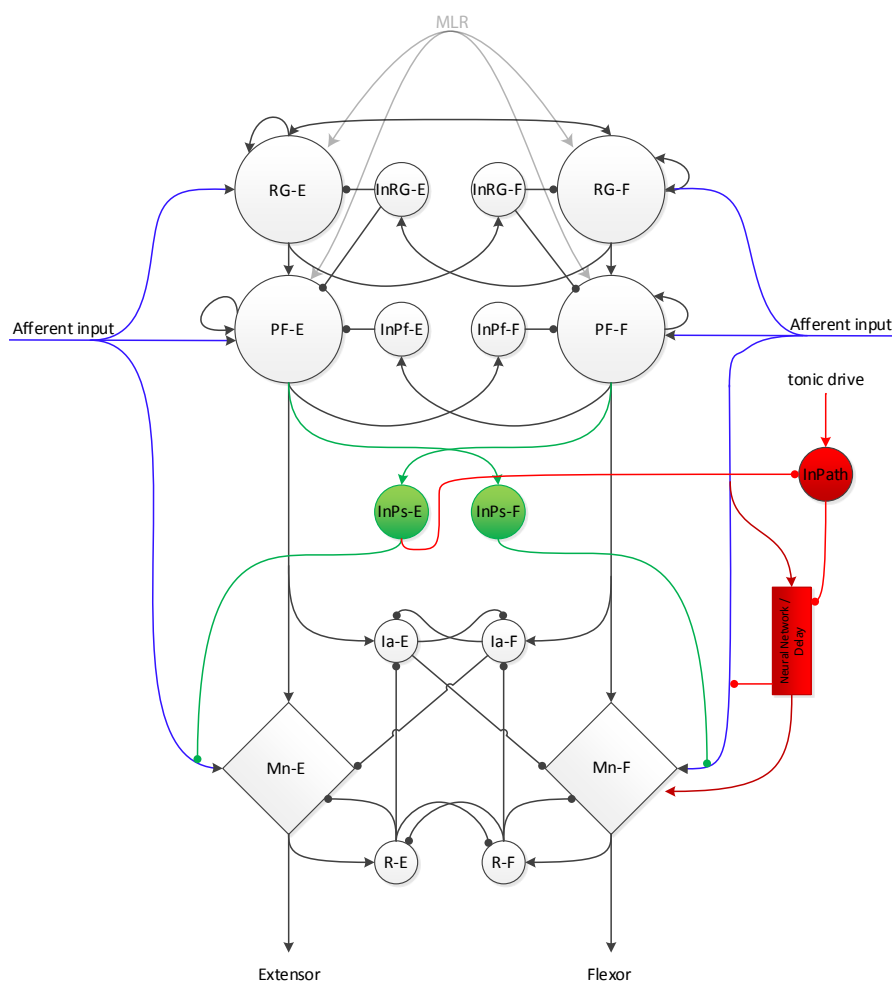


Figure 6.1: Design of the network model. Every node represents a class population of 20 neurons. All edges represent directed synaptic connections between all neurons of the source and all neurons of the target population. Arrows denote excitatory and dots inhibitory synapses. Black lines represent features present in all simulated models; gray lines features only present in the Rybak, Shevtsova, et al. (2006) model and colored lines, features that expand upon the latter. Abbreviations: Mn: motoneurons, R: Renshaw cells, Ia: Ia inhibitory neurons, InPs: inhibitory neurons of presynaptic inhibition, RG: rhythm generation neurons, PF: pattern formation neurons, InRg: inhibitory neurons of the rhythm generation network, InPf: inhibitory neurons of pattern formation network, InPath: inhibitory neurons of the inhibition of the polysynaptic flexor pathway, -E/-F: neurons part of the extensor and flexor half, respectively. To reduce computation complexity, InPs neurons were not modeled, presynaptic inhibition was modeled as originating from the InPf populations.



## 6.3 Simulation

The model was implemented using the simulation software Brian Version 1.4.1 (Goodman & Brette, 2008, 2009, 2013), which bases on Python (<http://www.python.org>). The utilized Python version was 2.7.5 (64 bit for Mac OS X 10.8.8). An exponential Euler integration mechanism with a time step of 0.1 ms was applied.

## 6.4 Parameters

In the following the model parameters are listed, beginning with the reproduction of the Rybak, Shevtsova, et al. (2006) model for validation. All following model descriptions only list the values that differ from this model.

### 6.4.1 Replication of Rybak's model

Table 6.1: Variables of the ion channel dynamics

Ion channel	Steady-state (in-)activation variables and time constants
Na <sup>+</sup>	$m_{\infty Na} = (1 + \exp(-(V + 35)/7.8))^{-1}$ $\tau_{mNa} = 0$ $h_{\infty Na} = (1 + \exp((V + 55)/7))^{-1}$ $\tau_{hNa} = 30 / (\exp((V + 50)/15) + \exp(-(V + 50)/16))$
NaP <sup>+</sup>	$m_{\infty NaP} = (1 + \exp(-(V + 47.1)/3.1))^{-1}$ $\tau_{mNaP} = 0$ $h_{\infty NaP} = (1 + \exp((V + 59)/8))^{-1}$ $\tau_{hNap} = \tau_{hNaP,max} / \cosh((V + 59)/16), \tau_{hNaP,max} = 1200$
K <sup>+</sup>	$m_{\infty K} = (1 + \exp(-(V + 28)/15))^{-1}$ $\tau_{mK} = 7 / (\exp((V + 40)/40) + \exp((-V + 40)/50))$
CaN <sup>2+</sup>	$m_{\infty CaN} = (1 + \exp(-(V + 30)/5))^{-1}$ $\tau_{mCaN} = 4$ $h_{\infty CaN} = (1 + \exp((V + 45)/5))^{-1}$ $\tau_{hCaN} = 40$
CaL <sup>2+</sup>	$m_{\infty CaL} = (1 + \exp(-(V + 40)/7))^{-1}$ $\tau_{mCaL} = 40$

V is measured in mV,  $\tau$  in ms

Table 6.1 lists all steady-state activation and inactivation variables as well as the time constants of all ionic currents, table 6.2 lists all connection weights and in the following all other parameters are listed.

Table 6.2: Weights of synaptic connections

Target	Source population (weights of synaptic input or drive)
RG-E	MLR (1); RG-E (0.0125); RG-F (0.0125); Inrg-E (-0.115)
RG-F	MLR (1); RG-F (0.0125); RG-E (0.0125); Inrg-F (-0.115)
Inrg-E	RG-F (0.45)
Inrg-F	RG-E (0.45)
PF-E	MLR(1); RG-E (0.0075); Inrg-E (-0.05); Inpf-E (-0.35)
PF-F	MLR(1); RG-F (0.0075); Inrg-F (-0.05); Inpf-F (-0.35)
Inpf-E	PF-F (0.2)
Inpf-F	PF-E (0.2)
Ia-E	PF-E (0.4); Ia-F (-0.1); R-E (-0.1)
Ia-F	PF-F (0.4); Ia-E (-0.1); R-F (-0.1)
R-E	Mn-E (0.25); R-F (-0.1)
R-F	Mn-F (0.25); R-E (-0.1)
Mn-E	PF-E (0.5); Ia-F (-0.6); R-E (-0.2)
Mn-F	PF-F (0.5); Ia-E (-0.6); R-F (-0.2)

Weights are  $w_{ij}$  for synaptic input or  $w_{dmi}$  for MLR drive. All abbreviations are explained elsewhere in the text; see also figure 6.1.

### General model parameters

- $E_{Na} = 55$  mV
- $E_k = -80$  mV
- $E_{Ca} = 80$  mV
- $C = 1$   $\mu\text{F cm}^{-2}$

### Parameters of synapses

- $E_{SynE} = -10$  mV
- $E_{SynI} = -70$  mV
- $\bar{g}_E = 0.05$  mS  $\text{cm}^{-2}$
- $\bar{g}_I = 0.05$  mS  $\text{cm}^{-2}$
- $\bar{g}_{Ed} = 0.05$  mS  $\text{cm}^{-2}$
- $\bar{g}_{Id} = 0.05$  mS  $\text{cm}^{-2}$
- $\tau_{SynE} = 5$  ms
- $\tau_{SynI} = 5$  ms

### Neuron parameters

## RG neurons

- $\bar{g}_{Na} = 30 \text{ mS cm}^{-2}$
- $\bar{g}_{NaP} = 0.25 \text{ mS cm}^{-2}$
- $\bar{g}_K = 1 \text{ mS cm}^{-2}$
- $g_L = 0.1 \text{ mS cm}^{-2}$
- $E_L = -64.0 \pm 0.64 \text{ mV}$

## PF neurons

- $\bar{g}_{Na} = 30 \text{ mS cm}^{-2}$
- $\bar{g}_{NaP} = 0.1 \text{ mS cm}^{-2}$
- $\bar{g}_K = 1.2 \text{ mS cm}^{-2}$
- $g_L = 0.1 \text{ mS cm}^{-2}$
- $E_L = -64.0 \pm 0.64 \text{ mV}$

## Motoneurons

- $\bar{g}_{Na(S)} = 120 \text{ mS cm}^{-2}$
- $\bar{g}_{K(S)} = 100 \text{ mS cm}^{-2}$
- $\bar{g}_{CaN(S)} = 14 \text{ mS cm}^{-2}$
- $\bar{g}_{K,Ca(S)} = 5 \text{ mS cm}^{-2}$
- $g_{L(S)} = 0.51 \text{ mS cm}^{-2}$
- $E_{L(S)} = -65.0 \pm 6.5 \text{ mV}$
- $\bar{g}_{CaN(D)} = 0.3 \text{ mS cm}^{-2}$
- $\bar{g}_{CaL(D)} = 0.33 \text{ mS cm}^{-2}$
- $\bar{g}_{K,Ca(D)} = 1.1 \text{ mS cm}^{-2}$
- $\bar{g}_{NaP(D)} = 0.1 \text{ mS cm}^{-2}$
- $g_{L(D)} = 0.51 \text{ mS cm}^{-2}$
- $E_{L(D)} = -65.0 \pm 3.25 \text{ mV}$
- $g_C = 0.1 \text{ mS cm}^{-2}$
- $p = 0.1$
- $f = 0.01$
- $\alpha = 0.009 \text{ mol C}^{-1} \mu\text{m}^{-1}$
- $k_{Ca} = 2 \text{ ms}^{-1}$
- $K_d = 0.2 \mu\text{M}$

## Other interneurons

- $\bar{g}_{Na} = 120 \text{ mS cm}^{-2}$
- $\bar{g}_K = 100 \text{ mS cm}^{-2}$
- $g_L = 0.51 \text{ mS cm}^{-2}$

- $E_L = -64.0 \pm 3.2$  mV (for all interneurons except Inrg)
- $E_L = -57.5^2 \pm 2.875$  mV (for Inrg)

### Other parameters

- $I_{app} = 0$   $\mu\text{A cm}^{-2}$
- $d_{pf-e} = 0.5$
- $d_{pf-f} = 0.5$
- $d_{rg-e/f} =$  (see text/figure legends)
- $\bar{f}_{pre} = 0$

All parameters are taken from Rybak, Shevtsova, et al. (2006). The parameters for the motoneuron model of Booth et al. (1997) were cross-checked—the value  $\alpha$  was reproduced from Booth et al. (1997). It is assumed that the presentation in Rybak, Shevtsova, et al. (2006) as  $\alpha = 0.0009$  mol C<sup>-1</sup>  $\mu\text{m}^{-1}$  must have been a typing error. Furthermore, it is not specified in the paper with what method a spike is detected.

### 6.4.2 Model A

Model A is a derivation of the Rybak, Shevtsova, et al. (2006) model that replaces the MLR drive by afferent input of variable frequencies. The updated synaptic connections can be found in table 6.3. The activation and inactivation variables as well as the time constants of the ion channels were left untouched and in the following the changed parameters are listed, all non-listed parameters are equal to the previous model.

#### Afferent input

- $f_q = 5 - 60$  Hz
- $off = 0$  ms  $\pm$  0 ms

#### Neuron parameters

##### RG neurons

- $\bar{g}_K = 2$  mS  $\text{cm}^{-2}$
- $a_{rg-e} = 1$
- $a_{rg-f} = \frac{15}{16}$

##### PF neurons

- $\bar{g}_K = 2$  mS  $\text{cm}^{-2}$

---

<sup>2</sup>Rybak, Shevtsova, et al. (2006) reported  $E_L$  to be 57.5 mV (without the negative sign) which is most likely a typing error.

Table 6.3: Weights of synaptic connections: Model **A**, **B** and **C**

Target	Source population (weights of synaptic input or drive)
RG-E	RG-E (0.0125); RG-F (0.0125); Inrg-E (-0.115); <b>Aff (0.064·<math>a_{rg-e}</math>)</b>
RG-F	RG-F (0.0125); RG-E (0.0125); Inrg-F (-0.115); <b>Aff (0.064·<math>a_{rg-f}</math>)</b>
Inrg-E	RG-F (0.45)
Inrg-F	RG-E (0.45)
PF-E	RG-E (0.0075); Inrg-E (-0.05); Inpf-E (-0.35); <b>Aff (0.064)</b>
PF-F	RG-F (0.0075); Inrg-F (-0.05); Inpf-F (-0.35); <b>Aff (0.064)</b>
Inpf-E	PF-F ( <b>0.6</b> )
Inpf-F	PF-E ( <b>0.6</b> )
Ia-E	PF-E (0.4); Ia-F (-0.1); R-E (-0.1)
Ia-F	PF-F (0.4); Ia-E (-0.1); R-F (-0.1)
R-E	Mn-E (0.25); R-F (-0.1)
R-F	Mn-F (0.25); R-E (-0.1)
Mn-E	PF-E (0.5); Ia-F ( <b>-0.8</b> ); R-E (-0.2); <b>Aff (0.4·<math>a_{mn-e}</math>)</b> ; <i>MnE (pre -0.8)</i>
Mn-F	PF-F (0.5); Ia-E ( <b>-0.8</b> ); R-F (-0.2); <b>Aff (0.4·<math>a_{mn-f}</math>)</b> ; <i>MnF (pre -0.8)</i> ; <a href="#">AP2 (0.75)</a> ; <a href="#">AP2in (pre -0.8)</a>
<a href="#">InPath</a>	<a href="#">Poisson (0.5)</a> ; <a href="#">InPF-E (-2)</a>
<a href="#">AP1</a>	<a href="#">InPath (-2)</a> ; <a href="#">Aff (0.75)</a>
<a href="#">AP2</a>	<a href="#">AP1 (0.75)</a>
<a href="#">AP2in</a>	<a href="#">AP1 (0.75)</a>

Weights are  $w_{ij}$  for synaptic input. All abbreviations are explained elsewhere in the text. The  $a_{rg-e/f}$ s are used to adjust the input to the RG population. Later models incorporate all features parameters from the previous ones.

#### Mn neurons

- $a_{mn-e} = 0.5$  or  $0.75$
- $a_{mn-f} = 0.5$  or  $0.75$

#### Other parameters

- $t_{cd} = 2 \text{ ms} \pm 0.5 \text{ ms}$

### 6.4.3 Model B

Model B builds upon model A and adds phasic, rhythmically modulated presynaptic inhibition to the afferents synapsing to the motoneurons. Furthermore the input weights from the afferents to the motoneurons are increased. All parameters are listed in table 6.3 and below.

#### Mn neurons

- $a_{mn-e} = 1.5$
- $a_{mn-f} = 1.5$
- $\bar{f}_{pre} = 0.65$

#### 6.4.4 Model C

Model C builds upon model B and adds an additional pathway from the afferent input to the motoneuron on the flexor side that is disinhibited by the pattern formation network when the CPG is active at the flexor side. This pathway is quiescent during the non-locomotor states. To reproduce this behavior a similar approach of disinhibition of alternative reflex pathways as in Rybak, Stecina, et al. (2006) is applied. The hypothetical InPath population, which inhibits the interneurons along the polysynaptic path, has been included in the model. Under non-locomoting conditions, excitatory external drive produces tonic activity of this population that prevents signal transmission along the polysynaptic pathway. However during the flexor phase of locomotion (i.e. when the RG-F, PF-F populations and the inhibitory InPf-E population are active), the InPf-E population inhibits InPath thereby removing the InPath inhibition of the polysynaptic pathway. This disinhibition permits the selection of the polysynaptic pathway that produces the higher delay of flexor muscle responses. This pathway has several synapses in between is modeled as two neural populations with feed forward connections. The monosynaptic pathway is inactivated by presynaptic inhibition of inhibitory interneurons along the polysynaptic pathway when the disinhibition is active. The connectivities are described in table 6.3 and additional parameters are listed below.

##### **Mn neurons**

- $\bar{f}_{pre} = 0.65$  (for the extensor side)
- $\bar{f}_{pre} = 0.95$  (for the flexor side)

##### **Poisson neuron group (tonic drive)**

- $f_{pois} = 75$  Hz

---

*Results*

First, the implementation was verified by replicating simulations of Booth et al. (1997) and Rybak, Shevtsova, et al. (2006). Figure 7.1 shows the simulation of a bistable firing pattern in response to an injected current ramp that should simulate apamine or 5-HT stimulation of the motoneuron as presented in figure 5 of Booth et al. (1997). The results are qualitatively identical and quantitatively within the margins of error that arise from using different integration mechanisms and spike detection algorithms.

The main properties of the model of Rybak, Shevtsova, et al. (2006) were replicated. Figures 7.2 and 7.3 illustrate the ability of the model to replicate resetting and non-resetting deletions. Resetting deletions occur when the population of rhythm generating neurons (RG-E and RG-F) are disturbed so that they stop firing in a reciprocal manner. In figure 7.2 this has been simulated by changing the drive to one side of the rhythm generating neurons. The drive to both RG pools ( $d_{rg-e/f}$ ) was set to 0.5. After the rhythmicity was established the drive to the extensor part of the rhythm generating network ( $d_{rg-e}$ ) was set to zero for four seconds. In this time period the extensor half of the excitatory rhythm generating neurons stopped firing and the flexor half started to fire tonically. Tonic and sporadic firing patterns were observed in all neurons of the pattern formation networks (PF-E/F) and in the motoneuron pools (MN-E/F). After the drive was reset to its normal value and a short initial phase the network started again to produce rhythmicity.

Figure 7.3 shows a simulated example of a non-resetting deletion. This was accomplished by changing the drive to the population of excitatory pattern formation neurons of the flexor side (PF-F) to the double of its initial value ( $d_{pf-f} = 1$ ) for four seconds. In this time the flexor pattern formation neurons started to fire tonically, the extensor pattern formation neurons fired only sporadically and the rhythm generation neurons were uninfluenced by this change and remained in their rhythmically firing state. The motoneuron pools strongly follow the behavior of the pattern formation neural pools. When the drive to the flexor pattern formation neurons was restored to its previous value ( $d_{pf-f} = 0.5$ ) they again started to fire rhythmically and assumed the rhythm phase and period from the rhythm generation networks (RG-E/-F).

The influence of relatively smaller changes to the drive of the rhythm generating neuron pools was tested in figure 7.4. Figure 7.4A and B shows equal drive values for the flexor and extensor sides. It can be observed that

## 7. RESULTS

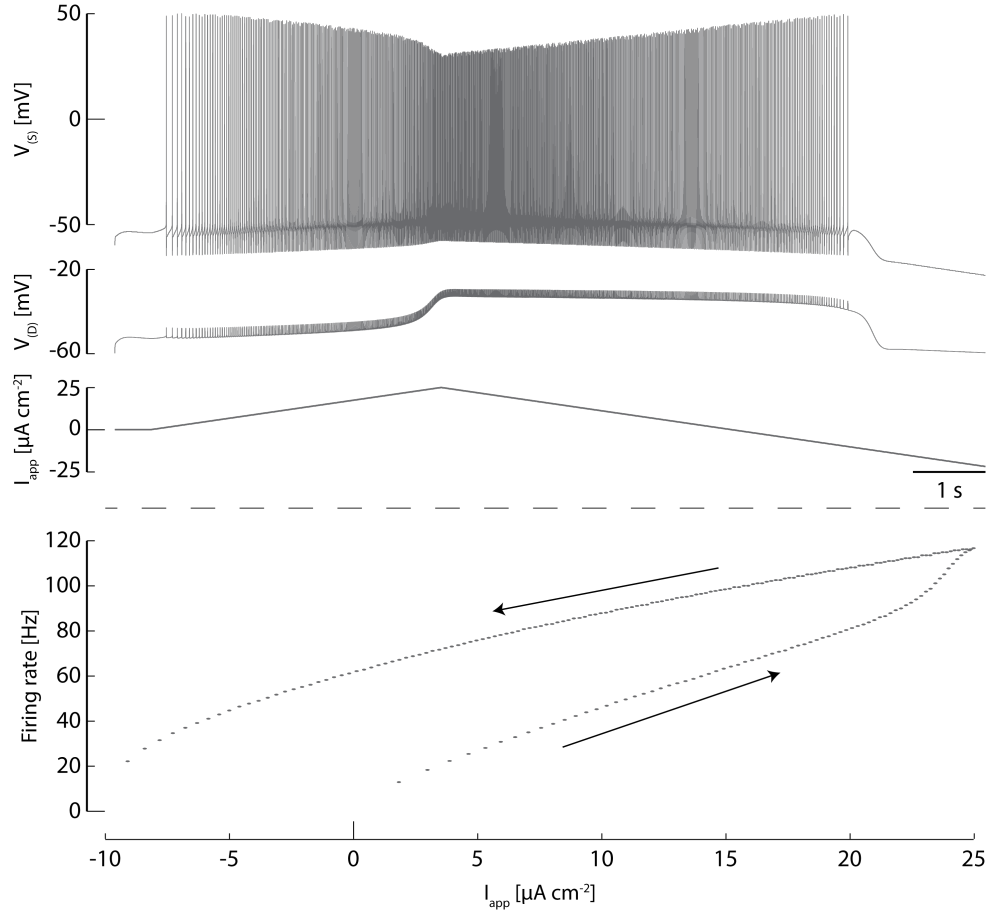


Figure 7.1: Motoneuron model under simulated influence of 5-HT or apamin. A bistable firing pattern can be observed. From to bottom: i) membrane potential of the soma and ii) dendrite in response to the iii) injected current (peak  $I_{app} = 25\mu\text{A cm}^{-2}$  reached after 4 s). Firing frequency computed depending on iv) the applied injected current  $I_{app}$ . The time course is illustrated by the arrows.  $\bar{g}_{K,Ca(S)} = 3.136 \text{ mS cm}^{-2}$ ,  $\bar{g}_{K,Ca(D)} = 0.69 \text{ mS cm}^{-2}$ ,  $E_{L(D)} = E_{L(D)} = -60.0 \text{ mV}$  and  $\bar{g}_{NaP(D)} = 0 \text{ mS cm}^{-2}$ .



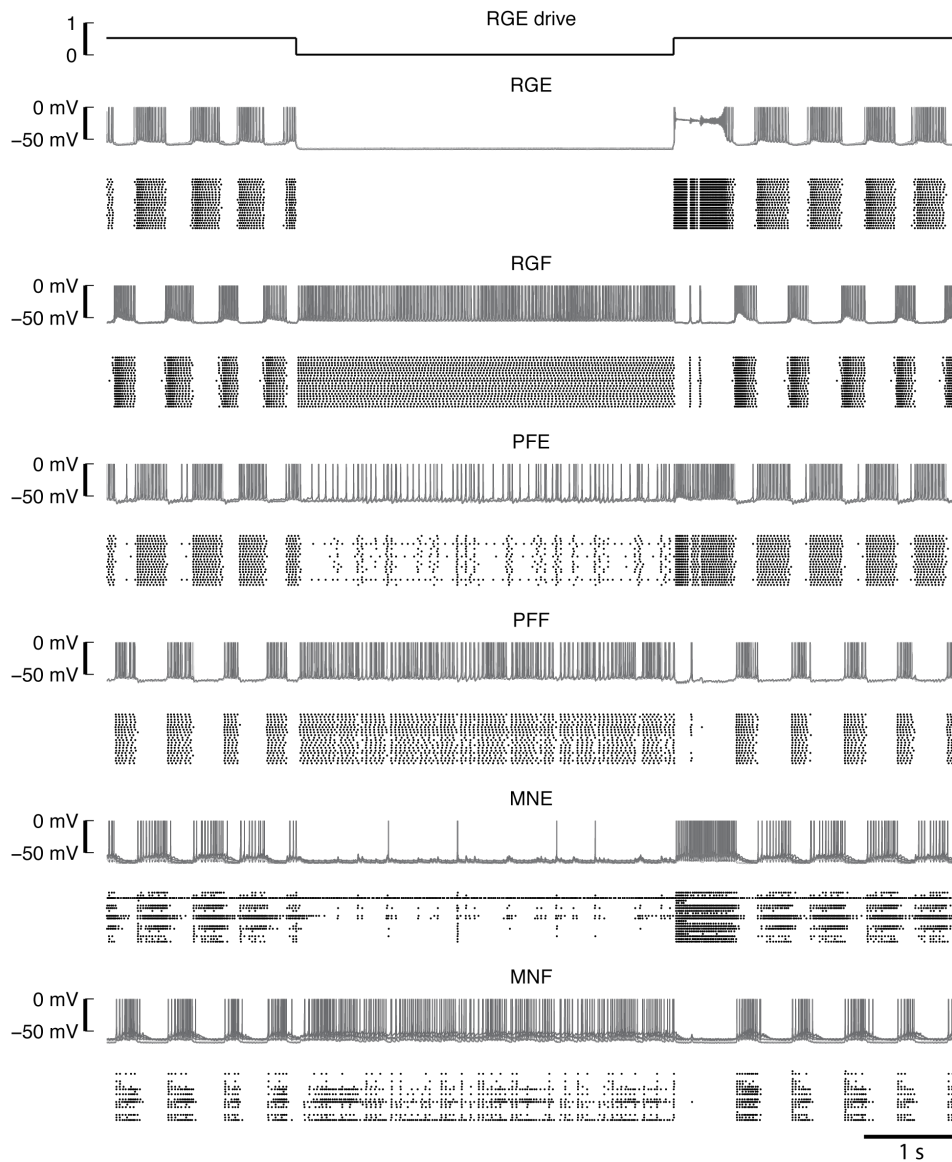


Figure 7.2: Example of the simulation of a resetting deletion. The drive to the rhythm generating neurons of the extensor half was removed for four seconds ( $d_{rg-e} = 0$ ). The established rhythm seized and was newly developed after the drive to the rhythm generating neurons was set back to 0.5, its initial value. For each population of neurons a superposition of the membrane potentials of five neurons (top) and a raster plot of the spikes (bottom) are depicted.

## 7. RESULTS

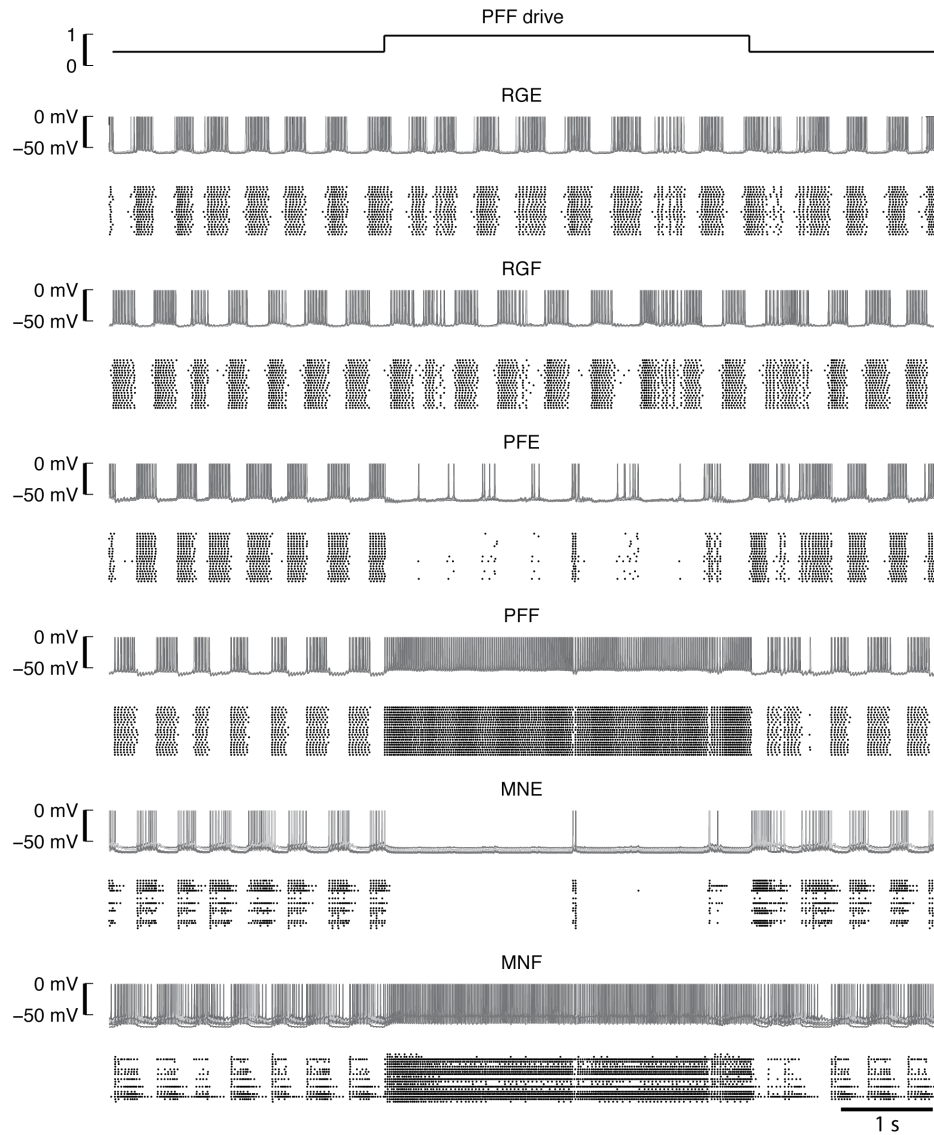


Figure 7.3: Example of the simulation of a non-resetting deletion. The drive to the pattern formation neurons of the flexor half was increased for four seconds ( $d_{p_{f-f}} = 1$ ). The established rhythm of the pattern generating network persisted but did not reach the motoneurons. After the drive to the pattern generating neurons was set back to 0.5, its initial value, the motoneurons continued to fire in a rhythmic fashion. Note that the overlap of the motoneuronal activity between flexor and extensor half is due to one highly excitable motoneuron. For each population of neurons a superposition of the membrane potentials of five neurons (top) and a raster plot of the spikes (bottom) are depicted.

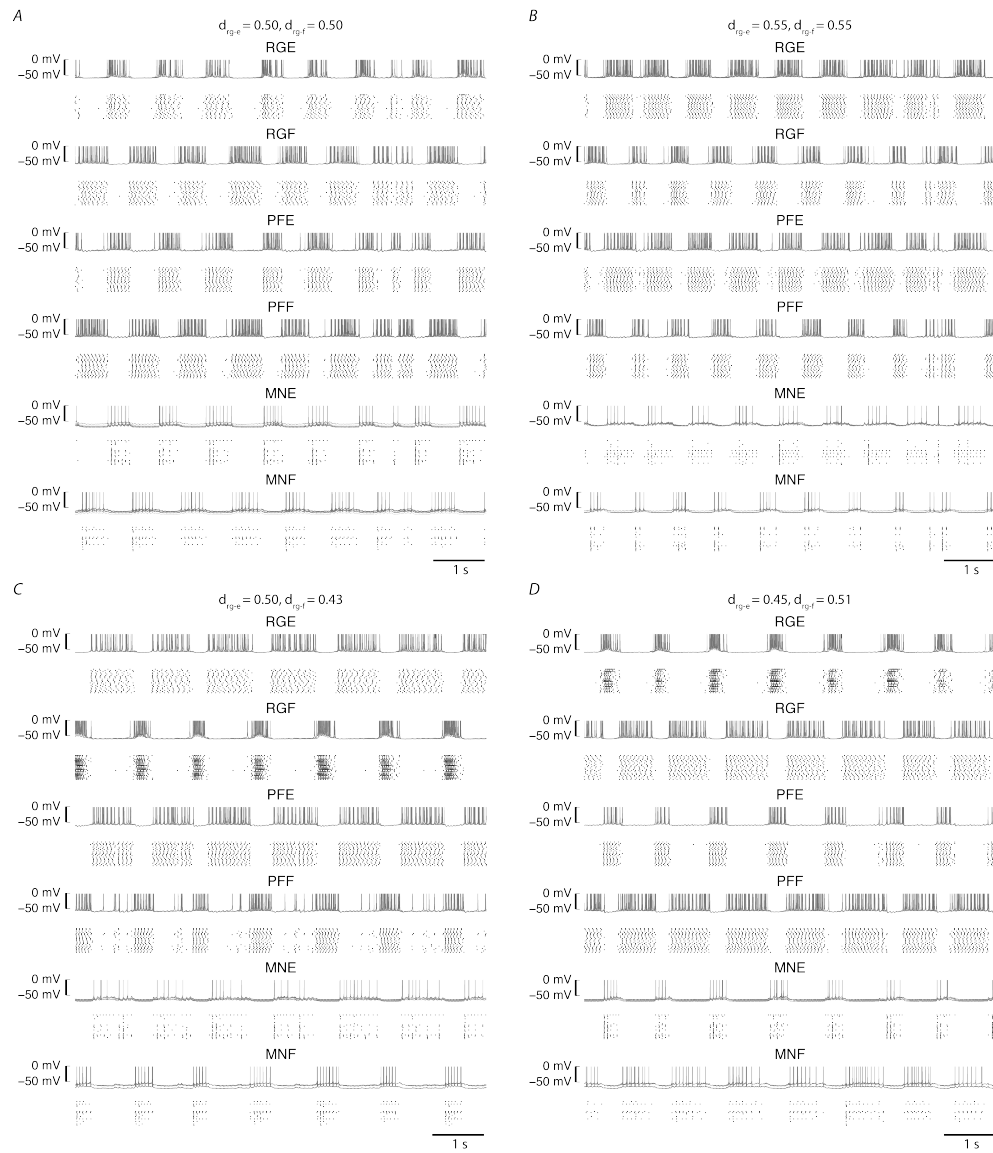


Figure 7.4: The influence of drive on the burst rate of the network's half-centers. For each population of neurons a superposition of the membrane potentials of five neurons (top) and a raster plot of the spikes (bottom) are depicted.

periods of activity were the same, for the flexor and for the extensor sides, in both cases. With the heightened value of the drive the rhythm frequency slightly increased. Furthermore, it can be seen that slight perturbation of the rhythmic activity can occur. In the lower traces of the figure, i.e. 7.4C and D, the values of the drive were changed asymmetrically, once in favor of the extensor and once of the flexor side. In both cases the side with the relatively higher value of the drive was subject to longer times of activity and shorter times of inactivity, while the reciprocity was preserved. Thus, the influence of the drive, including the ability to trigger deletions (both resetting and non-resetting) as well as the general ability of the model to produce rhythmic reciprocal activity was shown.

## 7.1 Model A

In model A the MLR drive is removed and instead pulsed stimulation of the afferent fibers was simulated by volleys of afferent spikes with a certain frequency. Such a stimulation was effective to activate the RG, PF and ultimately the motoneuron (Mn) populations to be reciprocally active in a cycle period similar to that of MLR stimulation. The effectiveness of the stimulation strongly depended on the input frequency. By varying the frequency of synchronous firing of the afferents in 5 Hz steps it can be observed that rhythmic, reciprocal activation of the flexor and extensor sides occurred with stimulation frequencies from 25 Hz–45 Hz (see figures 7.5 and 7.6). With frequencies above 45 Hz sudden, sporadic and short patterns of periodic firing can occur. These patterns were followed (and preceded) by longer tonic activation of the RG, PF and Mn populations.

The weight of the afferent input to the motoneurons ( $a_{mn-e/f}$ ) strongly influenced the behavior of the motoneuron output. Relatively higher values showed activation of the motoneurons in the silent phases of the RG and PF populations and lower values caused the motoneurons to fire seldomly. Whereas in the normal condition the motoneurons fired in the phase their side is active in and were not or sporadically (depending on their reversal potential) active in the other phase.

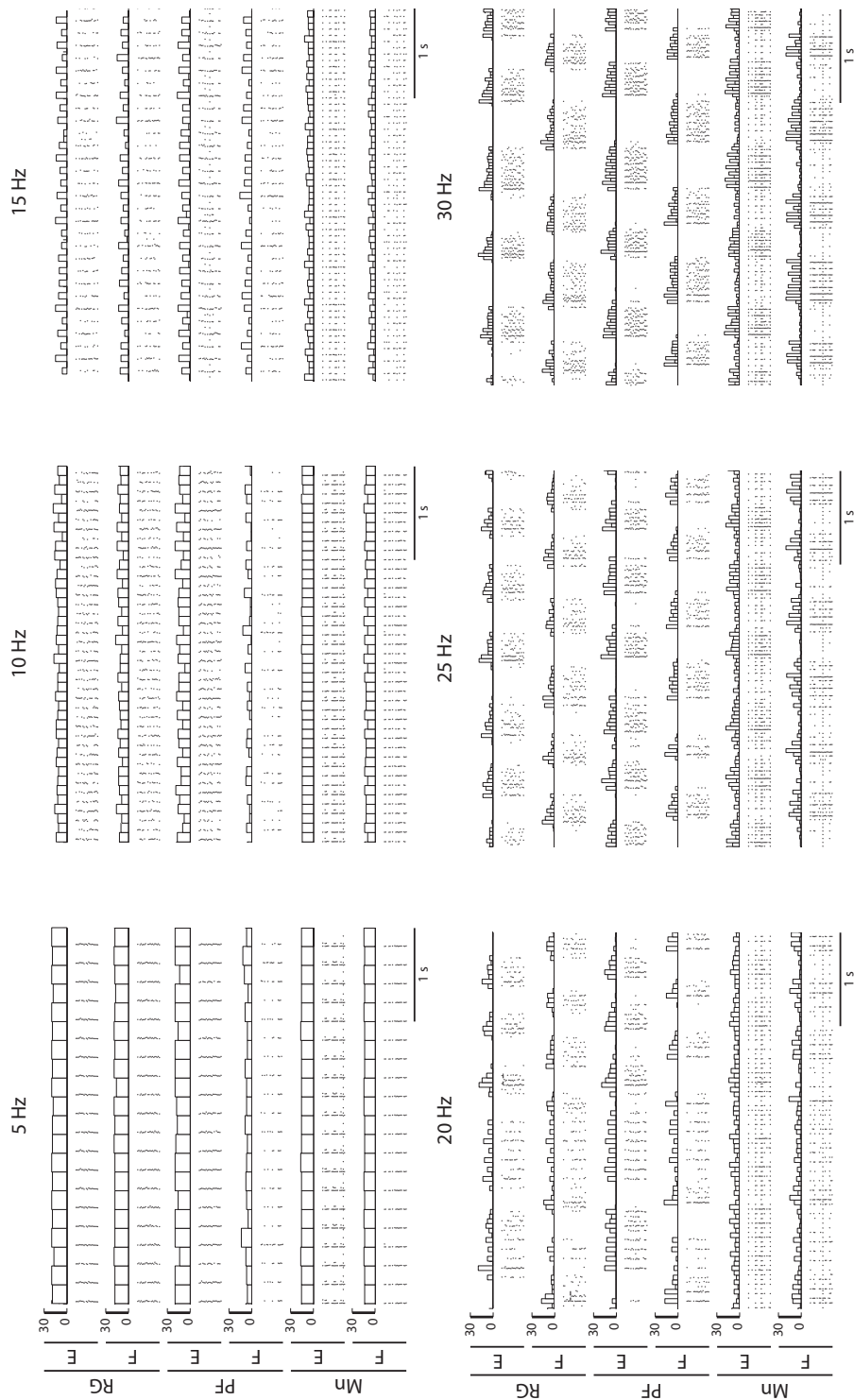


Figure 7.5: Stimulation frequencies ranging from 5 to 30 Hz with model A. Figure legend continues in figure 7.6.

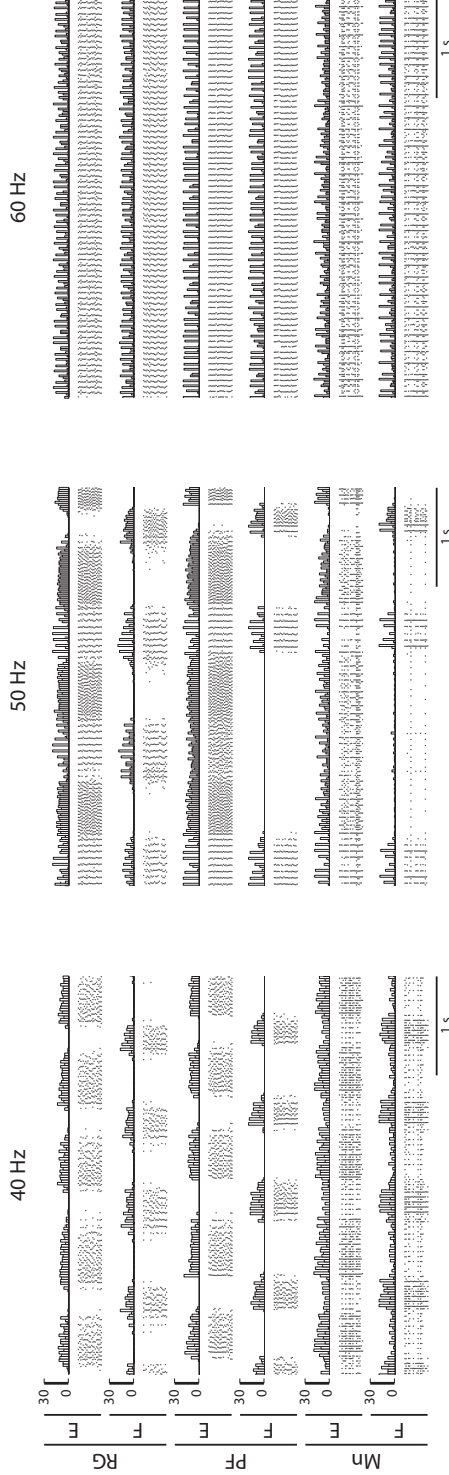


Figure 7.6: Continuation of figure 7.5 with stimulation frequencies ranging from 40 to 60 Hz using model A. For every neuron group two graphs are given i) a bar chart where every bar illustrates the recorded count of spikes in the neuron group in time bins delimited by the stimulation volleys, i.e. one time bin describes all spikes occurring between to stimulation volleys, and ii) a scatter plot of spikes where every line is a neuron belonging to the described group. The stimulation frequency is varied, while every other parameter is kept constant ( $a_{mn-e/f} = 0.75$ ). At low frequencies (< 20 Hz) it can be seen that all illustrated neurons fire stimulus time-locked to the afferent stimulation. Some motoneurons (Mn) respond to the stimulation with two spikes while others only with one. At 20 Hz stimulation frequency the RG and PF neurons start to fire in a reciprocal manner, although inconsistent, while the motoneuron pools only partially follow with fewer neurons firing in response to the stimulation in the "silent period" in comparison to the "active period". From 25 Hz to 40 Hz clear reciprocity is evident in the RG and PF neuron groups and the number of motoneurons responding is modulated this reciprocity, true "silent periods" are not reached. With 50 Hz stimulation frequency the rhythmic firing of the RG and PF populations becomes unstable and with 60 Hz all populations fire tonically. In various cases the spike count of the Mn tend to alternate between stimulation volleys, especially evident in Mn-F at 30 Hz. RG: rhythm generation and PF: pattern formation neurons, E: extensor and F: flexor side.

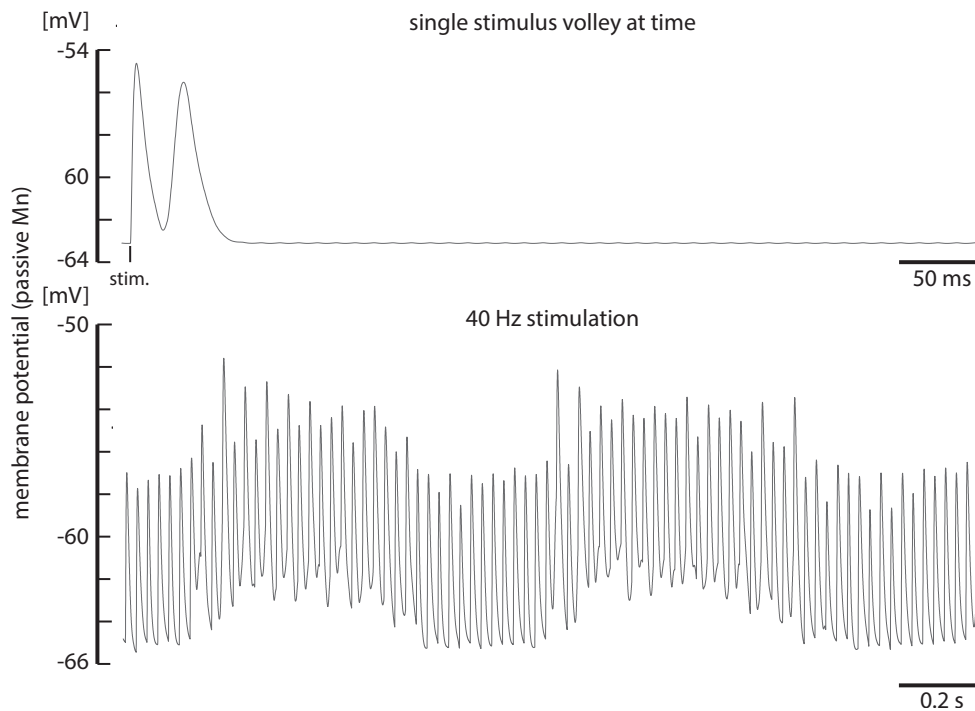


Figure 7.7: Model A: response of the membrane potential of a passive motoneuron to a single stimulation volley (top trace) and to 40 Hz repetitive stimulation (bottom trace). Both simulations were conducted with  $a_{mn-e/f} = 0.75$ . Each stimulation volley generated two peaks of the membrane potential of the passive motoneuron. One generated directly by the excitatory post synaptic potentials of the afferent input and the other by disynaptic excitatory post synaptic potentials originating from the pattern formation neuron population. Note that the lateness of the second spike was due to the time the pattern formation neurons need to generate an action potential in response to a stimulation volley. The lower trace shows the interplay of all excitatory and inhibitory mechanisms acting on the motoneurons when the network is rhythmically active. The effect of single afferent volleys on the motoneurons is rhythmically modulated.

Figure 7.7 shows a response of a passive motoneuron (i.e. without any ion channels) to a single afferent volley and to 40 Hz stimulation. It can be seen that the afferent stimulation generated large, fast, stimulus triggered changes in the membrane potential that were rhythmically modulated. This rhythmic modulation, influenced from PF, Ia and R neuron pools, was of a lower amplitude than the oscillations produced by the afferent stimulation and yet, the motoneurons might fire multiple times in response to a stimulus. Furthermore, the post-stimulus time histogram (figure 7.8) of motoneuron

## 7. RESULTS

---

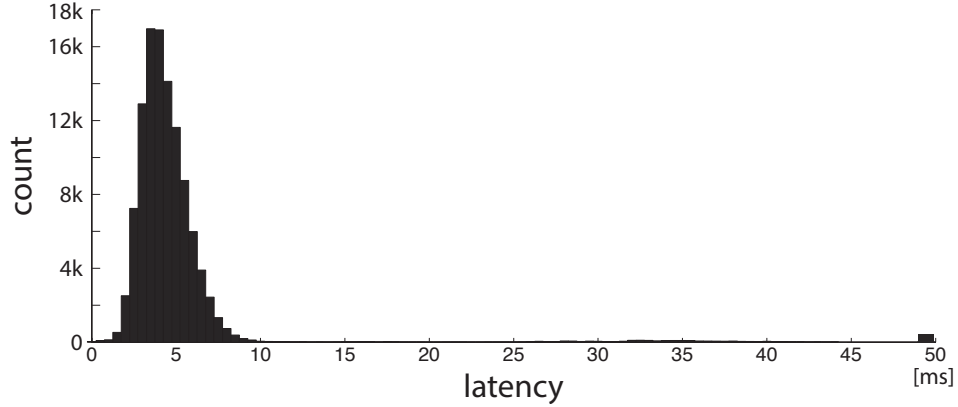


Figure 7.8: Model A: post-stimulus time histogram of motoneuron firing with stimulation frequencies of 2, 5, 10, 15, 20, 25, 30, 35, 40, 45, 50, 55 and 60 Hz and  $a_{mn-e/f} = 0.75$ . The main peak shows that action potential fired in response to excitatory post-synaptic potentials directly from afferents (median 4.2 ms, mean 5.7 ms). The second accumulation for spikes show activation in response to excitatory post-synaptic potentials from the pattern formation networks, these spikes mostly occurred with low stimulation frequencies (2 Hz and 5 Hz). Furthermore, there were spikes that were not stimulus time-locked and occurred with a latency of 50 ms and later (last bar summarizes these; stimulation frequency < 20 Hz).

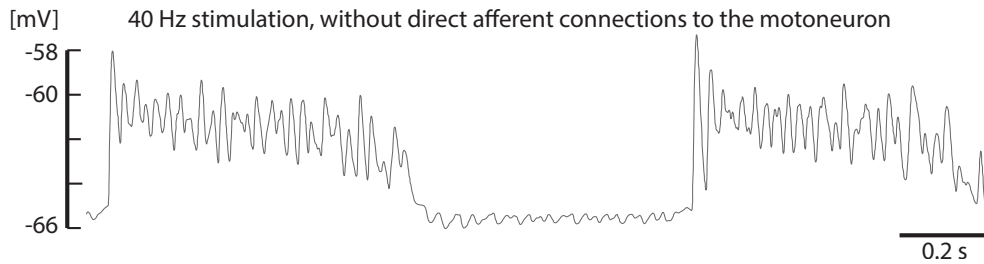


Figure 7.9: Model A: the reaction of a passive motoneuron to afferent stimulation (40 Hz) only of the rhythm generation (RG) and pattern formation (PF) networks but not to the motoneurons itself. In comparison to the passive motoneuron with afferent synapses modeled (see figure 7.7) the amount of depolarization was much smaller, there was no clear stimulus time-locked depolarization and in the ‘silent periods’ no depolarization was occurring.



spikes in response to the frequency range of 2 Hz–60 Hz show that most motoneurons fire within 10 ms after the stimulation volley; mean latency is 5.7 ms (median 4.2 ms). There is an accumulation of action potentials occurring at around 35 ms post stimulus.

When afferent stimulation to the motoneurons was removed fewer spikes were elicited in the motoneurons with no clear stimulus time relation. Figure 7.9 shows the membrane potential of a passive motoneuron only influenced by the PF, Ia and R neural populations and without afferent excitatory postsynaptic potentials under 40 Hz stimulation. Clear phases of depolarization can be observed, the amount of depolarization was clearly reduced in comparison to the one with afferent influence (see figure 7.7). The sum of the total occurring spikes in the 40 neurons comprising the two motoneuron pools during 20 s simulations for each, 2, 5, 10, 15, 20, 25, 30, 35, 40, 45, 50, 55 and 60 Hz afferent stimulation was 21,331 and 118,838 for the simulations without and with afferent input to the motoneurons. Thus, without afferent stimulation to the motoneurons only 17.9% of the counts of spikes with afferent stimulation to the motoneurons were elicited in the motoneuron pools.

## 7.2 Model B

Model B builds upon model A and introduces presynaptic inhibition that is rhythmically modulated and gates the afferent input to the motoneurons. The rhythmic modulation originates from the PF motoneuron groups. This presynaptic gating mechanism suppresses the afferent input in the phase where the corresponding side is in its inactive phase and allows the full afferent effect on the motoneurons in the active phase. This allowed for higher values of  $a_{mn-e/f}$  while still allowing for a true ‘silent period’ thus resulting in two main effects i) the synchronicity of the motoneuron firing was increased, i.e. the mean latency of action potentials was reduced as well as its standard deviation and ii) the “silent period” was retained without motoneuron firing. Figure 7.10 shows the models response to 40 Hz stimulation. The membrane potential changes of a passive motoneuron for each side (flexor and extensor) in a 2 seconds window of figure 7.10 are illustrated in figure 7.11. Furthermore, figure 7.12 shows a post-stimulus time histogram of motoneuron firing.

## 7.3 Model C

Model C builds upon model B and added the phase dependent disinhibition of an alternative pathway from the afferent input to the motoneuron on the flexor side. The results are presented in two figures, figure 7.13 shows the effect of the simulation on passive motoneurons on both, the extensor and flexor sides, under continuous 25 Hz afferent stimulation and figure 7.14 illustrates post-stimulus time histograms of motoneuron firing in response to afferent

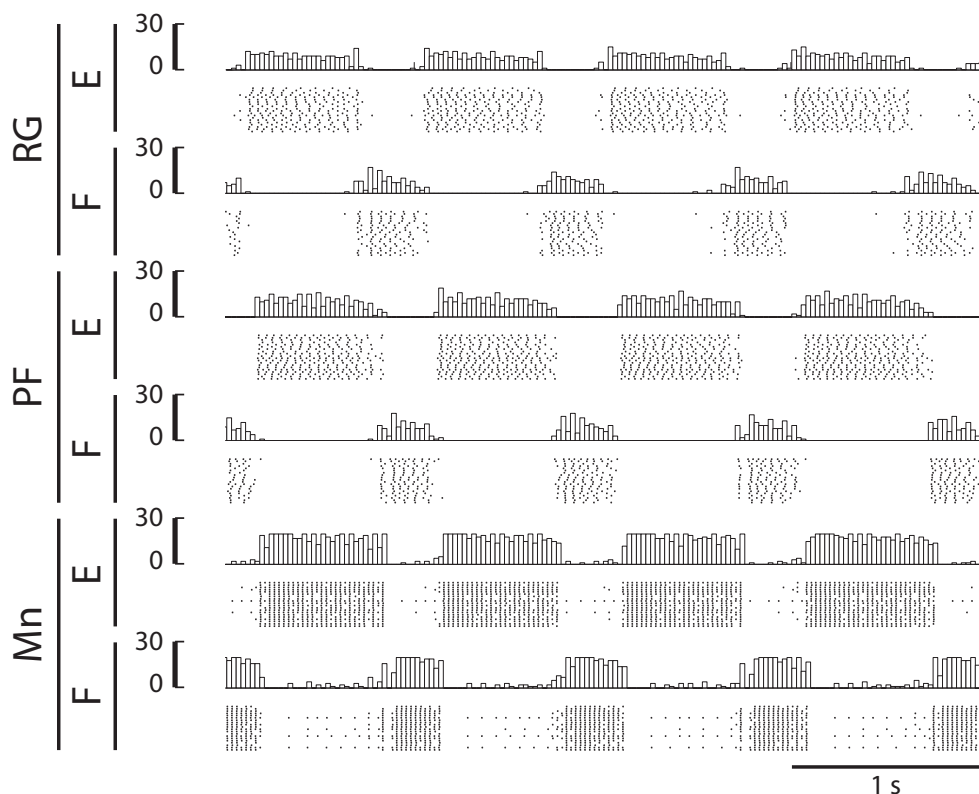


Figure 7.10: Model B: response to 40 Hz continuous afferent stimulation. Rhythmicity was produced similarly as in model A. The influence of the presynaptic inhibition on the afferents can be seen in the motoneuron’s firing patterns. During their “active phase” almost all motoneurons fired while very few were active during the ‘silent period’ of the respective side. RG: rhythm generation, PF: pattern formation and Mn: motoneuron pools. E: extensor and F: flexor side.

stimulation of different frequencies. The model exhibited following behavior, under low frequencies (i.e.  $< 15$  Hz) only the monosynaptic pathway from the afferents to the motoneurons was active, thus only short latency responses (i.e. latencies similar to those of model B) occurred both on the extensor and on the flexor side. When the frequency was increased the inhibiting influence of the CPG to the InPath motoneuron pool became stronger, thus disinhibiting the alternative pathway. This had the consequence of increasing the latency of the spikes occurring in the motoneuron pools of the flexor side in response to the afferent stimulation. Under these frequencies only the flexor side was influenced and the extensor side retained the same, low latency spike patterns of the motoneuron pools. The spike latencies were not only later but also

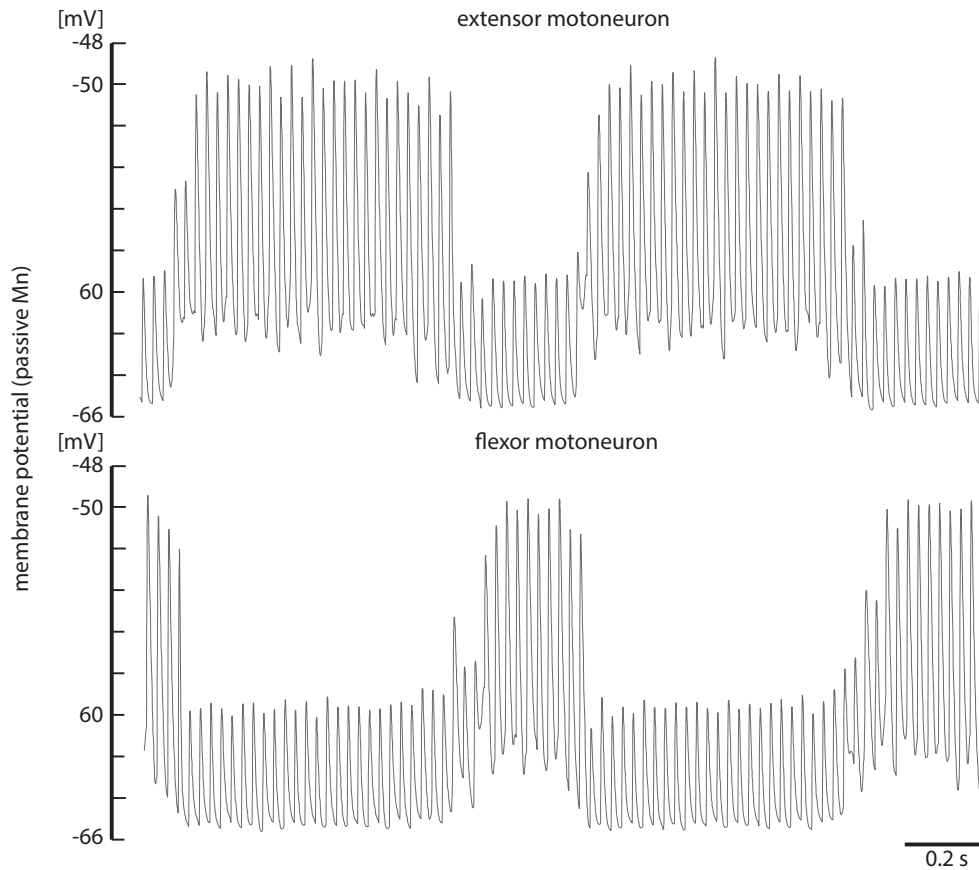


Figure 7.11: Model B: passive motoneurons of the flexor and extensor sides under 40 Hz continuous afferent stimulation and the network currently being in a rhythmic state. The top trace shows a passive motoneuron in the extensor and the bottom trace in the flexor motoneuron pool. The afferent stimulation volleys were the main visible influence on the membrane potential. They were offset, modulated by the excitatory influence of the pattern generator networks, from the pattern formation neuron pools and from reciprocal and recurrent inhibition of the Ia and Renshaw interneuronal pools. During the ‘silent period’ or phase of inactivity of the respective side the influence from the presynaptic inhibition can be seen. The afferent volleys generated smaller compound effects on the passive membrane potential, since their individual excitatory post synaptic potentials were reduced in size by the presynaptic inhibition. Furthermore, when compared to model B (see figure 7.7) the maximal depolarization during the ‘active phase’ was increased while the maximal depolarization during the ‘silent period’ was lowered.

## 7. RESULTS

---

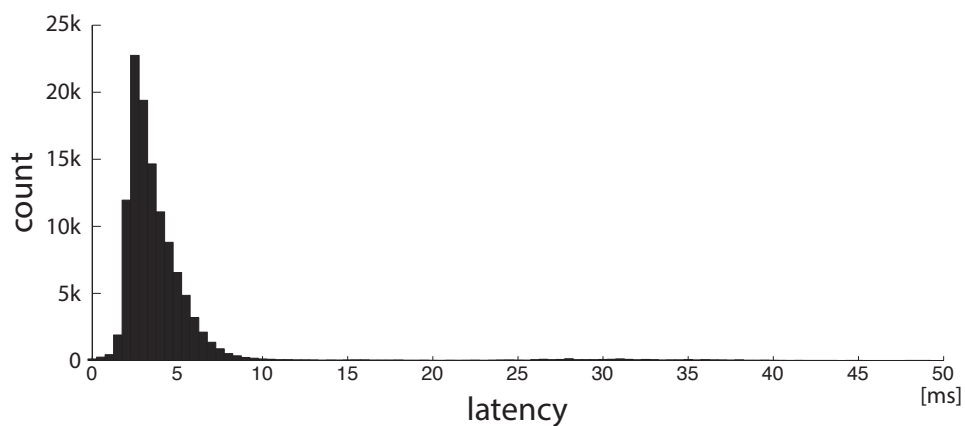


Figure 7.12: Model B: post-stimulus time histogram of motoneuron firing with stimulation frequencies of 2, 5, 10, 15, 20, 25, 30, 35, 40, 45, 50, 55 and 60 Hz. The mean latency was 4.2 ms with a standard deviation of 4.4 ms and a median of 3.3 ms. The spike timing was more synchronous than in model A (see figure 7.8), of shorter latency and with fewer long latency responses.

more spread when the alternative pathway was active. With the help of the illustration of the membrane potential of the passive motoneurons it can be seen that the stimulus time-locked effect of the afferent stimulation was less focused, later and longer on the flexor side with active alternative pathway than on the extensor side (see figure 7.14).

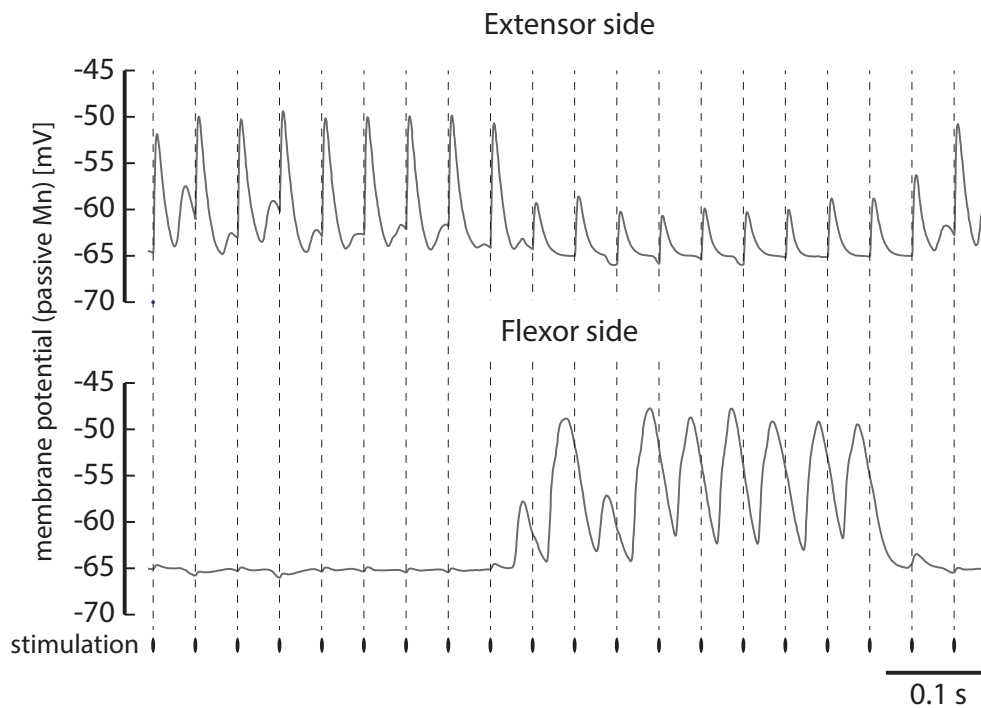


Figure 7.13: Model C: passive motoneuron under 25 Hz stimulation. The volleys of afferent input were affecting the passive motoneurons in a stimulus time-locked manner. On the extensor side, similar to the previous models, the main influence appeared immediately after the stimulation (dashed lines), whereas on the flexor side the deflections due to the afferent stimulation occurred later after the respective stimulation pulse, but still in a time-locked manner.

## 7. RESULTS

---

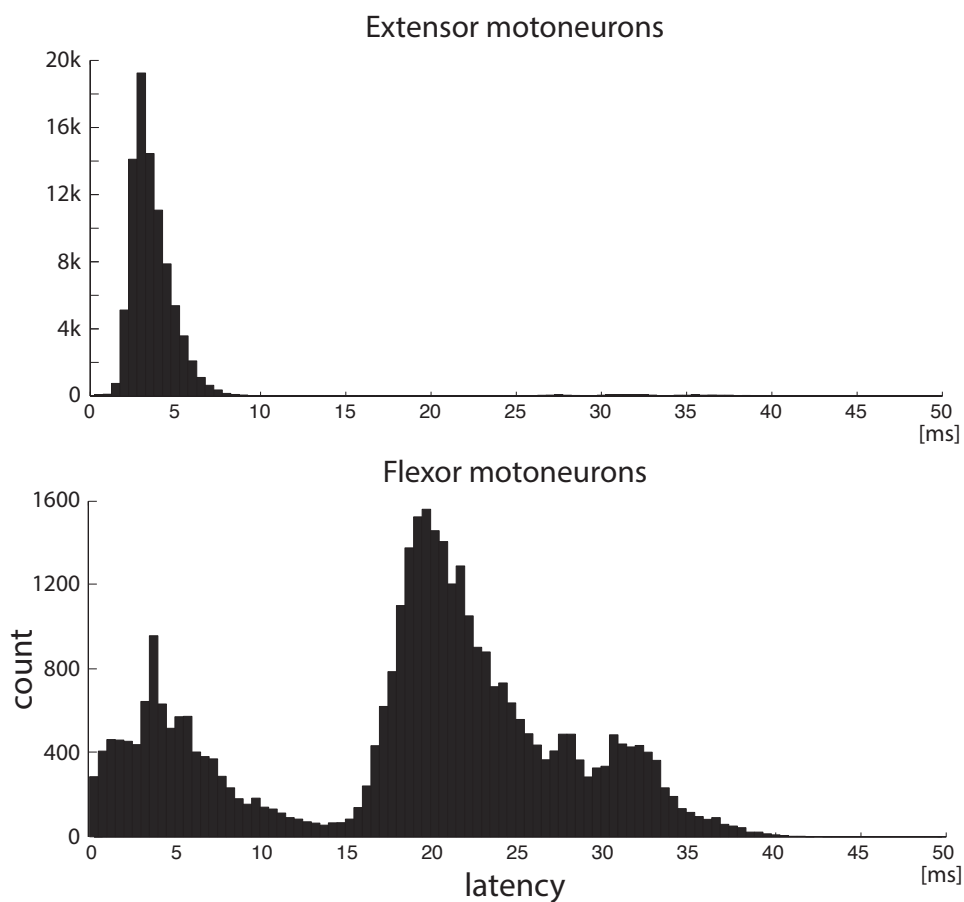


Figure 7.14: Model C: post-stimulus time histogram of extensor and flexor motor pools during stimulation frequencies of 2, 5, 10, 15, 20, 25, 30, 35, 40, 45, 50, 55 and 60 Hz. The distribution of spike latencies on the extensor side was similar to that of model B. The flexor side, on the other hand, had two peaks, an early one and a late one. The latter was due to the alternative pathway and peaked around 20 ms. The former had two origins partially the spikes occurred early at low stimulation frequencies over the monosynaptic afferent pathway and partially the spikes were elicited in response to the previous stimulation pulse, when the latency was longer than the post-stimulus time window (occurred mainly during high frequency afferent stimulation, i.e. > 30 Hz).

## Chapter Eight

---

### *Discussion*

The presented computer simulation modeled the effect of epidural posterior root (afferent) stimulation of the human lumbar spinal cord segments at different frequencies on the modulation of the stimulus time-locked CMAP responses. This was accomplished by translating a well established CPG model of the mammalian spinal cord (Rybak, Shevtsova, et al., 2006). This model consisted of several populations of neurons with Hodgkin and Huxley (1952)-like membrane dynamics and a two level CPG as well as first-order interneurons. To model the lumbar locomotor pattern generating circuits of motor complete spinal cord injured people under afferent stimulation involved the introduction of pulsed afferent input, phasic presynaptic inhibition and state-dependent disinhibition of an additional, polysynaptic pathway of the afferents to the motoneurons.

Following results were found. Pulsed stimulation can activate the pattern generating centers. This activation of the pattern generating circuits to generate rhythmicity is frequency dependent, occurs only after a certain threshold frequency and diminishes again when stimulation frequency is increase over another threshold. Rhythmic activity can be produced by non-bursting neurons, i.e. the excitatory interneurons could be presumably of bursting or non-bursting nature. In the presented simulation the excitatory interneurons of the rhythm and pattern formation network were firing with the same frequency as the input and a certain probability to skip a response to a stimulation volley. Stimulus-coupled responses as the only components comprising the rhythmic activity were explained by the interneuronal network is mainly exerting subthreshold modifications to the motoneurons membrane potential when activated by pulsed epidural stimulation, thus only modifying their excitability. In the extension half-center, direct afferent connections play a dominant role in exciting motoneurons as suggested by constant CMAP latencies. The existence of a mono- and a separate oligosynaptic pathway with presynaptic inhibition of the afferent fibers to the flexor motoneurons explained the substitution of the short latency CMAPs by prolonged ones. Furthermore, phasic presynaptic inhibition was shown to play a major role in reducing the motoneuron pool activity in the inactivity periods of the respective side while retaining and/or allowing for very synchronized, short latency responses of the motoneurons in response to the afferent volleys when the side is active.

The model from Rybak, Shevtsova, et al. (2006) represents to-date one of

the most detailed models of the mammalian CPG. It is accepted and was used here as a basis to model the influence of epidural spinal cord stimulation of different frequencies to the human spinal cord motor networks. The reimplementation was thoroughly tested and has been shown to reproduce, although with some minor deviations, the main model features.

A slowly inactivating (persistent) sodium current was modeled into the interneurons and motoneurons involved in pattern generation, because there exists indirect evidence for its involvement in rhythm genesis (McCrea & Rybak, 2008). Such sodium currents have been found in spinal interneurons and motoneurons (e.g., R. H. Lee & Heckman, 2001, Darbon, Yvon, Legrand, & Streit, 2004, Streit, Tschertter, & Darbon, 2005, Brocard, Tazerart, Viermari, Darbon, & Vinay, 2006, Dai & Jordan, 2006, Theiss, Kuo, & Heckman, 2007 after McCrea & Rybak, 2007), and their blockade abolishes the intrinsic cellular oscillations and rhythm generation in cultured rat spinal cord neurons (Darbon et al., 2004, Streit et al., 2005 after McCrea & Rybak, 2007). Furthermore, there is evidence of the existence of persistent sodium currents in subicular neurons in man (Vreugdenhil, Hoogland, van Veelen, & Wadman, 2004) and tuberomammillary neurons (Taddese & Bean, 2002). Recently Brocard, Shevtsova, et al. (2013) presented a concept of locomotor rhythm generation in the neonatal rodent rat in which persistent sodium current-dependent pacemaker properties are switched on and modified by activity dependent changes of extracellular  $\text{Ca}^{2+}$  and  $\text{K}^{+}$  concentration changes. Nonetheless, there is no conclusive evidence of such a current being part of excitatory interneurons of the CPG in man. The persistent sodium current, thus was hypothesized to be the main source of rhythm genesis and all results, except the frequency dependence of the functional activation of the rhythm and pattern generating networks do not depend on this assumption. Any other source of rhythm genesis would equally well describe all other findings as long as its influence upon the motoneurons is with a similar amount of excitation and inhibition.

The results of replacing the constant MLR drive with pulsed volleys of afferent spikes with different frequencies to the rhythm and pattern generating networks, showed a clear frequency dependence. Rhythmic firing is produced only with frequencies above 20 Hz, which is in accordance with the data of part I and the literature (Dimitrijevic et al., 1998b; Minassian, Gilge, et al., 2004; Minassian, Persy, Rattay, Pinter, et al., 2007). This matching frequency dependence of the functional activation of the rhythm and pattern generating networks to produce rhythmicity suggests that slowly-inactivating persistent sodium currents might be the source of rhythm genesis also in man. Furthermore, low frequency stimulation (below 20 Hz) produces tonic output, i.e. the count of motoneuron spikes per stimulation volley is not rhythmically modulated and remains rather constant. This has been also observed in human measurements, where stimulation frequencies of the range 5 Hz–16 Hz produce tonic CMAP modulations of the motor nuclei outputs that functionally induces the extension of the lower limbs (Gilge, Minassian, Rattay, Pinter,



---

et al., 2004). Similarly, the phenomenon that under 5 Hz afferent stimulation almost the same number of motoneurons fire in response to a stimulation volley while with gradually higher stimulation frequencies the response patterns become less stable has also been observed in measurements of motor complete spinal cord injury patients during epidural afferent stimulation (Danner, Rattay, et al., 2011; Danner, Hofstoetter, Minassian, et al., 2012). Furthermore, simple alternating patterns of high and low counts of motoneurons firing in one pool to individual consecutive afferent stimulation volleys were observed in the model output as well as in human measurements (Hofstoetter, 2009; Danner, Hofstoetter, Minassian, et al., 2012). The latter two phenomena were not explicitly modeled but emerged from the set of posed model assumptions.

The model incorporates the assumption that the output is predominately stimulus time-locked to the afferent stimulation and that the sum of the excitatory (from PF-E/F) and inhibitory (from R and Ia) input is modulating the amount of motoneurons firing in response to the afferent stimulation and is itself not the direct cause of action potential generation in the motoneurons (Degtyarenko et al., 1998; Kinoshita & Yamaguchi, 2001; Noga et al., 2003). The simulations have shown that a clear stimulus time relation between the afferent volleys and the motoneuron firing is evident by synchronous afferent stimulation even when the interneurons would, without afferent stimulation, excite the motoneurons themselves. In this case the afferent input was relatively stronger and directly induced action potentials in the motoneurons that afterwards became refractory, and thus the sum of the interneuronal effects was reduced to being modulatory. This result reveals that the assumption of subthreshold manipulation of the motoneurons' membrane potentials was too strong. To produce the observed results of human measurements it is sufficient that the excitatory influence of the interneurons on the motoneurons is comparably small to the afferent input acting upon the motoneurons.

The investigation of presynaptic inhibition that is phasically modulated (Nusbaum et al., 1999; Gosgnach et al., 2000; Rudomin & Schmidt, 1999) showed that rhythmic presynaptic inhibition allows for very synchronous activation of the motoneurons in response to afferent volleys while concomitantly reducing the activity in the 'silent periods'. Similar effects would be conceivable without presynaptic but with strong reciprocal Ia inhibition, but since there are evidences for both mechanisms it is more probable to hypothesize that they synergistically produce the necessary inhibition during the phases when the respective motoneurons are inactive. At the very least, rhythmic presynaptic inhibition was shown to widen the range of input intensities to the afferents that would produce reciprocal, alternating activity and inactivity phases of the motoneuron pools when the rhythm and pattern generating networks are active.

An essential difference to previous models of the mammalian CPG (Rybak, Shevtsova, et al., 2006; Rybak, Stecina, et al., 2006; Markin et al., 2010; Zhong, Shevtsova, Rybak, & Harris-Warrick, 2012) is the inclusion of axonal

delays. Connection delays can strongly influence network dynamics (Izhikevich, 2006). Furthermore, the experimental results this model based on deeply rely on the synchronicity of the input and thus delays are subject to play a very important role (e.g. delayed responses from the flexor muscles cannot be modeled without the addition of delays, and there is also evidence that the frequency dependency of the responses rely on the delay of the axons Jilge, Minassian, Rattay, & Dimitrijevic, 2004). An action potential of a neuron will generate a post synaptic potential on every synaptically connected neuron that is delayed by a certain amount and thus the introduction of the delays was necessary.

The model successfully demonstrated that an asymmetric organization of the reflex pathways that is modified, disinhibited depending on the state of the pattern formation networks viably reproduces the observation of prolonged latency reflex responses when the flexion side is active during CPG activity induced by pulsed afferent stimulation. Recently the idea of an asymmetric organization of the locomotor rhythm and/or pattern generating networks was revisited and differences between flexor and extensor side of the networks were suggested (Brownstone & Wilson, 2008; Duysens, De Groote, & Jonkers, 2013). McCrea and Rybak (2008) proposed that asymmetries of the CPG architecture most likely will involve the pattern formation and not the rhythm generation networks. S. Dietz, Shevtsova, Rybak, and Harris-Warrick (2013) suggest that the asymmetries are located in the rhythm generation layer. In the here presented model the asymmetries are hierarchically lower and are limited to the reflex pathways. It remains to be clarified whether there are similar circuits on the extensor side, since long latency responses were also recorded during the extension phase (see part I). It is not clear whether these were recorded due to imperfect classification of the phases, since all recorded muscle groups that are responsible for extension also include flexor muscles. The phenomenon seen in part I that there are cases where flexor muscle groups show tonically rather than rhythmically prolonged responses might be explained by a malfunction in the cessation of the disinhibition.

## 8.1 Conclusion

A first model of central locomotor rhythm and pattern generating networks in the lumbar spinal cord has been presented that reproduces numerous properties seen in measurements of humans with motor complete spinal cord injury under epidural posterior root stimulation. Stimulus time-locked responses were explained by relatively strong and highly synchronized depolarization of the motoneurons by the excitatory post synaptic potentials originating from afferents and relatively smaller depolarization due to the interneurons of the pattern formation networks. The main role of the interneurons was the modulation of the motoneuron excitability in response to the afferent stimulation.

The activation of the rhythm and pattern generating model was shown to be frequency dependent. Slowly-inactivating persistent sodium currents have been shown to be a viable candidate of rhythm genesis in the human lumbar cord. The role of presynaptic inhibition was investigated and an asymmetric model was proposed. Unraveling some of the tentative components of the human lumbar cord networks not only answered several questions but raised many more that previously could not have been posed.

## 8.2 Model limitations

The model presented here bases on the model by Rybak, Shevtsova, et al. (2006). Even after multiply crosschecking all parameters the behavior of the in the text presented model differs from the reference. Rybak, Shevtsova, et al. (2006) misses a clarification of how action potentials were detected and the INRG neuron population is intrinsically firing when replicated as presented in the text, even when the presumably missing negative sign of the leakage reversal potential was introduced. Following the illustrations in Rybak, Shevtsova, et al. (2006) these neurons should not fire if there is no input. The detection of action potentials greatly influences the amount of excitatory and inhibitory post-synaptic potentials generated. Especially, regarding the RG neural population that has a low maximal potassium conductance and is easily put into a resonating state, where depending on the detection algorithm bursts of spikes or even no spikes at all are detected. The maximal sodium conductance was increased for models A–C which removes the resonating property of the RG and PF neurons (Zhong et al., 2012). The MLR drive was modeled to include excitatory as well as inhibitory components instead of only excitatory ones. Nonetheless, model results suggest that the overall behavior can be replicated. Rhythmicity is generated through MLR input, asymmetric input lengthens the active period of the side with more input and shortens the active period of the other side and the two-layer CPG model can exhibit resetting as well as non-resetting deletions when introducing perturbation to one side of the PF or RG neuron populations.

Furthermore, there is evidence of tonic presynaptic inhibition, i.e. not influenced by the the CPG, that operates with three or more synapses, but has not been modeled here (Rudomin, 1990; Rudomin, Quevedo, & Eguibar, 1993; Rudomin & Schmidt, 1999; Rudomin, 2009; Hochman, Shreckengost, Kimura, & Quevedo, 2010). The underlying assumption is that tonic presynaptic inhibition is activated shortly after the first afferent volley arrived at the motoneuron and then reaches a plateau and has a constant influence on the post-synaptic potentials arriving through the Ia afferents at the motoneurons. Thus, under this assumption, the modeled afferent input can be seen as already affected by the tonic afferent stimulation and it is assumed that when investigating afferent input of sufficiently high frequency the effect is

negligible.

The structure and organization of the lumbar neural network involved in rhythm generation as well as the involved ion-channels are largely unknown for the human or even generally for vertebrates. Here, I followed the assumptions made by Rybak, Shevtsova, et al. (2006). Slowly inactivating, persistent sodium channels were assumed—in the interplay with a half-center organization—to be the source of rhythm genesis and the two-layer organization was preserved. In order to assess the generation stimulus time-locked rhythmically modulated responses, the influence of presynaptic inhibition and the involvement of disinhibition in prolonging the response latencies in a phase depending manner, the source of the rhythm genesis is not of importance. The modeled mechanism is activated in dependence of the phase the rhythm generating process is in and is not depending on any assumptions of their origin. On the other hand, the influence of the stimulation frequency on the rhythm generation is very much depending on these assumptions and can only be seen in the light of the specific implementation of the rhythm generating process. Nonetheless, the results of the model show the same preferred input frequencies as seen in human electrophysiological recordings (see part I; Dimitrijevic et al., 1998b; Minassian, Gilge, et al., 2004).

Moreover, the modeled interneurons are reacting rather slow to volleys of synchronized stimulation. The disinhibition of the alternative pathway that introduces two additional interneurons between the afferents and the motoneurons prolonged the latency by over 15 ms, while electrophysiological studies showed that the post synaptic potentials of disynaptic Ia reciprocal inhibition (one additional interneuron in comparison to the monosynaptic pathway of the afferents to the motoneurons) arrive only about 0.8 ms later to the motoneurons than those of the monosynaptic afferent synapses (Matthews, 1972; Pierrot-Desseilligny & Burke, 2005). This is a substantial difference that is caused by the ion channel configuration of the chosen interneurons. Due to the importance of spike timing no connections of the afferents to the Ia inhibitory interneurons were modeled, thus there is no disynaptic reciprocal inhibition in the model. Furthermore, interpretations of results depending on the spike-timing of interneurons need to be made under consideration of this limitation. Nonetheless, the disinhibition resulted in the observed prolonged latencies with the mere difference being in absolute numbers, thus the overall interpretation is not limited.

---

## Bibliography

- Akaike, H. (1974). A new look at the statistical model identification. *IEEE Transactions on Automatic Control*, *19*(6), 716–723. (Cit. on p. 12).
- Armstrong, D. (1988). The supraspinal control of mammalian locomotion. *The Journal of Physiology*, *405*, 1–37. (Cit. on p. 49).
- Barthélemy, D., Leblond, H., & Rossignol, S. (2007). Characteristics and mechanisms of locomotion induced by intraspinal microstimulation and dorsal root stimulation in spinal cats. *Journal of Neurophysiology*, *97*(3), 1986–2000. (Cit. on p. 56).
- Beres-Jones, J. A. & Harkema, S. J. (2004). The human spinal cord interprets velocity-dependent afferent input during stepping. *Brain*, *127*(10), 2232–2246. (Cit. on p. 49).
- Booth, V., Rinzel, J., & Kiehn, O. (1997). Compartmental model of vertebrate motoneurons for Ca<sup>2+</sup>-dependent spiking and plateau potentials under pharmacological treatment. *Journal of Neurophysiology*, *78*(6), 3371–3385. (Cit. on pp. 63–65, 74, 77).
- Brocard, F., Shevtsova, N. A., Bouhadfane, M., Tazerart, S., Heinemann, U., Rybak, I. A., & Vinay, L. (2013). Activity-dependent changes in extracellular Ca<sup>2+</sup> and K<sup>+</sup> reveal pacemakers in the spinal locomotor-related network. *Neuron*, *77*(6), 1047–1054. (Cit. on p. 94).
- Brocard, F., Tazerart, S., Viermari, J. C., Darbon, P., & Vinay, L. (2006). Persistent sodium inward current (INaP) in the neonatal rat lumbar spinal cord and its contribution to locomotor pattern generation. In *Society for Neuroscience Abstracts* (p. 252.16). (Cit. on p. 94).
- Brown, T. G. (1911). The intrinsic factors in the act of progression in the mammal. *Proceedings of the Royal Society of London. Series B, Containing Papers of a Biological Character*, *84*, 308–319. (Cit. on pp. 56, 68).
- Brown, T. G. (1914). On the nature of the fundamental activity of the nervous centres; together with an analysis of the conditioning of rhythmic activity in progression, and a theory of the evolution of function in the nervous system. *Journal of Physiology*, *48*, 18–46. (Cit. on pp. 3, 56, 68).
- Brownstone, R. M. & Wilson, J. M. (2008). Strategies for delineating spinal locomotor rhythm-generating networks and the possible role of Hb9 interneurons in rhythmogenesis. *Brain Research Reviews*, *57*(1), 64–76. (Cit. on p. 96).

- Burnham, K. P. & Anderson, D. R. (2002). *Model selection and multimodel inference: a practical information-theoretic approach* (2nd ed). New York: Springer. (Cit. on pp. 14, 15).
- Bussel, B., Roby-Brami, A., Azouvi, P., Biraben, A., Yakovleff, A., & Held, J. P. (1988). Myoclonus in a patient with spinal cord transection. *Brain*, *111*(5), 1235–1245. (Cit. on p. 56).
- Calabrese, R. L. & Prinz, A. A. (2010). Realistic modeling of small neuronal networks. In E. De Shutter (Ed.), *Computational modeling methods for neuroscientists* (pp. 285–316). Cambridge, MA: MIT Press. (Cit. on pp. 60, 62, 63).
- Calancie, B. (2006). Spinal myoclonus after spinal cord injury. *The Journal of Spinal Cord Medicine*, *29*(4), 413–424. (Cit. on pp. 44, 56).
- Calancie, B., Needham-Shropshire, B., Jacobs, P., Willer, K., Zych, G., & Green, B. A. (1994). Involuntary stepping after chronic spinal cord injury. *Brain*, *117*(5), 1143–1159. (Cit. on pp. 44, 56).
- Dai, Y. & Jordan, L. M. (2006). Characterization of persistent inward currents (PICs) in locomotor activity-related neurons of Cfos-EGFP mice. In *Society for Neuroscience Abstracts* (p. 130.6). (Cit. on p. 94).
- Danner, S. M., Hofstoetter, U. S., Ladenbauer, J., Rattay, F., & Minassian, K. (2011). Can the human lumbar posterior columns be stimulated by transcutaneous spinal cord stimulation? A modeling study. *Artificial Organs*, *35*(3), 257–262. (Cit. on p. 51).
- Danner, S. M., Hofstoetter, U. S., & Minassian, K. (in-press). Finite element models of transcutaneous spinal cord stimulation. In D. Jaeger & R. Jung (Eds.), *Encyclopedia of Computational Neuroscience: SpringerReference*. Springer-Verlag. DOI: 10.1007/SpringerReference\_348669. (Cit. on p. 51).
- Danner, S. M., Hofstoetter, U. S., Minassian, K., Krenn, M., Rattay, F., Mayr, W., & Dimitrijevic, M. R. (2012). The human lumbar cord circuitry disconnected from the brain can generate a variety of motor outputs in response to non-patterned spinal cord stimulation at different frequencies. In *Cellular and network functions in the spinal cord* (p. P13). Madison, WI. (Cit. on pp. 57, 95).
- Danner, S. M., Rattay, F., Bijak, M., Mayr, W., Minassian, K., Hofstoetter, U. S., & Dimitrijevic, M. R. (2011). Human lumbar cord can process spinal cord stimulation of different frequencies. In *Neuroscience Meeting Planner Program Nr. 182.06*. Washington, DC: Society for Neuroscience. (Cit. on pp. 57, 62, 95).
- Darbon, P., Yvon, C., Legrand, J.-C., & Streit, J. (2004). INaP underlies intrinsic spiking and rhythm generation in networks of cultured rat spinal cord neurons. *The European Journal of Neuroscience*, *20*(4), 976–988. (Cit. on p. 94).

- De Schutter, E., Ekeberg, O., Kotaleski, J. H., Achard, P., & Lansner, A. (2005). Biophysically detailed modelling of microcircuits and beyond. *Trends in Neurosciences*, *28*(10), 562–569. (Cit. on pp. 60, 63).
- Degtyarenko, A. M., Simon, E. S., & Burke, R. E. (1998). Locomotor modulation of disynaptic EPSPs from the mesencephalic locomotor region in cat motoneurons. *Journal of Neurophysiology*, *80*(6), 3284–3296. (Cit. on pp. 58, 95).
- Dietz, S., Shevtsova, N. A., Rybak, I. A., & Harris-Warrick, R. M. (2013). An asymmetric model of the spinal locomotor central pattern generator: insights from afferent stimulations. *BMC Neuroscience*, *14*(Suppl 1), P161. (Cit. on p. 96).
- Dietz, V., Colombo, G., Jensen, L., & Baumgartner, L. (1995). Locomotor capacity of spinal cord in paraplegic patients. *Annals of Neurology*, *37*(5), 574–582. (Cit. on p. 3).
- Dietz, V., Müller, R., & Colombo, G. (2002). Locomotor activity in spinal man: significance of afferent input from joint and load receptors. *Brain*, *125*(12), 2626–2634. (Cit. on p. 4).
- Dimitrijevic, M. R., Gerasimenko, Y., & Pinter, M. M. (1998a). Effect of reduced afferent input on lumbar CPG in spinal cord injury subjects. In *Society for Neuroscience*, *24* (pp. 623–624). (Cit. on p. 56).
- Dimitrijevic, M. R., Gerasimenko, Y., & Pinter, M. M. (1998b). Evidence for a spinal central pattern generator in humans. *Annals of the New York Academy of Sciences*, *860*, 360–376. (Cit. on pp. 3, 4, 46, 47, 56, 61, 94, 98).
- Dobkin, B. H., Harkema, S. J., Requejo, P., & Edgerton, V. R. (1995). Modulation of locomotor-like emg activity in subjects with complete and incomplete spinal cord injury. *Journal of Neurologic Rehabilitation*, *9*(4), 183–190. (Cit. on p. 3).
- Dominici, N., Ivanenko, Y. P., Cappellini, G., d’Avella, A., Mondì, V., Cicchese, M., . . . Lacquaniti, F. (2011). Locomotor primitives in newborn babies and their development. *Science*, *334*(6058), 997–999. (Cit. on pp. 11, 45).
- Duysens, J., De Groote, F., & Jonkers, I. (2013). The flexion synergy, mother of all synergies and father of new models of gait. *Frontiers in Computational Neuroscience*, *7*, 14. (Cit. on p. 96).
- Edgley, S. A. (2001). Organisation of inputs to spinal interneurone populations. *The Journal of Physiology*, *533*(1), 51–56. (Cit. on p. 55).
- Fedirchuk, B., Nielsen, J., Petersen, N., & Hultborn, H. (1998). Pharmacologically evoked fictive motor patterns in the acutely spinalized marmoset monkey (*Callithrix jacchus*). *Experimental Brain Research*, *122*(3), 351–361. (Cit. on p. 55).
- Gerasimenko, Y., Daniel, O., Regnaud, J., Combeaud, M., & Bussel, B. (2001). Mechanisms of locomotor activity generation under epidural spinal cord

- stimulation. In R. Dengler & A. Kosssev (Eds.), *Sensorimotor control* (pp. 164–171). Washington, DC: IOS Press. (Cit. on pp. 3, 46).
- Gerasimenko, Y., Ichiyama, R. M., Lavrov, I. A., Courtine, G., Cai, L., Zhong, H., ... Edgerton, V. R. (2007). Epidural spinal cord stimulation plus quipazine administration enable stepping in complete spinal adult rats. *Journal of Neurophysiology*, *98*(5), 2525–2536. (Cit. on pp. 46, 50).
- Gerasimenko, Y., Roy, R. R., & Edgerton, V. R. (2008). Epidural stimulation: comparison of the spinal circuits that generate and control locomotion in rats, cats and humans. *Experimental Neurology*, *209*(2), 417–425. (Cit. on pp. 46, 50, 56).
- Goodman, D. F. M. & Brette, R. (2008). Brian: a simulator for spiking neural networks in python. *Frontiers in Neuroinformatics*, *2*, 5. (Cit. on pp. 63, 71).
- Goodman, D. F. M. & Brette, R. (2009). The brian simulator. *Frontiers in Neuroscience*, *3*(2), 192–197. (Cit. on pp. 63, 71).
- Goodman, D. F. M. & Brette, R. (2013). Brian simulator. *Scholarpedia*, *8*(1), 10883. (Cit. on p. 71).
- Gosgnach, S., Quevedo, J., Fedirchuk, B., & McCrea, D. a. (2000). Depression of group Ia monosynaptic EPSPs in cat hindlimb motoneurons during fictive locomotion. *The Journal of Physiology*, *526*(3), 639–652. (Cit. on pp. 60, 95).
- Gossard, J. P., Brownstone, R. M., Barajon, I., & Hultborn, H. (1994). Transmission in a locomotor-related group Ib pathway from hindlimb extensor muscles in the cat. *Experimental Brain Research*, *98*(2), 213–228. (Cit. on pp. 50, 56).
- Grillner, S. (1981). Control of locomotion in bipeds, tetrapods, and fish. In J. M. Brookhart & V. B. Mountcastle (Eds.), *Handbook of physiology—The nervous system II*. (pp. 1179–1236). Bethesda, MD: American Physiological Society. (Cit. on pp. 3, 55).
- Grillner, S. (1985). Neurobiological bases of rhythmic motor acts in vertebrates. *Science*, *228*(4696), 143–149. (Cit. on p. 3).
- Grillner, S. (2003). The motor infrastructure: from ion channels to neuronal networks. *Nature Reviews Neuroscience*, *4*(7), 573–586. (Cit. on p. 55).
- Grillner, S. (2006). Biological pattern generation: the cellular and computational logic of networks in motion. *Neuron*, *52*(5), 751–766. (Cit. on p. 3).
- Grillner, S. (2011). Human locomotor circuits conform. *Science*, *334*(6058), 912–913. (Cit. on pp. 3, 45).
- Grillner, S., Markram, H., De Schutter, E., Silberberg, G., & LeBeau, F. E. N. (2005). Microcircuits in action—from CPGs to neocortex. *Trends in Neurosciences*, *28*(10), 525–533. (Cit. on pp. 60, 63).
- Guertin, P. A. (2009). The mammalian central pattern generator for locomotion. *Brain Research Reviews*, *62*(1), 45–56. (Cit. on p. 55).



- Guertin, P. A. (2013). Central pattern generator for locomotion: anatomical, physiological and pathophysiological considerations. *Frontiers in Neurology*, 3, 183. (Cit. on p. 55).
- Guru, K., Mailis, A., Ashby, P., & Vanderlinden, G. (1987). Postsynaptic potentials in motoneurons caused by spinal cord stimulation in humans. *Electroencephalography and Clinical Neurophysiology*, 66(3), 275–280. (Cit. on p. 48).
- Harkema, S. J., Hurley, S. L., Patel, U. K., Requejo, P. S., Dobkin, B. H., & Edgerton, V. R. (1997). Human lumbosacral spinal cord interprets loading during stepping. *Journal of Neurophysiology*, 77(2), 797–811. (Cit. on pp. 3, 49).
- Hochman, S., Shreckengost, J., Kimura, H., & Quevedo, J. (2010). Presynaptic inhibition of primary afferents by depolarization: observations supporting nontraditional mechanisms. *Annals of the New York Academy of Sciences*, 1198, 140–152. (Cit. on p. 97).
- Hodgkin, A. L. & Huxley, A. F. (1952). A quantitative description of membrane current and its application to conduction and excitation in nerve. *The Journal of Physiology*, 117(4), 500–544. (Cit. on pp. 61, 63, 93).
- Hofstoetter, U. S. (2009). *Model of spinal cord reflex circuits in humans: stimulation frequency-dependence of segmental activities and their interactions* (Doctoral dissertation, Vienna University of Technology). (Cit. on p. 95).
- Holsheimer, J., den Boer, J. A., Struijk, J. J., & Rozeboom, A. R. (1994). MR assessment of the normal position of the spinal cord in the spinal canal. *American Journal of Neuroradiology*, 15(5), 951–959. (Cit. on p. 6).
- Hultborn, H., Conway, B. A., Gossard, J. P., Brownstone, R., Fedirchuk, B., Schomburg, E. D., . . . Perreault, M. C. (1998). How do we approach the locomotor network in the mammalian spinal cord? *Annals of the New York Academy of Sciences*, 860, 70–82. (Cit. on pp. 48, 50, 55, 56).
- Hultborn, H. & Nielsen, J. B. (2007). Spinal control of locomotion—from cat to man. *Acta physiologica (Oxford, England)*, 189(2), 111–121. (Cit. on pp. 49, 50).
- Hultborn, H., Petersen, N., Prownstone, P., & Nielsen, J. (1993). Evidence of fictive spinal locomotion in the marmoset (*Callithrix jacchus*). In *Society for Neuroscience*, 19 (p. 539). (Cit. on p. 55).
- Hunter, J. P. & Ashby, P. (1994). Segmental effects of epidural spinal cord stimulation in humans. *Journal of Physiology*, 474(3), 407–419. (Cit. on p. 48).
- Hurvich, C. M. & Tsai, C.-L. (1989). Regression and time series model selection in small samples. *Biometrika*, 76(2), 297–307. (Cit. on p. 14).
- Izhikevich, E. M. (2006). Polychronization: Computation with spikes. *Neural Computation*, 18, 245–282. (Cit. on p. 96).
- Jankowska, E. (1992). Interneuronal relay in spinal pathways from proprioceptors. *Progress in Neurobiology*, 38(4), 335–378. (Cit. on pp. 48, 69).

- Jankowska, E. (2001). Spinal interneuronal systems: identification, multifunctional character and reconfigurations in mammals. *The Journal of Physiology*, *533*(1), 31–40. (Cit. on pp. 47, 48).
- Jankowska, E. & Hammar, I. (2002). Spinal interneurons; how can studies in animals contribute to the understanding of spinal interneuronal systems in man? *Brain Research. Brain Research Reviews*, *40*(1-3), 19–28. (Cit. on p. 48).
- Jilge, B., Minassian, K., Rattay, F., & Dimitrijevic, M. R. (2004). Frequency-dependent selection of alternative spinal pathways with common periodic sensory input. *Biological Cybernetics*, *91*(6), 359–376. (Cit. on pp. 46, 96).
- Jilge, B., Minassian, K., Rattay, F., Pinter, M. M., Gerstenbrand, F., Binder, H., & Dimitrijevic, M. R. (2004). Initiating extension of the lower limbs in subjects with complete spinal cord injury by epidural lumbar cord stimulation. *Experimental Brain Research*, *154*(3), 308–326. (Cit. on pp. 61, 94).
- Kiehn, O. (2006). Locomotor circuits in the mammalian spinal cord. *Annual Review of Neuroscience*, *29*, 279–306. (Cit. on p. 55).
- Kinoshita, M. & Yamaguchi, T. (2001). Stimulus time-locked responses of motoneurons during forelimb fictive locomotion evoked by repetitive stimulation of the lateral funiculus. *Brain Research*, *904*(1), 31–42. (Cit. on pp. 58, 95).
- Lavrov, I., Dy, C. J., Fong, A. J., Gerasimenko, Y., Courtine, G., Zhong, H., ... Edgerton, V. R. (2008). Epidural stimulation induced modulation of spinal locomotor networks in adult spinal rats. *Journal of Neuroscience*, *28*(23), 6022–6029. (Cit. on p. 46).
- Lee, D. D. & Seung, H. S. (1999). Learning the parts of objects by non-negative matrix factorization. *Nature*, *401*(6755), 788–791. (Cit. on p. 11).
- Lee, R. H. & Heckman, C. J. (2001). Essential Role of a Fast Persistent Inward Current in Action Potential Initiation and Control of Rhythmic Firing. *Journal of Neurophysiology*, *85*(1), 472–475. (Cit. on p. 94).
- Lloyd, D. P. (1943). Reflex action in relation to pattern and peripheral source of afferent stimulation. *Journal of Neurophysiology*, *6*, 111–120. (Cit. on p. 47).
- Marder, E., Bucher, D., Schulz, D. J., & Taylor, A. L. (2005). Invertebrate central pattern generation moves along. *Current Biology*, *15*(17), R685–R699. (Cit. on p. 63).
- Marder, E. & Calabrese, R. L. (1996). Principles of rhythmic motor pattern generation. *Physiological Reviews*, *76*(3), 687–717. (Cit. on p. 55).
- Markin, S. N., Klishko, A. N., Shevtsova, N. A., Lemay, M. A., Prilutsky, B. I., & Rybak, I. A. (2010). Afferent control of locomotor CPG: insights from a simple neuromechanical model. *Annals of the New York Academy of Sciences*, *1198*, 21–34. (Cit. on p. 95).

- Matthews, P. B. C. (1972). *Mammalian muscle receptors and their central actions*. Monographs of the Physiological Society, No. 23. London: Edward Arnold. (Cit. on p. 98).
- McCrea, D. A. (1998). Neuronal basis of afferent-evoked enhancement of locomotor activity. *Annals of the New York Academy of Sciences*, 860, 216–225. (Cit. on p. 50).
- McCrea, D. A. (2001). Spinal circuitry of sensorimotor control of locomotion. *The Journal of Physiology*, 533(1), 41–50. (Cit. on pp. 50, 56).
- McCrea, D. A., Pratt, C. A., & Jordan, L. M. (1980). Renshaw cell activity and recurrent effects on motoneurons during fictive locomotion. *Journal of Neurophysiology*, 44(3), 475–488. (Cit. on p. 69).
- McCrea, D. A. & Rybak, I. A. (2007). Modeling the mammalian locomotor CPG: insights from mistakes and perturbations. *Progress in Brain Research*, 165, 235–253. (Cit. on p. 94).
- McCrea, D. A. & Rybak, I. A. (2008). Organization of mammalian locomotor rhythm and pattern generation. *Brain Research Reviews*, 57(1), 134–146. (Cit. on pp. 56, 94, 96).
- McGraw, M. B. (1940). Neuromuscular development of the human infant as exemplified in the achievement of erect locomotion. *Journal of Pediatrics*, 17, 747–771. (Cit. on p. 45).
- Minassian, K., Hofstoetter, U. S., Tansey, K., & Mayr, W. (2012). Neuromodulation of lower limb motor control in restorative neurology. *Clinical Neurology and Neurosurgery*, 114(5), 489–497. (Cit. on p. 51).
- Minassian, K., Gilge, B., Rattay, F., Pinter, M. M., Binder, H., Gerstenbrand, F., & Dimitrijevic, M. R. (2004). Stepping-like movements in humans with complete spinal cord injury induced by epidural stimulation of the lumbar cord: electromyographic study of compound muscle action potentials. *Spinal Cord*, 42(7), 401–416. (Cit. on pp. 3, 4, 16, 45–48, 58, 60–62, 94, 98).
- Minassian, K., Persy, I., Rattay, F., Dimitrijevic, M. R., Hofer, C., & Kern, H. (2007). Posterior root-muscle reflexes elicited by transcutaneous stimulation of the human lumbosacral cord. *Muscle & Nerve*, 35(3), 327–336. (Cit. on p. 51).
- Minassian, K., Persy, I., Rattay, F., Pinter, M. M., Kern, H., & Dimitrijevic, M. R. (2007). Human lumbar cord circuitries can be activated by extrinsic tonic input to generate locomotor-like activity. *Human Movement Science*, 26(2), 275–295. (Cit. on pp. 4, 45–48, 58, 60, 94).
- Murg, M., Binder, H., & Dimitrijevic, M. R. (2000). Epidural electric stimulation of posterior structures of the human lumbar spinal cord: 1. muscle twitches - a functional method to define the site of stimulation. *Spinal Cord*, 38(7), 394–402. (Cit. on p. 8).
- Noga, B. R., Kriellaars, D. J., Brownstone, R. M., & Jordan, L. M. (2003). Mechanism for activation of locomotor centers in the spinal cord by

- stimulation of the mesencephalic locomotor region. *Journal of Neurophysiology*, *90*(3), 1464–1478. (Cit. on pp. 60, 95).
- Nusbaum, M. P., El Manira, A., Gossard, J.-P., & Rossignol, S. (1999). Presynaptic mechanisms during rhythmic activity in vertebrates and invertebrates. In P. S. G. Stein, S. Grillner, A. I. Selverston, & D. G. Stuart (Eds.), *Neurons, networks and motor behavior* (pp. 257–267). Cambridge, MA: MIT Press. (Cit. on pp. 60, 95).
- Oberg, T., Karsznia, A., & Oberg, K. (1993). Basic gait parameters: reference data for normal subjects, 10–79 years of age. *Journal of Rehabilitation Research & Development*, *30*(2), 210–223. (Cit. on p. 44).
- Okamoto, T., Okamoto, K., & Andrew, P. D. (2001). Electromyographic study of newborn stepping in neonates and young infants. *Electromyography and Clinical Neurophysiology*, *41*(5), 289–296. (Cit. on p. 45).
- Parker, D. (2009). Descending interactions with spinal cord networks: a time to build? *The Journal of Physiology*, *587*(20), 4761. (Cit. on p. 49).
- Pearson, K. & Gordon, J. (2000). Locomotion. In E. R. Kandel, J. H. Schwartz, & T. M. Jessell (Eds.), *Principles of neural science 4th edition* (pp. 737–755). New York: McGraw-Hill. (Cit. on pp. 3, 49, 56).
- Pierrot-Desseilligny, E. & Burke, D. C. (2005). *The circuitry of the human spinal cord: its role in motor control and movement disorders*. Cambridge: Cambridge University Press. (Cit. on p. 98).
- Pinter, M. M., Gerstenbrand, F., & Dimitrijevic, M. R. (2000). Epidural electrical stimulation of posterior structures of the human lumbosacral cord: 3. control of spasticity. *Spinal Cord*, *38*(9), 524–531. (Cit. on pp. 5, 8, 56).
- Rattay, F., Minassian, K., & Dimitrijevic, M. R. (2000). Epidural electrical stimulation of posterior structures of the human lumbosacral cord: 2. quantitative analysis by computer modeling. *Spinal Cord*, *38*(8), 473–489. (Cit. on pp. 4, 45, 56).
- Roberts, A., Soffee, S. R., Wolf, E. S., Yoshida, M., & Zhao, F.-Y. (1998). Central circuits controlling locomotion in young frog tadpoles. *Annals of the New York Academy of Sciences*, *860*, 19–34. (Cit. on p. 55).
- Roby-Brami, A. & Bussel, B. (1987). Long-latency spinal reflex in man after flexor reflex afferent stimulation. *Brain*, *110*(3), 707–725. (Cit. on p. 56).
- Rossignol, S. (1996). Neural control of stereotypic limb movements. In L. B. Rowell & J. Sheperd (Eds.), *Handbook of physiology, section 12. Exercise: regulation and integration of multiple systems* (pp. 173–216). Washington DC: American Physiology Society. (Cit. on p. 55).
- Rudomin, P. (1990). Presynaptic inhibition of muscle spindle and tendon organ afferents in the mammalian spinal cord. *Trends in Neurosciences*, *13*(12), 499–505. (Cit. on p. 97).
- Rudomin, P. (2009). In search of lost presynaptic inhibition. *Experimental Brain Research*, *196*(1), 139–151. (Cit. on p. 97).

- Rudomin, P., Quevedo, J., & Eguibar, J. R. (1993). Presynaptic modulation of spinal reflexes. *Current Opinion in Neurobiology*, 3(6), 997–1004. (Cit. on p. 97).
- Rudomin, P. & Schmidt, R. F. (1999). Presynaptic inhibition in the vertebrate spinal cord revisited. *Experimental Brain Research*, 129(1), 1–37. (Cit. on pp. 60, 95, 97).
- Rybak, I. A., Shevtsova, N. A., Lafreniere-Roula, M., & McCrea, D. A. (2006). Modelling spinal circuitry involved in locomotor pattern generation: insights from deletions during fictive locomotion. *The Journal of Physiology*, 577(2), 617–639. (Cit. on pp. 47, 56, 63, 65, 67–71, 74, 77, 93, 95, 97, 98).
- Rybak, I. A., Stecina, K., Shevtsova, N. A., & McCrea, D. A. (2006). Modelling spinal circuitry involved in locomotor pattern generation: insights from the effects of afferent stimulation. *The Journal of Physiology*, 577(2), 641–658. (Cit. on pp. 49, 56, 63, 76, 95).
- Sherwood, A. M., Dimitrijevic, M. R., & McKay, W. B. (1992). Evidence of subclinical brain influence in clinically complete spinal cord injury: discomplete sci. *Journal of the Neurological Sciences*, 110(1-2), 90–98. (Cit. on p. 43).
- Sherwood, A. M., McKay, W. B., & Dimitrijevic, M. R. (1996). Motor control after spinal cord injury: assessment using surface emg. *Muscle & Nerve*, 19(8), 966–979. (Cit. on pp. 5, 43).
- Streit, J., Tscherter, A., & Darbon, P. (2005). Rhythm generation in spinal culture: Is it the neuron or the network? In M. Taketani & M. Baudry (Eds.), *Advances in network electrophysiology using multi-electrode arrays* (pp. 377–408). New York: Springer. (Cit. on p. 94).
- Taddese, A. & Bean, B. P. (2002). Subthreshold sodium current from rapidly inactivating sodium channels drives spontaneous firing of tuberomammillary neurons. *Neuron*, 33(4), 587–600. (Cit. on p. 94).
- Theiss, R. D., Kuo, J. J., & Heckman, C. J. (2007). Persistent inward currents in rat ventral horn neurones. *The Journal of Physiology*, 580(2), 507–522. (Cit. on p. 94).
- Vilensky, J. a. & O'Connor, B. L. (1998). Stepping in nonhuman primates with a complete spinal cord transection: old and new data, and implications for humans. *Annals of the New York Academy of Sciences*, 860, 528–530. (Cit. on p. 55).
- Vreugdenhil, M., Hoogland, G., van Veelen, C. W. M., & Wadman, W. J. (2004). Persistent sodium current in subicular neurons isolated from patients with temporal lobe epilepsy. *European Journal of Neuroscience*, 19(10), 2769–2778. (Cit. on p. 94).
- Wernig, A. & Müller, S. (1992). Laufband locomotion with body weight support improved walking in persons with severe spinal cord injuries. *Paraplegia*, 30(4), 229–238. (Cit. on p. 3).

## BIBLIOGRAPHY

---

- Zelazo, P. R., Zelazo, N. A., & Kolb, S. (1972). “Walking” in the newborn. *Science*, *176*, 314–315. (Cit. on p. 45).
- Zhong, G., Shevtsova, N. A., Rybak, I. A., & Harris-Warrick, R. M. (2012). Neuronal activity in the isolated mouse spinal cord during spontaneous deletions in fictive locomotion: insights into locomotor central pattern generator organization. *The Journal of Physiology*, *590*(19), 4735–4759. (Cit. on pp. 95, 97).

## Appendix A

### *Appendix*

#### A.1 Tables

Table A.1: Onset latency of every subject and muscle group

RID	MG	Controls		Extension		Flexion		sig. post-hoc		
		n	M(SD)	n	M(SD)	n	M(SD)	c-f	e-f	c-e
1	1	46	10.12 (0.22)	1	20.51 (0.00)	35	12.03 (2.61)	***		
1	2	46	11.24 (0.13)	57	13.74 (1.03)	47	12.81 (0.62)	***	***	***
1	3	46	18.95 (0.49)	19	20.71 (1.50)	41	18.45 (0.92)	**	***	***
1	4	46	18.91 (0.22)	11	19.09 (0.83)	46	18.76 (0.51)			
2	1	38	10.11 (0.22)	4	9.28 (0.00)	22	11.45 (0.86)	***	**	***
2	2	38	10.33 (0.21)	0		13	12.32 (1.95)	***		
2	3	0		2	32.96 (1.73)	20	20.95 (1.86)			
2	4	0		1	18.07 (0.00)	10	22.61 (3.34)			
3	1	38	10.11 (0.22)	6	9.68 (0.20)	29	11.16 (0.52)	***	***	**
3	2	38	10.33 (0.21)	0		22	12.98 (2.47)	***		
3	3	0		23	33.39 (5.34)	28	20.35 (2.11)		***	
3	4	0		23	31.36 (6.63)	24	21.44 (1.80)		***	
4	1	38	9.71 (0.15)	48	10.18 (0.93)	1	30.76 (0.00)	*		***
4	2	38	10.36 (0.20)	0		0				
4	3	0		2	17.82 (3.11)	23	17.68 (1.06)			
4	4	0		0		6	18.96 (0.78)			
5	1	26	10.31 (0.42)	2	10.50 (0.35)	60	9.38 (0.72)	***		
5	2	25	11.39 (0.74)	7	19.60 (2.48)	18	11.18 (1.13)		***	***
5	3	0		71	27.93 (1.63)	31	23.56 (3.96)		***	
5	4	0		0		1	15.14 (0.00)			
6	1	46	10.12 (0.22)	11	10.92 (0.82)	72	9.02 (0.80)	***	***	**
6	2	46	11.24 (0.13)	3	16.28 (8.31)	21	12.72 (4.16)			
6	3	46	18.95 (0.49)	58	27.61 (2.27)	29	22.06 (3.67)	***	***	***
6	4	46	18.91 (0.22)	0		14	21.66 (2.45)	***		
7	1	29	10.69 (0.53)	84	10.90 (1.15)	57	10.43 (0.46)	**	***	
7	2	29	11.43 (0.28)	60	13.40 (2.88)	39	10.98 (1.95)		***	***
7	3	0		38	25.67 (3.22)	23	24.27 (5.37)			
7	4	14	21.10 (1.05)	32	19.58 (1.79)	14	27.73 (3.73)	***	***	**
8	1	23	10.64 (0.36)	72	10.96 (0.50)	30	10.91 (0.47)			*
8	2	23	11.00 (0.32)	72	11.56 (0.41)	30	11.44 (0.44)	**		***
8	3	18	22.11 (1.39)	64	21.75 (1.75)	21	22.02 (2.16)			*
8	4	23	21.19 (0.46)	72	21.62 (0.97)	29	20.98 (1.51)			
9	1	23	10.64 (0.36)	77	11.09 (0.51)	48	10.49 (0.35)		***	***
9	2	23	11.00 (0.32)	77	11.77 (0.65)	48	11.32 (0.37)	**	***	***
9	3	18	22.11 (1.39)	57	21.92 (1.38)	47	25.99 (2.75)	***	***	
9	4	23	21.19 (0.46)	77	21.66 (0.85)	48	21.42 (1.64)		*	**
10	1	23	9.83 (0.34)	66	10.86 (1.02)	59	10.68 (0.66)	***		***
10	2	23	10.98 (0.39)	66	11.38 (0.77)	58	10.83 (0.63)		***	**
10	3	0		19	23.23 (2.20)	41	21.47 (1.72)		*	
10	4	4	22.83 (1.28)	41	24.57 (1.91)	14	22.57 (2.21)		**	

Continued on next page

A. APPENDIX

Table A.1 Onset latency of every subject and muscle group (continued)

RID	MG	n	Controls		Extension		Flexion		sig. post-hoc		
			M(SD)	n	M(SD)	n	M(SD)	n	c-f	e-f	c-e
11	1	102	12.15 (0.16)	78	11.79 (1.20)	46	10.70 (0.41)	***	***	***	
11	2	102	13.78 (0.21)	79	12.96 (0.28)	46	13.09 (1.35)	***	***	***	
11	3	102	22.69 (0.24)	79	21.08 (0.58)	31	22.11 (1.82)	***	***	***	
11	4	102	21.84 (0.61)	79	20.79 (0.82)	42	20.71 (1.74)	***		***	
12	1	32	11.75 (0.12)	66	13.27 (2.28)	35	10.67 (0.45)	***	***	***	
12	2	32	13.31 (0.21)	66	13.27 (1.06)	35	13.31 (0.92)			***	
12	3	32	20.57 (0.21)	66	21.32 (0.50)	26	21.67 (1.50)	***		***	
12	4	32	21.23 (0.57)	66	20.85 (0.74)	22	21.35 (0.97)		*	***	
13	1	32	11.75 (0.12)	78	11.39 (0.37)	24	11.23 (0.63)	***		***	
13	2	32	13.31 (0.21)	78	13.62 (0.52)	36	13.66 (1.07)			***	
13	3	32	20.57 (0.21)	78	21.28 (0.48)	36	24.74 (3.88)	***	***	***	
13	4	32	21.23 (0.57)	78	21.10 (0.66)	36	20.78 (0.75)	*	*		
14	1	70	11.47 (0.25)	74	11.26 (0.30)	17	11.14 (0.50)	**		***	
14	2	70	12.86 (0.23)	74	13.85 (0.94)	48	13.80 (1.13)	***		***	
14	3	70	20.12 (0.28)	74	21.29 (0.40)	48	22.52 (2.61)	***	***	***	
14	4	70	22.17 (0.44)	74	21.31 (0.65)	48	21.43 (0.79)	***		***	
15	1	76	10.52 (0.25)	1	13.67 (0.00)	46	13.77 (1.73)	***			
15	2	76	10.92 (0.24)	87	13.58 (1.34)	46	13.06 (0.24)	***		***	
15	3	15	19.08 (0.47)	18	20.35 (0.84)	46	19.98 (0.31)	***	*	***	
15	4	72	20.14 (0.82)	17	20.22 (1.67)	46	20.81 (0.63)	***			
16	1	75	11.06 (0.26)	90	13.72 (1.85)	13	11.34 (2.35)		***	***	
16	2	0		106	13.55 (1.18)	27	14.78 (1.00)		***		
16	3	0		101	19.56 (0.67)	27	25.59 (1.41)		***		
16	4	0		104	19.64 (1.00)	12	19.90 (2.68)				
17	1	75	11.06 (0.26)	66	13.73 (1.91)	22	10.85 (1.46)	**	***	***	
17	2	0		66	13.61 (1.14)	45	14.92 (0.91)		***		
17	3	0		66	19.48 (0.48)	44	24.75 (1.77)		***		
17	4	0		65	19.97 (0.73)	24	19.67 (1.13)		*		
18	1	76	10.69 (0.17)	8	13.55 (2.33)	8	15.69 (4.89)	**		***	
18	2	76	11.42 (0.24)	66	14.58 (1.51)	37	15.35 (1.98)	***		***	
18	3	70	18.67 (0.46)	62	19.83 (0.87)	37	27.59 (1.30)	***	***	***	
18	4	75	18.49 (0.66)	64	20.86 (0.80)	35	21.85 (2.69)	***		***	
19	1	76	10.52 (0.25)	101	13.64 (1.91)	5	10.94 (1.88)		*	***	
19	2	76	10.92 (0.24)	109	13.21 (0.75)	30	13.80 (1.75)	***		***	
19	3	15	19.08 (0.47)	107	19.83 (0.73)	30	26.35 (0.68)	***	***	***	
19	4	72	20.14 (0.82)	94	20.50 (0.95)	3	21.48 (4.96)				
20	1	76	10.52 (0.25)	0		46	14.04 (2.11)	***			
20	2	76	10.92 (0.24)	53	14.48 (1.76)	46	12.94 (0.29)	***	***	***	
20	3	15	19.08 (0.47)	7	28.60 (3.65)	46	19.88 (0.39)	***	***	***	
20	4	72	20.14 (0.82)	0		46	20.73 (0.49)	***			
21	1	76	10.69 (0.17)	54	12.45 (1.98)	16	13.00 (3.83)			***	
21	2	76	11.42 (0.24)	126	14.42 (1.43)	22	15.54 (2.06)	***	***	***	
21	3	70	18.67 (0.46)	112	20.03 (0.93)	22	26.15 (1.34)	***	***	***	
21	4	75	18.49 (0.66)	121	20.55 (1.33)	8	24.41 (4.44)	***		***	
22	1	75	11.06 (0.26)	101	14.03 (2.33)	9	12.42 (1.64)	**		***	
22	2	0		109	13.46 (1.03)	30	15.17 (1.34)		***		
22	3	0		107	19.57 (1.08)	29	25.36 (1.62)		***		
22	4	0		109	20.23 (0.62)	3	23.93 (6.78)				
23	1	4	11.84 (0.24)	24	17.01 (1.96)	33	14.43 (3.42)		**	**	
23	2	4	11.96 (0.28)	100	13.83 (2.20)	33	11.30 (0.18)	***	***		
23	3	4	19.65 (0.24)	50	20.14 (1.07)	26	27.87 (3.86)	*	***		
23	4	4	20.63 (0.47)	74	19.63 (0.90)	0				*	
24	1	22	11.10 (1.68)	4	15.02 (3.99)	13	12.21 (3.44)				
24	2	22	12.23 (0.24)	57	12.90 (0.36)	46	12.69 (0.82)	***		***	
24	3	22	18.42 (0.66)	56	20.64 (1.15)	40	20.04 (1.82)	***	***	***	
24	4	22	19.07 (0.35)	57	19.30 (0.40)	43	20.11 (0.82)	***	***	*	
25	1	33	10.45 (0.27)	1	11.23 (0.00)	4	11.72 (2.67)				

Continued on next page



Table A.1 Onset latency of every subject and muscle group (continued)

RID	MG	n	Controls		Extension		Flexion		sig. post-hoc		
			M(SD)	n	M(SD)	n	M(SD)	n	c-f	e-f	c-e
25	2	33	11.62 (0.24)	89	13.63 (0.97)	39	13.15 (2.13)	***		***	
25	3	33	19.25 (1.06)	90	21.34 (1.27)	14	24.48 (4.05)	***	*	***	
25	4	33	17.67 (0.26)	97	19.56 (0.33)	22	20.09 (3.25)	***		***	
26	1	33	10.45 (0.27)	36	13.51 (2.58)	42	12.27 (2.67)	***	**	***	
26	2	33	11.62 (0.24)	53	13.17 (0.92)	45	13.12 (0.89)	***		***	
26	3	33	19.25 (1.06)	51	21.64 (0.77)	43	21.73 (2.62)	***	***	***	
26	4	33	17.67 (0.26)	53	20.00 (0.25)	45	20.17 (0.37)	***		***	
27	1	33	10.45 (0.27)	3	11.88 (1.13)	17	14.59 (2.18)	***		**	
27	2	33	11.62 (0.24)	90	13.38 (1.12)	33	13.21 (1.53)	***		***	
27	3	33	19.25 (1.06)	89	21.02 (1.30)	29	27.18 (3.62)	***	***	***	
27	4	33	17.67 (0.26)	98	19.80 (0.26)	28	20.16 (1.12)	***	**	***	
28	1	33	10.14 (0.25)	6	15.14 (1.16)	4	8.91 (0.73)	***	*	***	
28	2	33	12.73 (0.21)	96	13.16 (0.42)	25	13.03 (1.21)			***	
28	3	33	19.38 (0.33)	78	21.20 (1.63)	3	27.67 (3.66)	**	**	***	
28	4	33	19.04 (0.27)	98	19.46 (0.27)	7	20.93 (1.34)	***	***	***	
29	1	33	10.45 (0.27)	56	14.87 (1.43)	75	17.39 (1.19)	***	***	***	
29	2	33	11.62 (0.24)	74	13.71 (0.98)	79	12.69 (1.23)	***	***	***	
29	3	33	19.25 (1.06)	41	22.25 (2.08)	56	25.77 (2.81)	***	***	***	
29	4	33	17.67 (0.26)	72	18.87 (0.74)	47	18.10 (0.93)	**	***	***	
30	1	16	10.77 (0.22)	79	11.22 (1.07)	11	11.41 (2.45)				
30	2	16	14.47 (0.30)	83	12.83 (0.47)	32	13.12 (0.44)	***	*	***	
30	3	16	20.72 (0.31)	23	23.42 (6.03)	33	27.24 (1.56)	***			
30	4	16	21.09 (0.27)	17	20.08 (1.14)	32	23.94 (1.76)	***	***	***	
31	1	16	10.77 (0.22)	84	11.67 (0.80)	18	12.42 (2.13)	*		***	
31	2	16	14.47 (0.30)	78	13.70 (1.04)	36	13.78 (0.55)	***		***	
31	3	16	20.72 (0.31)	14	21.80 (5.51)	36	27.83 (1.57)	***	***		
31	4	16	21.09 (0.27)	10	22.61 (5.72)	30	25.81 (2.38)	***			
32	1	23	10.95 (0.38)	109	11.65 (0.83)	6	11.31 (2.40)			***	
32	2	23	14.39 (0.36)	106	14.25 (0.96)	42	14.79 (1.12)		**	*	
32	3	23	21.68 (0.32)	28	19.69 (1.82)	41	26.93 (1.73)	***	***	***	
32	4	23	21.78 (0.35)	38	21.32 (3.28)	9	28.70 (2.53)	***	***		
33	1	23	10.83 (0.32)	80	11.49 (0.69)	8	14.22 (1.26)	***	***	***	
33	2	23	16.26 (1.08)	81	14.12 (0.72)	41	14.93 (1.46)	**	**	***	
33	3	23	20.42 (0.28)	21	20.60 (4.83)	41	29.05 (1.00)	***	***		
33	4	23	21.00 (0.36)	10	22.85 (5.02)	34	25.98 (2.76)	***	*		
34	1	24	11.05 (0.24)	161	11.58 (0.53)	11	10.88 (0.69)		***	***	
34	2	24	13.02 (0.24)	163	13.87 (1.03)	47	14.68 (1.03)	***	***	***	
34	3	24	18.41 (0.49)	58	20.35 (1.47)	34	29.11 (2.32)	***	***	***	
34	4	24	18.31 (0.25)	76	21.30 (2.88)	1	28.81 (0.00)			***	
35	1	21	8.86 (0.18)	20	16.58 (0.56)	28	15.70 (1.13)	***	***	***	
35	2	21	11.30 (0.18)	0		22	17.93 (1.70)	***			
35	3	21	18.11 (0.15)	26	26.99 (2.24)	28	26.72 (1.66)	***		***	
35	4	21	17.23 (0.23)	1	27.34 (0.00)	26	27.61 (1.90)	***			
36	1	21	8.86 (0.18)	0		92	18.54 (0.62)	***			
36	2	21	11.30 (0.18)	74	12.05 (0.30)	21	11.88 (0.45)	***		***	
36	3	21	18.11 (0.15)	3	27.67 (1.02)	87	27.56 (1.38)	***		***	
36	4	21	17.23 (0.23)	0		49	29.62 (3.07)	***			
37	1	21	9.14 (0.23)	43	16.95 (0.68)	19	15.75 (0.81)	***	***	***	
37	2	21	10.51 (0.25)	1	18.07 (0.00)	0					
37	3	21	18.16 (0.20)	60	25.59 (1.46)	51	25.21 (1.54)	***		***	
37	4	21	16.97 (0.21)	33	29.82 (2.04)	67	25.19 (1.52)	***	***	***	
38	1	21	9.14 (0.23)	0		8	17.52 (0.96)	***			
38	2	21	10.51 (0.25)	89	13.61 (1.13)	51	12.98 (1.32)	***	*	***	
38	3	21	18.16 (0.20)	4	28.44 (1.46)	82	26.13 (1.08)	***	*	***	
38	4	21	16.97 (0.21)	1	19.04 (0.00)	58	26.70 (1.67)	***			
39	1	12	8.71 (0.35)	9	20.29 (0.85)	23	18.19 (0.81)	***	***	***	
39	2	12	10.25 (0.29)	63	13.10 (0.39)	17	13.16 (0.53)	***		***	

Continued on next page

A. APPENDIX

**Table A.1 Onset latency of every subject and muscle group (continued)**

RID	MG	n	Controls		Extension		Flexion		sig. post-hoc		
			M(SD)	n	M(SD)	n	M(SD)	n	c-f	e-f	c-e
39	3	12	18.31 (0.39)	79	27.35 (1.42)	55	25.25 (1.05)	***	***	***	
39	4	12	17.54 (0.44)	19	28.24 (1.06)	27	25.35 (1.00)	***	***	***	

RID: recording identification number, MG: muscle group (1: quadriceps, 2: hamstrings, 3: tibialis anterior, 4: triceps surae), \*:  $p < .05$ , \*\*:  $p < .01$ , \*\*\*:  $p < .001$  (of pairwise Whitney-Mann-U tests, Bonferroni corrected).

Table A.2: Center of gravity of every subject and muscle group

RID	MG	n	Controls		Extension		Flexion		sig. post-hoc		
			M(SD)	n	M(SD)	n	M(SD)	n	c-f	e-f	c-e
1	1	46	23.03 (0.21)	54	27.93 (3.64)	47	23.82 (2.61)		***	***	***
1	2	46	22.81 (0.22)	60	20.83 (1.54)	47	20.86 (2.99)	***			***
1	3	46	24.48 (0.35)	60	29.94 (4.06)	47	26.75 (3.43)	**	***		***
1	4	46	22.75 (0.24)	60	31.16 (4.18)	47	22.74 (1.50)	***	***		***
2	1	38	23.99 (0.34)	160	21.44 (1.91)	37	23.00 (1.60)	*	***		***
2	2	38	23.78 (0.28)	101	22.94 (2.26)	29	22.93 (2.55)				**
2	3	0		159	29.14 (5.22)	37	27.83 (2.34)				
2	4	34	34.42 (2.15)	160	29.54 (4.19)	37	30.41 (3.20)	***			***
3	1	38	23.99 (0.34)	133	21.10 (1.54)	30	22.40 (0.73)	***	***		***
3	2	38	23.78 (0.28)	133	22.02 (1.93)	30	23.75 (1.77)		***		***
3	3	0		122	30.95 (5.99)	30	27.49 (1.40)		*		
3	4	34	34.42 (2.15)	125	31.41 (4.72)	30	29.64 (1.92)	***			***
4	1	38	23.53 (0.32)	126	22.16 (2.82)	34	28.35 (4.10)	***	***		*
4	2	38	23.72 (0.33)	126	25.34 (2.55)	34	27.78 (3.05)	***	***		***
4	3	0		126	31.89 (4.04)	34	24.20 (1.27)		***		
4	4	35	37.70 (3.11)	126	33.31 (2.61)	34	28.03 (4.00)	***	***		***
5	1	29	24.09 (8.32)	81	23.58 (1.96)	69	18.27 (1.02)	***	***		**
5	2	26	23.01 (9.64)	81	25.52 (2.96)	69	21.44 (3.26)		***		***
5	3	0		81	36.10 (2.05)	69	34.13 (3.55)		*		
5	4	0		81	32.75 (2.11)	69	32.80 (2.91)				
6	1	46	23.03 (0.21)	76	23.94 (1.78)	72	17.84 (0.97)	***	***		***
6	2	46	22.81 (0.22)	75	24.64 (3.57)	72	21.30 (3.62)	*	***		***
6	3	46	24.48 (0.35)	73	36.81 (1.35)	72	33.73 (3.96)	***	***		***
6	4	46	22.75 (0.24)	76	33.05 (2.54)	72	31.32 (2.95)	***	***		***
7	1	29	20.79 (2.51)	87	21.88 (2.40)	58	17.87 (2.22)	***	***		*
7	2	29	21.18 (1.20)	87	24.95 (3.15)	58	24.06 (4.74)	*			***
7	3	0		87	34.66 (2.76)	58	31.67 (5.49)		*		
7	4	12	53.06 (39.34)	87	29.67 (4.07)	58	33.56 (3.65)		***		
8	1	23	19.55 (0.74)	72	19.31 (1.71)	30	19.50 (1.81)				
8	2	23	21.76 (1.17)	72	20.60 (1.07)	30	20.12 (0.65)	***	*		***
8	3	18	28.02 (0.65)	70	28.53 (3.91)	30	34.47 (3.74)	***	***		
8	4	23	25.45 (0.40)	72	26.23 (0.92)	30	26.04 (1.35)	*			***
9	1	23	19.55 (0.74)	77	19.40 (1.65)	48	17.78 (2.00)	**	***		
9	2	23	21.76 (1.17)	77	21.18 (1.45)	48	20.42 (0.68)	***	*		*
9	3	18	28.02 (0.65)	77	30.56 (4.43)	48	36.41 (1.59)	***	***		
9	4	23	25.45 (0.40)	77	26.37 (1.77)	48	28.63 (2.83)	***	***		***
10	1	23	17.66 (0.32)	66	19.87 (3.26)	59	19.73 (3.38)				*
10	2	23	17.92 (0.34)	66	20.15 (1.50)	58	19.86 (1.67)	***			***
10	3	0		66	31.57 (1.70)	59	31.77 (2.02)				
10	4	17	35.24 (4.91)	66	31.35 (2.21)	58	32.61 (4.90)				*
11	1	102	22.69 (0.25)	79	24.32 (1.40)	46	22.54 (2.19)		***		***
11	2	102	19.49 (0.20)	79	19.88 (0.70)	46	21.27 (1.74)	***	***		***
11	3	102	26.77 (0.22)	79	29.80 (4.46)	46	34.86 (3.23)	***	***		***
11	4	102	26.99 (0.44)	79	26.53 (1.23)	46	32.12 (3.53)	***	***		***
12	1	32	22.46 (0.00)	66	24.34 (1.52)	35	21.97 (1.69)	*	***		***
12	2	32	19.85 (0.24)	66	20.18 (0.99)	35	21.64 (2.10)	***	***		
12	3	32	26.11 (0.25)	66	29.13 (3.30)	35	33.72 (3.38)	***	***		***
12	4	32	27.65 (0.24)	66	26.50 (1.03)	35	30.47 (2.52)	***	***		***
13	1	32	22.46 (0.00)	78	22.47 (0.50)	36	27.63 (3.39)	***	***		
13	2	32	19.85 (0.24)	78	18.71 (1.11)	36	20.49 (1.64)		***		***
13	3	32	26.11 (0.25)	78	28.67 (3.82)	36	38.56 (2.28)	***	***		***
13	4	32	27.65 (0.24)	78	26.26 (0.84)	36	29.19 (3.15)		***		***
14	1	70	21.82 (0.23)	74	22.63 (0.44)	48	27.38 (3.57)	***	***		***
14	2	70	19.50 (0.14)	74	19.53 (1.61)	48	20.42 (1.48)		***		**
14	3	70	25.61 (0.32)	74	27.88 (2.87)	48	38.55 (2.93)	***	***		***
14	4	70	26.35 (0.36)	74	25.53 (0.50)	48	26.89 (1.07)		***		***

Continued on next page

A. APPENDIX

Table A.2 Center of gravity of every subject and muscle group (continued)

RID	MG	n	Controls		Extension		Flexion		sig. post-hoc		
			M(SD)	n	M(SD)	n	M(SD)	n	c-f	e-f	c-e
15	1	76	20.68 (0.27)	88	23.53 (2.00)	46	22.14 (1.02)	***	***	***	
15	2	76	20.64 (0.22)	88	21.52 (1.47)	46	19.72 (0.47)	***	***	**	
15	3	0		88	32.26 (4.74)	46	25.76 (0.31)		***		
15	4	2	25.64 (1.04)	88	28.61 (2.50)	46	26.97 (1.00)		***		
16	1	75	22.25 (0.31)	106	22.59 (1.34)	27	22.14 (2.18)	*		**	
16	2	0		106	21.96 (1.61)	27	23.66 (0.63)		***		
16	3	0		106	25.74 (0.52)	27	33.76 (2.02)		***		
16	4	0		106	26.20 (1.42)	27	32.30 (4.29)		***		
17	1	75	22.25 (0.31)	66	22.32 (1.38)	45	22.47 (1.82)			*	
17	2	0		66	22.16 (1.55)	45	23.98 (0.54)		***		
17	3	0		66	25.52 (0.46)	45	34.19 (1.70)		***		
17	4	0		66	26.37 (1.35)	45	29.81 (4.06)		***		
18	1	76	21.47 (0.22)	66	22.95 (1.96)	37	26.58 (2.32)	***	***	***	
18	2	76	20.55 (0.18)	66	21.94 (1.57)	37	22.73 (1.61)	***	**	***	
18	3	6	28.00 (0.86)	66	26.23 (0.84)	37	35.43 (1.18)	***	***	***	
18	4	76	27.01 (0.91)	65	26.04 (1.47)	37	34.01 (2.01)	***	***	***	
19	1	76	20.68 (0.27)	109	23.23 (1.39)	29	22.93 (2.39)	***		***	
19	2	76	20.64 (0.22)	109	20.64 (1.01)	30	22.01 (1.35)	***	***	***	
19	3	0		109	25.85 (0.67)	30	34.95 (1.50)		***		
19	4	2	25.64 (1.04)	109	27.17 (1.64)	30	35.30 (2.50)		***		
20	1	76	20.68 (0.27)	53	23.34 (2.64)	46	21.47 (1.28)	***	***	***	
20	2	76	20.64 (0.22)	53	22.91 (1.39)	46	19.51 (0.83)	***	***	***	
20	3	0		53	32.99 (4.71)	46	25.52 (0.39)		***		
20	4	2	25.64 (1.04)	53	28.38 (3.53)	46	26.88 (0.78)				
21	1	76	21.47 (0.22)	125	23.22 (1.85)	22	25.19 (2.60)	***	**	***	
21	2	76	20.55 (0.18)	126	21.39 (1.71)	22	22.35 (1.22)	***	**	*	
21	3	6	28.00 (0.86)	126	26.62 (1.50)	22	36.29 (1.49)	***	***	**	
21	4	76	27.01 (0.91)	123	25.77 (2.28)	22	36.53 (1.13)	***	***	***	
22	1	75	22.25 (0.31)	109	21.70 (1.40)	30	23.29 (1.77)	*	***	***	
22	2	0		109	21.42 (1.45)	30	24.20 (1.23)		***		
22	3	0		108	25.96 (1.49)	30	33.55 (1.61)		***		
22	4	0		109	26.53 (0.97)	30	32.41 (4.16)		***		
23	1	4	22.95 (0.40)	100	21.92 (1.26)	33	23.01 (1.09)		***		
23	2	4	24.54 (1.08)	100	20.70 (0.93)	33	19.92 (0.29)	**	***	**	
23	3	4	26.00 (0.24)	99	26.54 (2.17)	28	35.02 (3.81)	**	***		
23	4	4	25.39 (0.40)	100	25.32 (1.47)	33	27.65 (3.35)		***		
24	1	22	23.28 (0.57)	57	30.92 (2.89)	47	26.58 (3.17)	***	***	***	
24	2	22	19.98 (0.58)	57	16.97 (0.56)	47	22.28 (3.21)	***	***	***	
24	3	22	26.59 (0.33)	57	28.99 (3.07)	47	35.15 (3.55)	***	***	***	
24	4	22	23.93 (0.21)	57	24.04 (0.47)	47	27.02 (3.73)	***	***		
25	1	33	23.29 (0.31)	100	22.05 (2.64)	58	22.85 (2.98)			**	
25	2	33	21.71 (0.30)	100	19.64 (1.56)	58	21.43 (2.31)		***	***	
25	3	33	28.37 (1.05)	100	26.87 (1.19)	57	32.31 (2.86)	***	***	***	
25	4	33	22.98 (0.21)	100	25.03 (1.16)	57	30.41 (3.89)	***	***	***	
26	1	33	23.29 (0.31)	53	26.36 (2.79)	45	23.31 (2.69)		***	***	
26	2	33	21.71 (0.30)	53	19.90 (1.94)	45	21.50 (3.18)		*	***	
26	3	33	28.37 (1.05)	53	26.52 (2.17)	45	34.36 (5.99)	***	***	***	
26	4	33	22.98 (0.21)	53	24.67 (0.31)	45	25.30 (2.51)	***		***	
27	1	33	23.29 (0.31)	98	23.58 (2.08)	57	22.24 (2.78)		**		
27	2	33	21.71 (0.30)	98	19.83 (2.26)	57	21.84 (2.77)		***	***	
27	3	33	28.37 (1.05)	98	25.99 (0.99)	56	34.15 (3.89)	***	***	***	
27	4	33	22.98 (0.21)	98	24.75 (0.51)	56	28.01 (3.43)	***	***	***	
28	1	33	24.12 (0.30)	94	21.75 (2.35)	55	21.78 (3.48)	**		***	
28	2	33	18.24 (0.29)	98	17.82 (0.97)	55	20.61 (2.43)	***	***	***	
28	3	33	23.82 (0.27)	95	29.10 (2.53)	54	31.96 (2.99)	***	***	***	
28	4	33	24.21 (0.27)	98	25.27 (0.67)	56	31.80 (2.67)	***	***	***	
29	1	33	23.29 (0.31)	74	19.78 (1.75)	79	23.88 (1.47)		***	***	

Continued on next page

Table A.2 Center of gravity of every subject and muscle group (continued)

RID	MG	n	Controls		Extension		Flexion		sig. post-hoc		
			M(SD)	n	M(SD)	n	M(SD)	n	c-f	e-f	c-e
29	2	33	21.71 (0.30)	74	19.44 (1.37)	79	20.54 (0.83)	***	***	***	
29	3	33	28.37 (1.05)	65	30.50 (3.80)	78	33.15 (2.28)	***	***		
29	4	33	22.98 (0.21)	74	24.33 (1.02)	79	26.63 (2.85)	***	***	***	
30	1	16	20.36 (0.29)	86	21.41 (1.45)	33	23.90 (1.66)	***	***	**	
30	2	16	22.10 (0.38)	86	18.59 (1.69)	33	18.26 (0.74)	***	***	***	
30	3	16	27.80 (0.22)	81	30.71 (3.99)	33	33.87 (1.56)	***	***	**	
30	4	16	27.10 (0.31)	85	31.47 (5.18)	33	32.72 (0.83)	***	***	**	
31	1	16	20.36 (0.29)	88	21.50 (1.11)	36	23.00 (1.27)	***	***	***	
31	2	16	22.10 (0.38)	88	21.58 (1.58)	36	20.83 (0.33)	***	***	***	
31	3	16	27.80 (0.22)	83	32.06 (4.87)	36	35.83 (1.53)	***	***	***	
31	4	16	27.10 (0.31)	85	31.27 (5.37)	34	35.47 (2.17)	***	***	***	
32	1	23	21.51 (0.40)	111	20.83 (0.63)	42	22.38 (1.79)	**	***	***	
32	2	23	21.61 (0.45)	108	21.36 (0.63)	42	20.64 (0.76)	***	***	*	
32	3	23	29.02 (0.53)	109	28.06 (2.84)	42	34.96 (1.30)	***	***	**	
32	4	23	28.70 (1.06)	109	27.84 (3.20)	42	33.67 (2.86)	***	***	**	
33	1	23	20.19 (0.32)	86	21.18 (0.82)	41	24.56 (1.08)	***	***	***	
33	2	23	22.12 (0.34)	86	21.47 (0.71)	41	21.21 (0.50)	***	**	***	
33	3	23	27.28 (0.34)	86	30.97 (4.30)	41	37.07 (1.34)	***	***	***	
33	4	23	26.86 (0.42)	83	31.64 (5.34)	41	36.76 (1.69)	***	***	***	
34	1	24	21.53 (0.14)	163	20.23 (0.51)	47	19.55 (2.06)	***	*	***	
34	2	24	19.76 (0.25)	163	20.37 (0.70)	47	19.82 (0.97)	***	***	***	
34	3	24	26.29 (0.28)	161	26.13 (2.00)	31	32.59 (2.39)	***	***		
34	4	24	24.74 (0.28)	154	26.61 (2.52)	43	26.73 (3.79)	*		***	
35	1	21	26.90 (0.46)	26	24.10 (0.52)	28	23.14 (0.50)	***	***	***	
35	2	21	22.65 (0.24)	26	27.42 (0.94)	28	26.14 (0.63)	***	***	***	
35	3	21	24.28 (0.23)	26	35.66 (1.13)	28	34.09 (1.44)	***	***	***	
35	4	21	26.09 (0.25)	26	35.65 (0.90)	28	33.83 (0.89)	***	***	***	
36	1	21	26.90 (0.46)	83	21.03 (2.32)	93	24.48 (1.42)	***	***	***	
36	2	21	22.65 (0.24)	83	18.88 (0.45)	94	21.78 (2.64)	***	***	***	
36	3	21	24.28 (0.23)	82	33.88 (3.88)	89	34.76 (1.72)	***		***	
36	4	21	26.09 (0.25)	83	29.39 (1.55)	94	35.23 (2.58)	***	***	***	
37	1	21	24.21 (1.09)	85	23.66 (0.99)	70	22.50 (1.17)	***	***		
37	2	21	24.39 (0.19)	85	24.53 (1.24)	70	24.30 (1.28)				
37	3	21	24.60 (0.24)	85	33.13 (1.72)	70	33.15 (1.92)	***		***	
37	4	21	26.51 (0.23)	85	33.84 (0.67)	70	32.92 (0.48)	***	***	***	
38	1	21	24.21 (1.09)	89	20.08 (1.97)	97	23.75 (1.42)		***	***	
38	2	21	24.39 (0.19)	89	19.38 (0.93)	97	20.06 (1.66)	***	***	***	
38	3	21	24.60 (0.24)	83	32.80 (3.70)	97	33.62 (1.43)	***		***	
38	4	21	26.51 (0.23)	89	26.80 (2.71)	97	34.98 (1.13)	***	***		
39	1	12	24.13 (1.63)	112	20.69 (2.46)	57	21.42 (0.83)	***		***	
39	2	12	25.27 (0.37)	118	20.50 (1.63)	56	20.92 (1.26)	***		***	
39	3	12	24.94 (0.44)	100	32.47 (1.99)	56	31.36 (1.24)	***	***	***	
39	4	12	25.07 (0.56)	61	30.50 (2.93)	56	31.04 (1.93)	***		***	

RID: recording identification number, MG: muscle group (1: quadriceps, 2: hamstrings, 3: tibialis anterior, 4: triceps surae), \*:  $p < .05$ , \*\*:  $p < .01$ , \*\*\*:  $p < .001$  (of pairwise Whitney-Mann-U tests, Bonferroni corrected).

## A.2 Source code

Listing A.1: SuperNeuron.py

```

1 from brian import *
2 from brian.library.random_processes import *
3 from brian.library.synapses import *
4 from MyConstants import *
5
6 class SuperNeuron:
7     def init(self):
8         return
9     def add_rand_curr(self, rand):
10        if rand:
11            self.eqgs+= '''dIrand/dt = (mu-Irand)*invtau_rand+sigma*((2.*
12                        invtau_rand)**.5)*xi : uA*cm**-2
13                        '''
14        else:
15            self.eqgs+= '''Irand : uA*cm**-2
16                        '''
17            Irand=0*uA*cm**-2
18
19    def add_synapses(self, synapse, tau1, tau2=1*ms):
20        if synapse=='alpha':
21            self.eqgs+=Equations( '''dge/dt = -ge*invtau : siemens*metre**-2
22                                dgi/dt = -gi*invtau : siemens*metre**-2
23                                dipsp/dt = (gi-ipsp)*invtau : siemens*metre**-2
24                                depsp/dt = (ge-epsp)*invtau : siemens*metre**-2
25                                ''' , invtau=1/tau1)
26        elif synapse=='exp':
27            self.eqgs+=Equations( '''
28                                dipsp/dt = -ipsp*invtau : siemens*metre**-2
29                                depsp/dt = -epsp*invtau : siemens*metre**-2
30                                ge = epsp
31                                gi = ipsp
32                                ''' , invtau=1/tau1)
33        elif synapse=='biexp':
34            self.eqgs+=Equations( '''dge/dt = -ge*invtau2 : siemens*metre**-2
35                                depsp/dt = (invpeak*ge-epsp)*invtau1 : siemens*metre**-2
36                                dgi/dt = -gi*invtau2 : siemens*metre**-2
37                                dipsp/dt = (invpeak*gi-ipsp)*invtau1 : siemens*metre**-2
38                                ''' , invtau1=1/tau1, invtau2=1/tau2, invpeak = (tau2 / tau1) **
39                                (tau1 / (tau2 - tau1)))
40        else:
41            self.eqgs+= '''ipsp = 0 *siemens*metre**-2:siemens*metre**-2
42                        epsp = 0 *siemens*metre**-2:siemens*metre**-2
43                        '''

```

Listing A.2: MoNeuron.py

```

1 from brian import *
2 from brian.library.random_processes import *
3 from brian.library.synapses import *
4 import SuperNeuron as SuperNeuronCl
5 from MyConstants import *
6
7 mS = msiemens
8
9 # Conductances (mS/cm^2)
10 GNa = 120 * mS/cm**2
11 GK_dr = 100 * mS/cm**2
12 GCa_NS = 14 * mS/cm**2
13 GCa_ND = .3 * mS/cm**2
14 GK_CaS = 5 * mS/cm**2 # 3.136
15 GK_CaD = 1.1 * mS/cm**2 # 0.69
16 GCa_L = 0.33 * mS/cm**2
17 gleak = 0.51 * mS/cm**2

```

```

18 GNapD = 0.1 *mS/cm**2#####
19
20 # Static parameters
21 gc = 0.1 * mS/cm**2 # coupling conductance (mS/cm^2)
22 p = 0.1
23 Kd = 0.2 * 10**-2*mole*dmetre**-3 # uM
24 f = 0.01 # percent free to bound Ca
25 alpha = 0.009 *mole/(amp*second)*um**-1# mol/C/um
26 kca = 2 * ms**-1 # Ca removal rate
27 base_eqs=Equations( '''
28     dh/dt= (hinf-h)/Tauh : 1
29     dn/dt= (ninf-n)/Taub : 1
30     dmnS/dt = (mnSinf-mnS)/TaubmN : 1
31     dhnS/dt = (hnSinf-hnS)/TaubhN : 1
32     dmnD/dt = (mnDinf-mnD)/TaubmN : 1
33     dhnD/dt = (hnDinf-hnD)/TaubhN : 1
34     dmnap/dt = (mnapinf-mnap)/Taubmap : 1
35     dhnap/dt = (hnapinf-hnap)/Taubhnap : 1
36     dm/dt = (minf-m)/Taubm : 1
37     dml/dt = (mlinf-ml)/TaubmL : 1
38     dCaS/dt = f*(-alpha*ICaS-kca*CaS) : mole*dmetre**-3
39     dCaD/dt = f*(-alpha*ICaD-kca*CaD) : mole*dmetre**-3
40     dvm/dt = 1/C*(-INaS-IKS-ICaS-IleakS-IcouplingS-Irand) : mV
41     dvd/dt = 1/C*(-INaD-IKD-ICaD-IleakD-IcouplingD-ISynI-ISynE) : mV
42
43     Tauh = 30/(exp((vm/mV+50)/15)+exp(-(vm/mV+50)/16))*ms : ms
44     Taub = 7/(exp((vm/mV+40)/40)+exp(-(vm/mV+40)/50))*ms : ms
45     Tauhnap = 1200/(cosh((vm/mV + 59)/16))*ms : ms
46     minf = 1/(1+exp((vm-Vhm)/Sm)) : 1
47     hinf = 1/(1+exp((vm-Vhh)/Sh)) : 1
48     ninf = 1/(1+exp((vm-Vhn)/Sn)) : 1
49     mnapinf = 1/(1+exp((vd-Vhmap)/Smnap)) : 1
50     hnapinf = 1/(1+exp((vd-Vhhnap)/Shnap)) : 1
51     mnSinf = 1/(1+exp((vm-VhmN)/SmN)) : 1
52     hnSinf = 1/(1+exp((vm-VhhN)/ShN)) : 1
53     mnDinf = 1/(1+exp((vd-VhmN)/SmN)) : 1
54     hnDinf = 1/(1+exp((vd-VhhN)/ShN)) : 1
55    mlinf = 1/(1+exp((vd-VhmL)/SmL)) : 1
56
57     INaD = dyn*GNapD*mnap*hnap*(vd-ENa) : mA*umetre**-2
58     INaS = dyn*GNaS*m**3*h*(vm-ENa) : mA*umetre**-2
59     IKS = dyn*(GK_dr*n**4 + GK_CaS*CaS/(CaS+Kd))*(vm-EK) : mA*umetre**-2
60     ICaS = dyn*GCa_NS*mnS**2*hnS*(vm-ECa) : mA*umetre**-2
61     IleakS = leak*(vm-ElleakS) : mA*umetre**-2
62     IcouplingS = gc/p*(vm-vd) : mA*umetre**-2
63     IKD = dyn*(GK_CaD*CaD/(CaD+Kd))*(vd-EK) : mA*umetre**-2
64     ICaD = dyn*(GCa_ND*mnD**2*hnD+GCa_L*ml)*(vd-ECa) : mA*umetre**-2
65     IleakD = leak*(vd-ElleakD) : mA*umetre**-2
66     IcouplingD = gc/(1-p)*(vd-vm) : mA*umetre**-2
67
68     ISynI = ipsp*(vd-Ei) : amp*umetre**-2
69     ISynE = (epsp+epsp_Aff*(1-Prsyn*f-presyn))*(vd-Ee) : amp*umetre**-2
70
71     depsp_Aff/dt = -epsp_Aff/tausyn : siemens*umetre**-2
72
73     dPrsyn/dt=(Prinf-Prsyn)/(0.0001*second) : 1
74     Prinf=1/(1+exp(6-xprsyn)) : 1
75     dxprsyn/dt=-xprsyn/(0.05*second) : 1
76
77     ElleakS : mV
78     ElleakD : mV
79
80     dyn : 1
81     f-presyn : 1
82     '''
83
84 class MnNeuronFactory (SuperNeuronCl.SuperNeuron):
85     def init(self, size,synapse='exp',Evariable=1,rand=False):
86         self.size = size
87         self.eqs = base_eqs
88         self.rand = rand
89         self.Evariable = Evariable
90         self.add_synapses(synapse,taul=tausyn)
91         self.add_rand_curr(rand)

```

## A. APPENDIX

```

92
93     self.Group=NeuronGroup( self.size , model=self.eqs ,
94                             threshold=EmpiricalThreshold( threshold=-20*mV,
95                                                             refractory=2*ms) ,
96                             implicit=True)
97
98     self.reinit()
99
100    return self.Group
101
102    def reinit( self ):
103        MnNeuronFactory.reinitNG( self.Group, self.Evariable)
104
105    @staticmethod
106    def reinitNG( Group, var ):
107        size = len(Group)
108        ivs= -60*mV
109        ivd= -60*mV
110        Group.vm= ivs
111        Group.vd= ivd
112        Group.dyn = 1
113        Group.h = 1/(1+exp((ivs-Vhh)/Sh))
114        Group.n = 1/(1+exp((ivs-Vhn)/Sn))
115        Group.mnS = 1/(1+exp((ivs-VhmN)/SmN))
116        Group.hnS = 1/(1+exp((ivs-VhhN)/ShN))
117        Group.mmD = 1/(1+exp((ivd-VhmN)/SmN))
118        Group.hnD = 1/(1+exp((ivd-VhhN)/ShN))
119        Group.ml = 1/(1+exp((ivd-VhmL)/SmL))
120        Group.m = 1/(1+exp((ivs-Vhm)/Sm))
121        Group.mnap = 1/(1+exp((ivd-Vhmnap)/Smnap))
122        Group.hnap = 1/(1+exp((ivd-Vhhnap)/Shnap))
123        Group.CaS = 0
124        Group.CaD = 0
125        Group.EleakS = (-65.0+randn(size)*6.5*var)*mV
126        Group.EleakD = (-65.0+randn(size)*3.25*var)*mV
127        Group.Prsyn = 0
128        Group.xprsyn = 0
129        Group.f_presyn = 0

```

Listing A.3: InNeuron.py

```

1  from brian import *
2  from brian.library.random_processes import *
3  from brian.library.synapses import *
4  import SuperNeuron as SuperNeuronCl
5  from MyConstants import *
6
7  class InNeuronFactory (SuperNeuronCl.SuperNeuron):
8      eqs=Equations( '''
9          dh/dt= (hinf-h)/Tauh : 1
10         dn/dt= (ninf-n)/Taubn : 1
11         dmnnap/dt = (mnnapinf-mnnap)/Taubmnap : 1
12         dhnap/dt = (hnnapinf-hnap)/Tauhnnap : 1
13         dm/dt = (minf-m)/Taubm : 1
14         dvm/dt = 1/C*(-INa-INap-IK-Ileak-ISynI-ISynE-Irand) : mV
15
16         Tauh = 30/(exp((vm/mV+50)/15)+exp(-(vm/mV+50)/16))*ms : ms
17         Taubn = 7/(exp((vm/mV+40)/40)+exp(-(vm/mV+40)/50))*ms : ms
18         Tauhnnap = 1200/(cosh((vm/mV + 59)/16))*ms : ms
19
20         minf = 1/(1+exp((vm-Vhm)/Sm)) : 1
21         hinf = 1/(1+exp((vm-Vhh)/Sh)) : 1
22         ninf = 1/(1+exp((vm-Vhn)/Sn)) : 1
23         mnnapinf = 1/(1+exp((vm-Vhmnap)/Smnap)) : 1
24         hnnapinf = 1/(1+exp((vm-Vhhnap)/Shnap)) : 1
25
26         INa = GNa*mnap*hnnap*(vm-ENa) : mA*umetre**-2
27         INa = GNa*m**3*h*(vm-ENa) : mA*umetre**-2
28         IK = GK*n**4*(vm-EK) : mA*umetre**-2
29         Ileak = gleak*(vm-Eleak) : mA*umetre**-2
30
31         gMlr = gEd * drive : siemens*umetre**-2

```



```

32
33
34 ISynI = (gMlr+ipsp)*(vm-Ei) : amp*metre**-2
35 ISynE = (gMlr+epsp)*(vm-Ee) : amp*metre**-2
36
37 GNa : msiemens*cm**-2
38 GNap : msiemens*cm**-2
39 GK : msiemens*cm**-2
40 gleak : msiemens*cm**-2
41 Eleak : mV
42
43 drive : 1
44 ''')
45 def init(self, N_RG=0,N_PF=0,N_IN=0,N_INRG=0,synapse='exp',Evariable=1,
46         rand=False):
47     self.add_synapses(synapse,tau1=tausyn)
48     self.add_rand_curr(rand)
49     self.rand=rand
50     self.Evariable = Evariable
51     self.N_RG = N_RG
52     self.N_PF = N_PF
53     self.N_IN = N_IN
54     self.N_INRG = N_INRG
55     self.Group=NeuronGroup(self.N_RG+self.N_PF+self.N_IN+self.N_INRG,
56                             model=self.eqs,
57                             threshold=EmpiricalThreshold(threshold=0*mV,refractory=3*ms),
58                             implicit=True)
59     self.SG_RG = self.Group.subgroup(self.N_RG)
60     self.SG_PF = self.Group.subgroup(self.N_PF)
61     self.SG_IN = self.Group.subgroup(self.N_IN)
62     self.SG_INRG = self.Group.subgroup(self.N_INRG)
63     #print self.eqs
64     self.reinit()
65     return self.Group
66
67 def reinit(self):
68     if self.N_RG != 0:
69
70         self.SG_RG.GNa = 30 * msiemens*cm**-2
71         self.SG_RG.GNap = 0.25 * msiemens*cm**-2
72         self.SG_RG.GK = 1 * msiemens*cm**-2
73         self.SG_RG.gleak = 0.1 * msiemens*cm**-2
74         self.SG_RG.Eleak = (-64+randn(self.N_RG)*0.64*self.Evariable) *
75             mV
76
77         self.SG_RG.drive = 0.5
78
79     if self.N_PF != 0:
80
81         self.SG_PF.GNa = 30 * msiemens*cm**-2
82         self.SG_PF.GNap = 0.1 * msiemens*cm**-2
83         self.SG_PF.GK = 1.2 * msiemens*cm**-2
84         self.SG_PF.gleak = 0.1 * msiemens*cm**-2
85         self.SG_PF.Eleak = (-64+randn(self.N_PF)*0.64*self.Evariable) *
86             mV
87
88         self.SG_PF.drive = 0.5
89
90     if self.N_IN != 0:
91
92         self.SG_IN.GNa = 120 * msiemens*cm**-2
93         self.SG_IN.GNap = 0 * msiemens*cm**-2
94         self.SG_IN.GK = 100 * msiemens*cm**-2
95         self.SG_IN.gleak = 0.51 * msiemens*cm**-2
96         self.SG_IN.Eleak = (-64+randn(self.N_IN)*3.2*self.Evariable) * mV
97
98         self.SG_IN.drive = 0
99
100     if self.N_INRG != 0:
101
102         self.SG_INRG.GNa = 120 * msiemens*cm**-2
103         self.SG_INRG.GNap = 0 * msiemens*cm**-2
104         self.SG_INRG.GK = 100 * msiemens*cm**-2
105         self.SG_INRG.gleak = 0.51 * msiemens*cm**-2

```

## A. APPENDIX

---

```
102         self.SG_INRG.Eleak = (-57.5+randn(self.N_INRG)*2.875*self.  
103             Evariable) * mV  
104         self.SG_INRG.drive = 0  
105         self.Group.v_m = -70*mV  
106         self.Group.m_nap = 1/(1+exp((self.Group.v_m-V_hmnap)/S_mnap))  
107         self.Group.h_nap = 1/(1+exp((self.Group.v_m-V_hhnap)/S_hnap))  
108         self.Group.m = 1/(1+exp((self.Group.v_m-V_hm)/S_m))  
109         self.Group.h = 1/(1+exp((self.Group.v_m-V_hh)/S_h))  
110         self.Group.n = 1/(1+exp((self.Group.v_m-V_hn)/S_n))
```

Listing A.4: MyConstants.py

```
1  from brian import *  
2  
3  # Half Activation V_h, Slopes S, Time Constants Tau  
4  V_hm = -35*mV  
5  S_m = -7.8*mV  
6  V_hh = -55*mV  
7  S_h = 7*mV  
8  V_hn = -28*mV  
9  S_n = -15*mV  
10 V_hmN = -30*mV  
11 S_mN = -5*mV  
12 V_hhN = -45*mV  
13 S_hN = 5*mV  
14 V_hmL = -40*mV  
15 S_mL = -7*mV  
16 V_hmnap = -47.1*mV  
17 S_mnap = -3.1*mV  
18 V_hhnap = -59*mV  
19 S_hnap = 8*mV  
20 Tau_mN = 4 *ms  
21 Tau_hN = 40*ms  
22 Tau_mL = 40*ms  
23 Tau_m = 0.00001*ms  
24 Tau_mnap = Tau_m  
25 C = 1 * uF/cm**2  
26  
27 tau_syn = 5*ms  
28  
29 # Reversal potentials in mV  
30 E_Na = 55 * mV  
31 E_K = -80 * mV  
32 E_Ca = 80 * mV  
33 E_e = -10*mV  
34 E_i = -70*mV  
35  
36 g_Id = 0.05*msiemens*cm**-2  
37 g_Ed = 0.05*msiemens*cm**-2  
38 g_SynE = 0.05*msiemens*cm**-2  
39 g_SynI = 0.05*msiemens*cm**-2  
40  
41  
42 mu = 0*uA*cm**-2  
43 sigma = .08*uA*cm**-2  
44 invtau_rand = 1/(20*ms)
```

Listing A.5: Rybak.py

```
1  from brian import *  
2  from brian.library.random_processes import *  
3  from brian.library.synapses import *  
4  import random  
5  import MoNeuron as Moto  
6  import InNeuron as IN  
7  import time  
8  from MyConstants import g_SynE, g_SynI
```

```

9  from matplotlib.backends.backend_pdf import PdfPages, new_figure_manager
10 import h5py
11 import os
12
13 class rybak(object):
14     additional_in=0
15     binsize = 30*ms
16     stype = 'exp'
17     Mstype = 'exp'
18     def plot_hist(self, ratemonitor):
19         bar(ratemonitor.times/ms, ratemonitor.rate, width=self.binsize/ms, color
            ='w')
20
21     def plot_spike(self, spikemon):
22         raster_plot(spikemon)
23
24     def plot_simple(self, trace):
25         plot(trace.times/ms, trace[0]/mV)
26
27     def plot_all(self, n, fun, lst):
28         fig=figure(n)
29         for i in xrange(0, lst.__len__()):
30             subplot(lst.__len__(), 1, i+1)
31             fun(lst[i])
32             fig.axes[i].set_xlim(0, self.DUR/ms)
33
34     return fig
35
36     def reinit_monitors(self, lst):
37         for i in xrange(0, lst.__len__()):
38             lst[i].reinit()
39
40     def __init__(self, Evar=1, rand=False):
41         random.seed(os.getpid()+int(round(time.time() * 1e6)))
42         self.Evar=Evar
43         self.rand=rand
44         self.setup_neurons()
45         self.setup_connections()
46         self.setup_monitors()
47         self.setup_network_operations()
48
49
50     def setup_neurons(self):
51         self.MNFactory=Moto.MnNeuronFactory()
52         self.MN=self.MNFactory.init(42, self.Mstype, self.Evar, self.rand)
53         self.INFactory=IN.InNeuronFactory()
54         self.P=self.INFactory.init(40,40,120+self.additional_in,40, self.stype
            , self.Evar, self.rand)
55         print 'init'
56         self.RG_E = self.INFactory.SG_RG.subgroup(20)
57         self.RG_F = self.INFactory.SG_RG.subgroup(20)
58
59
60         self.PF_E = self.INFactory.SG_PF.subgroup(20)
61         self.PF_F = self.INFactory.SG_PF.subgroup(20)
62
63         #uncomment one of those lines to simulate resetting or non-resetting
64         deletions
65         #self.PF_F.drive = TimedArray([0.5, 0.95, 0.5], start=0*ms, dt=5*second
66         )
67         #self.PF_F.drive = TimedArray([0.5,0.5, 0.5, 0.5,0.0,0.5,0.95,0.5],
68         start=0*ms, dt=4*second)
69         #self.PF_F.drive = TimedArray([0.5,0.5, 0, 0.5,1.5,0.5,1.0,0.5], start
70         =0*ms, dt=4*second)
71
72         self.INRG_E = self.INFactory.SG_INRG.subgroup(20)
73         self.INRG_F = self.INFactory.SG_INRG.subgroup(20)
74
75         self.INPF_E = self.INFactory.SG_IN.subgroup(20)
76         self.INPF_F = self.INFactory.SG_IN.subgroup(20)
77
78         self.IA_E = self.INFactory.SG_IN.subgroup(20)
79         self.IA_F = self.INFactory.SG_IN.subgroup(20)
80

```

## A. APPENDIX

---

```

77     self.R_E = self.INFactory.SG.IN.subgroup(20)
78     self.R_F = self.INFactory.SG.IN.subgroup(20)
79
80     self.MN_E = self.MN.subgroup(21)
81     self.MN_F = self.MN.subgroup(21)
82
83     self.realMN_E = self.MN_E.subgroup(20)
84     self.fakeMN_E = self.MN_E.subgroup(1)
85
86     self.realMN_F = self.MN_F.subgroup(20)
87     self.fakeMN_F = self.MN_F.subgroup(1)
88
89     self.net = Network(self.P, self.MN)
90
91     def setup_connections(self, use_delay=False):
92         #Connections
93         delay_mean=2*ms
94         delay_std=0.5*ms
95         self.RG_E_INRG_F=Connection(self.RG_E, self.INRG_F, 'ge', weight=gSynE
          *0.45, sparseness=1, structure='dense', max_delay=10*ms if
          use_delay else 0 *ms, delay= lambda i, j: delay_mean+randn(20)*
          delay_std if use_delay else 0*ms);
96         self.RG_F_INRG_E=Connection(self.RG_F, self.INRG_E, 'ge', weight=gSynE
          *0.45, sparseness=1, structure='dense', max_delay=10*ms if
          use_delay else 0 *ms, delay= lambda i, j: delay_mean+randn(20)*
          delay_std if use_delay else 0*ms);
97         self.net.add(self.RG_E_INRG_F, self.RG_F_INRG_E)
98
99         self.RG_E_self=Connection(self.RG_E, self.RG_E, 'ge', weight=gSynE
          *0.0125, sparseness=1, structure='dense', max_delay=10*ms if
          use_delay else 0 *ms, delay= lambda i, j: delay_mean+randn(20)*
          delay_std if use_delay else 0*ms);
100        self.RG_F_self=Connection(self.RG_F, self.RG_F, 'ge', weight=gSynE
          *0.0125, sparseness=1, structure='dense', max_delay=10*ms if
          use_delay else 0 *ms, delay= lambda i, j: delay_mean+randn(20)*
          delay_std if use_delay else 0*ms);
101        self.net.add(self.RG_E_self, self.RG_F_self)
102
103        self.RG_E_RG_F=Connection(self.RG_E, self.RG_F, 'ge', weight=gSynE
          *0.0125, sparseness=1, structure='dense', max_delay=10*ms if
          use_delay else 0 *ms, delay= lambda i, j: delay_mean+randn(20)*
          delay_std if use_delay else 0*ms);
104        self.RG_F_RG_E=Connection(self.RG_F, self.RG_E, 'ge', weight=gSynE
          *0.0125, sparseness=1, structure='dense', max_delay=10*ms if
          use_delay else 0 *ms, delay= lambda i, j: delay_mean+randn(20)*
          delay_std if use_delay else 0*ms);
105        self.net.add(self.RG_E_RG_F, self.RG_F_RG_E)
106
107        self.INRG_E_RG_E=Connection(self.INRG_E, self.RG_E, 'gi', weight=gSynI
          *0.115, sparseness=1, structure='dense', max_delay=10*ms if
          use_delay else 0 *ms, delay= lambda i, j: delay_mean+randn(20)*
          delay_std if use_delay else 0*ms);
108        self.INRG_F_RG_E=Connection(self.INRG_F, self.RG_F, 'gi', weight=gSynI
          *0.115, sparseness=1, structure='dense', max_delay=10*ms if
          use_delay else 0 *ms, delay= lambda i, j: delay_mean+randn(20)*
          delay_std if use_delay else 0*ms);
109        self.net.add(self.INRG_E_RG_E, self.INRG_F_RG_E)
110
111        self.RG_E_PF_E=Connection(self.RG_E, self.PF_E, 'ge', weight=gSynE
          *0.0075, sparseness=1, structure='dense', max_delay=10*ms if
          use_delay else 0 *ms, delay= lambda i, j: delay_mean+randn(20)*
          delay_std if use_delay else 0*ms);
112        self.RG_F_PF_F=Connection(self.RG_F, self.PF_F, 'ge', weight=gSynE
          *0.0075, sparseness=1, structure='dense', max_delay=10*ms if
          use_delay else 0 *ms, delay= lambda i, j: delay_mean+randn(20)*
          delay_std if use_delay else 0*ms);
113        self.net.add(self.RG_E_PF_E, self.RG_F_PF_F)
114
115        self.INRG_E_PF_E=Connection(self.INRG_E, self.PF_E, 'gi', weight=gSynI
          *0.05, sparseness=1, structure='dense', max_delay=10*ms if
          use_delay else 0 *ms, delay= lambda i, j: delay_mean+randn(20)*
          delay_std if use_delay else 0*ms);
116        self.INRG_F_PF_E=Connection(self.INRG_F, self.PF_F, 'gi', weight=gSynI
          *0.05, sparseness=1, structure='dense', max_delay=10*ms if

```

```

    use_delay else 0 *ms, delay= lambda i, j: delay_mean+randn(20)*
    delay_std if use_delay else 0*ms);
117 self.net.add(self.INRG_E_PPF_E, self.INRG_F_PPF_E)
118
119 self.INPF_E_PPF_E=Connection(self.INPF_E, self.PPF_E, 'gi', weight=gSynI
    *0.35, sparseness=1, structure='dense', max_delay=10*ms if
    use_delay else 0 *ms, delay= lambda i, j: delay_mean+randn(20)*
    delay_std if use_delay else 0*ms);
120 self.INPF_F_PPF_F=Connection(self.INPF_F, self.PPF_F, 'gi', weight=gSynI
    *0.35, sparseness=1, structure='dense', max_delay=10*ms if
    use_delay else 0 *ms, delay= lambda i, j: delay_mean+randn(20)*
    delay_std if use_delay else 0*ms);
121 self.net.add(self.INPF_E_PPF_E, self.INPF_F_PPF_F)
122
123 self.PPF_E_INPF_F=Connection(self.PPF_E, self.INPF_F, 'ge', weight=gSynE
    *0.2, sparseness=1, structure='dense', max_delay=10*ms if use_delay
    else 0 *ms, delay= lambda i, j: delay_mean+randn(20)*delay_std if
    use_delay else 0*ms);
124 self.PPF_F_INPF_E=Connection(self.PPF_F, self.INPF_E, 'ge', weight=gSynE
    *0.2, sparseness=1, structure='dense', max_delay=10*ms if use_delay
    else 0 *ms, delay= lambda i, j: delay_mean+randn(20)*delay_std if
    use_delay else 0*ms);
125 self.net.add(self.PPF_E_INPF_F, self.PPF_F_INPF_E)
126
127 self.PPF_E_IA_E=Connection(self.PPF_E, self.IA_E, 'ge', weight=gSynE*0.4,
    sparseness=1, structure='dense', max_delay=10*ms if use_delay else
    0 *ms, delay= lambda i, j: delay_mean+randn(20)*delay_std if
    use_delay else 0*ms);
128 self.PPF_F_IA_F=Connection(self.PPF_F, self.IA_F, 'ge', weight=gSynE*0.4,
    sparseness=1, structure='dense', max_delay=10*ms if use_delay else
    0 *ms, delay= lambda i, j: delay_mean+randn(20)*delay_std if
    use_delay else 0*ms);
129 self.net.add(self.PPF_E_IA_E, self.PPF_F_IA_F)
130
131 self.IA_F_IA_E=Connection(self.IA_F, self.IA_E, 'gi', weight=gSynI*0.1,
    sparseness=1, structure='dense', max_delay=10*ms if use_delay else
    0 *ms, delay= lambda i, j: delay_mean+randn(20)*delay_std if
    use_delay else 0*ms);
132 self.IA_E_IA_F=Connection(self.IA_E, self.IA_F, 'gi', weight=gSynI*0.1,
    sparseness=1, structure='dense', max_delay=10*ms if use_delay else
    0 *ms, delay= lambda i, j: delay_mean+randn(20)*delay_std if
    use_delay else 0*ms);
133 self.net.add(self.IA_F_IA_E, self.IA_E_IA_F)
134
135 self.R_E_IA_E=Connection(self.R_E, self.IA_E, 'gi', weight=gSynI*0.1,
    sparseness=1, structure='dense', max_delay=10*ms if use_delay else
    0 *ms, delay= lambda i, j: delay_mean+randn(20)*delay_std if
    use_delay else 0*ms);
136 self.R_F_IA_F=Connection(self.R_F, self.IA_F, 'gi', weight=gSynI*0.1,
    sparseness=1, structure='dense', max_delay=10*ms if use_delay else
    0 *ms, delay= lambda i, j: delay_mean+randn(20)*delay_std if
    use_delay else 0*ms);
137 self.net.add(self.IA_F_IA_E, self.IA_E_IA_F)
138
139 self.MN_E_R_E=Connection(self.MN_E, self.R_E, 'ge', weight=gSynE*0.25,
    sparseness=1, structure='dense', max_delay=10*ms if use_delay else
    0 *ms, delay= lambda i, j: delay_mean+randn(20)*delay_std if
    use_delay else 0*ms);
140 self.MN_F_R_F=Connection(self.MN_F, self.R_F, 'ge', weight=gSynE*0.25,
    sparseness=1, structure='dense', max_delay=10*ms if use_delay else
    0 *ms, delay= lambda i, j: delay_mean+randn(20)*delay_std if
    use_delay else 0*ms);
141 self.net.add(self.MN_E_R_E, self.MN_F_R_F)
142
143 self.R_F_R_E=Connection(self.R_F, self.R_E, 'gi', weight=gSynI*0.1,
    sparseness=1, structure='dense', max_delay=10*ms if use_delay else
    0 *ms, delay= lambda i, j: delay_mean+randn(20)*delay_std if
    use_delay else 0*ms);
144 self.R_E_R_F=Connection(self.R_E, self.R_F, 'gi', weight=gSynI*0.1,
    sparseness=1, structure='dense', max_delay=10*ms if use_delay else
    0 *ms, delay= lambda i, j: delay_mean+randn(20)*delay_std if
    use_delay else 0*ms);
145 self.net.add(self.R_F_R_E, self.R_E_R_F)
146

```

## A. APPENDIX

---

```

147     self.PF_E_MN_E=Connection(self.PF_E, self.MN_E, 'ge', weight=gSynE*0.5,
148                               sparseness=1, structure='dense', max_delay=10*ms if use_delay else
149                               0 *ms, delay= lambda i, j: delay_mean+randn(21)*delay_std if
150                               use_delay else 0*ms);
151     self.PF_F_MN_F=Connection(self.PF_F, self.MN_F, 'ge', weight=gSynE*0.5,
152                               sparseness=1, structure='dense', max_delay=10*ms if use_delay else
153                               0 *ms, delay= lambda i, j: delay_mean+randn(21)*delay_std if
154                               use_delay else 0*ms);
155     self.net.add(self.PF_E_MN_E, self.PF_F_MN_F)
156
157     self.R_E_MN_E=Connection(self.R_E, self.MN_E, 'gi', weight=gSynI*0.2,
158                               sparseness=1, structure='dense', max_delay=10*ms if use_delay else
159                               0 *ms, delay= lambda i, j: delay_mean+randn(21)*delay_std if
160                               use_delay else 0*ms);
161     self.R_F_MN_F=Connection(self.R_F, self.MN_F, 'gi', weight=gSynI*0.2,
162                               sparseness=1, structure='dense', max_delay=10*ms if use_delay else
163                               0 *ms, delay= lambda i, j: delay_mean+randn(21)*delay_std if
164                               use_delay else 0*ms);
165     self.net.add(self.R_E_MN_E, self.R_F_MN_F)
166
167     self.IA_F_MN_E=Connection(self.IA_F, self.MN_E, 'gi', weight=gSynI*0.6,
168                               sparseness=1, structure='dense', max_delay=10*ms if use_delay else
169                               0 *ms, delay= lambda i, j: delay_mean+randn(21)*delay_std if
170                               use_delay else 0*ms);
171     self.IA_E_MN_F=Connection(self.IA_E, self.MN_F, 'gi', weight=gSynI*0.6,
172                               sparseness=1, structure='dense', max_delay=10*ms if use_delay else
173                               0 *ms, delay= lambda i, j: delay_mean+randn(21)*delay_std if
174                               use_delay else 0*ms);
175     self.net.add(self.IA_F_MN_E, self.IA_E_MN_F)
176
177     def setup_monitors(self):
178         self.traceRGE=StateMonitor(self.RG_E, 'vm', record=True)
179         self.traceRGF=StateMonitor(self.RG_F, 'vm', record=True)
180         self.spikesRGE=SpikeMonitor(self.RG_E)
181         self.spikesRGF=SpikeMonitor(self.RG_F)
182
183         self.traceINRGE=StateMonitor(self.INRG_E, 'vm', record=True)
184         self.traceINRGF=StateMonitor(self.INRG_F, 'vm', record=True)
185         self.spikesINRGE=SpikeMonitor(self.INRG_E)
186         self.spikesINRGF=SpikeMonitor(self.INRG_F)
187
188         self.tracePFE=StateMonitor(self.PF_E, 'vm', record=True)
189         self.tracePFF=StateMonitor(self.PF_F, 'vm', record=True)
190         self.spikesPFE=SpikeMonitor(self.PF_E)
191         self.spikesPFF=SpikeMonitor(self.PF_F)
192
193         self.traceMNE=StateMonitor(self.MN_E, 'vm', record=True)
194         self.traceMNF=StateMonitor(self.MN_F, 'vm', record=True)
195         self.spikesMNE=SpikeMonitor(self.MN_E)
196         self.spikesMNF=SpikeMonitor(self.MN_F)
197
198         self.PRRGE=PopulationRateMonitor(self.RG_E, self.binsize)
199         self.PRRGF=PopulationRateMonitor(self.RG_F, self.binsize)
200
201         self.PRPFE=PopulationRateMonitor(self.PF_E, self.binsize)
202         self.PRPFF=PopulationRateMonitor(self.PF_F, self.binsize)
203
204         self.PRMNE=PopulationRateMonitor(self.MN_E, self.binsize)
205         self.PRMNF=PopulationRateMonitor(self.MN_F, self.binsize)
206
207         self.net.add(self.PRRGE, self.PRRGF, self.PRPFE, self.PRPFF, self.PRMNE,
208                     self.PRMNF, self.traceINRGE, self.traceINRGF, self.spikesINRGE, self.
209                     spikesINRGF, self.traceRGE, self.traceRGF, self.spikesRGE, self.
210                     spikesRGF, self.spikesPFE, self.spikesPFF, self.traceMNE, self.
211                     traceMNF, self.spikesMNE, self.spikesMNF, self.tracePFE, self.
212                     tracePFF)
213
214         self.SPMonitorNames = list()
215         self.SPMonitorNames.append("RGE")
216         self.SPMonitorNames.append("RGF")
217         self.SPMonitorNames.append("PFE")
218         self.SPMonitorNames.append("PFF")

```

```

198     self.SPMonitorNames.append("MNE")
199     self.SPMonitorNames.append("MNF")
200
201     self.TrMonitorNames = list()
202     self.TrMonitorNames.append("RGE")
203     self.TrMonitorNames.append("RGF")
204     self.TrMonitorNames.append("PFE")
205     self.TrMonitorNames.append("PFF")
206     self.TrMonitorNames.append("MNE")
207     self.TrMonitorNames.append("MNF")
208
209     self.Tracelist = list()
210     self.Tracelist.append(self.traceRGE)
211     self.Tracelist.append(self.traceRGF)
212     self.Tracelist.append(self.tracePFE)
213     self.Tracelist.append(self.tracePFF)
214     self.Tracelist.append(self.traceMNE)
215     self.Tracelist.append(self.traceMNF)
216
217     self.PRlist = list()
218     self.PRlist.append(self.PRRGE)
219     self.PRlist.append(self.PRRGF)
220     self.PRlist.append(self.PRPFE)
221     self.PRlist.append(self.PRPF)
222     self.PRlist.append(self.PRMNE)
223     self.PRlist.append(self.PRMNF)
224
225     self.Spikelist = list()
226     self.Spikelist.append(self.spikesRGE)
227     self.Spikelist.append(self.spikesRGF)
228     self.Spikelist.append(self.spikesPFE)
229     self.Spikelist.append(self.spikesPFF)
230     self.Spikelist.append(self.spikesMNE)
231     self.Spikelist.append(self.spikesMNF)
232
233     self.trace_MNE_ipsp=StateMonitor(self.MN_E, 'epsp_Aff', record=True)
234     self.trace_MNE_epsp=StateMonitor(self.MN_E, 'epsp', record=True)
235     self.trace_MNF_ipsp=StateMonitor(self.MN_F, 'epsp_Aff', record=True)
236     self.trace_MNF_epsp=StateMonitor(self.MN_F, 'epsp', record=True)
237     self.net.add(self.trace_MNE_epsp, self.trace_MNE_ipsp, self.
        trace_MNF_epsp, self.trace_MNF_ipsp)
238
239     self.MN_PSPlist = list()
240     self.MN_PSPlist.append(self.trace_MNE_ipsp)
241     self.MN_PSPlist.append(self.trace_MNE_epsp)
242     self.MN_PSPlist.append(self.trace_MNF_ipsp)
243     self.MN_PSPlist.append(self.trace_MNF_epsp)
244
245     #trace fake (no ion dynamics) MN
246     self.trace_fakeMNE = StateMonitor(self.fakeMN_E, 'vm', record=True)
247     self.trace_fakeMNF = StateMonitor(self.fakeMN_F, 'vm', record=True)
248     self.net.add(self.trace_fakeMNE, self.trace_fakeMNF)
249
250     self.fakeMNlist=list()
251     self.fakeMNlist.append(self.trace_fakeMNE)
252     self.fakeMNlist.append(self.trace_fakeMNF)
253
254     def setup_network_operations(self):
255         @network_operation(clock=EventClock(dt=200*ms))
256         def progress(clk):
257             print clk._t
258             return
259         self.net.add(progress)
260
261     def __call__(self, para, value, DUR=20*second, report=0, display=False,
262         filename='run', run=True):
263         self.net.reinit(states=True)
264         self.MNFactory.reinit()
265         self.INFactory.reinit()
266         self.reinit_monitors(self.Spikelist + self.PRlist + self.Tracelist)
267
268         Moto.MnNeuronFactory.reinitNG(self.fakeMN_E, 0)
269         Moto.MnNeuronFactory.reinitNG(self.fakeMN_F, 0)
270         self.fakeMN_E.dyn = 0

```

## A. APPENDIX

---

```

270         self.fakeMN_F.dyn = 0
271
272         self.filename = filename + str(int(round(time.time() * 1000)))
273         for i in range(0, len(para)):
274             self.filename = self.filename + '-' + para[i] + '=' + value[i]
275         self.filename = self.filename + '.pdf'
276         self.DUR = DUR
277         self.report = report
278         self.display = display
279         #self.RG.E.drive = TimedArray([0, 0.5, 0.5, 0.9], dt=1*second)
280         if run:
281             self.inject_assignments(para, value)
282             self.run()
283         #return self
284
285     def inject_assignments(self, para, value):
286         if len(para) == len(value):
287             for i in range(0, len(para)):
288                 exec 'self.' + para[i] + '=' + value[i]
289                 print 'self.' + para[i] + '=' + value[i]
290
291     def run(self):
292         start = time.clock()
293         if self.report == 0:
294             self.net.run(self.DUR)
295         else:
296             self.net.run(self.DUR, report=self.report)
297         stop = time.clock()
298         print 'Duration: ' + str(stop-start)
299         print 'Time to simulate 1 s : ' + str((stop-start)/(self.DUR/second))
300         self.plot(self.display)
301
302     def plot(self, display=False):
303         self.filename=self.filename.replace('*', '.')
304         self.filename=self.filename.replace('/', '.')
305         lt = time.localtime(time.time())
306         self.path = './output/' + str(lt[0]) + ("%02d" % lt[1]) + ("%02d" % lt
307             [2])
308         if not os.path.isdir(self.path):
309             os.makedirs(self.path)
310         self.filename=self.path + '/' +self.filename
311         pp = PdfPages(self.filename)
312
313         fig1 = self.plot_all(1, self.plot_simple, self.Tracelist)
314         fig2 = self.plot_all(2, self.plot_spike, self.Spikelist)
315         fig3 = self.plot_all(3, self.plot_hist, self.PRlist)
316         fig4 = self.plot_all(4, self.plot_simple, self.MN_PSPlist)
317         fig5 = self.plot_all(5, self.plot_simple, self.fakeMNlist)
318
319         fig1.set_size_inches(40,20)
320         fig2.set_size_inches(40,20)
321         fig3.set_size_inches(40,20)
322         fig4.set_size_inches(40,20)
323         fig5.set_size_inches(40,20)
324
325         f=h5py.File(self.filename+'.hdf5', 'w')
326         f.filename
327         for i in xrange(0, self.TrMonitorNames.__len__()):
328             if len(self.Tracelist)>i:
329                 if i<6:
330                     nspikes=zeros((self.Tracelist[i].values.shape[0],1))
331                     for j in xrange(0, self.Tracelist[i].values.shape[0]-1):
332                         nspikes[j]=size(self.Spikelist[i].spiketimes[j])
333
334                     f.create_dataset('trace'+self.TrMonitorNames[i],
335                                     data=self.Tracelist[i].values[[
336                                         argmax(nspikes), argsort(
337                                             nspikes,0)[10][0], argmin(
338                                                 nspikes)]] .astype(float32),
339                                     compression='gzip',
340                                     compression_opts=9)
341
342                 else:
343                     f.create_dataset('trace'+self.TrMonitorNames[i],
344                                     data=self.Tracelist[i].values

```



```

339         .astype(float32),
340         compression="gzip",
341         compression_opts=9)
342     for i in xrange(0, self.SPMonitorNames.__len__()):
343         if len(self.Spikelist)>i:
344             f.create_dataset('spikes'+self.SPMonitorNames[i],
345                             data=self.Spikelist[i].spikes,
346                             compression="gzip", compression_opts
347                             =9)
348     f.create_dataset('traceFakeMNE', data=self.trace_fakeMNE.values.astype
349                     (float32),
350                     compression="gzip", compression_opts=9)
351     f.create_dataset('traceFakeMNF', data=self.trace_fakeMNF.values.astype
352                     (float32),
353                     compression="gzip", compression_opts=9)
354     f.flush()
355     f.close()
356     pp.savefig(fig1)
357     pp.savefig(fig2)
358     pp.savefig(fig3)
359     pp.savefig(fig4)
360     pp.savefig(fig5)
361     pp.close()
362     if display==True:
363         show()
364     else:
365         close('all')
366
367 @staticmethod
368 def showarraysmem(obj, name='', n=0):
369     if n>30:
370         return
371     if isinstance(obj, ndarray):
372         size_MB = obj.nbytes/1024.**2
373         if size_MB>1.0:
374             print name, int(size_MB), 'MB'
375     else:
376         if hasattr(obj, '__dict__'):
377             for x, y in obj.__dict__.iteritems():
378                 if len(name):
379                     namex = name+'.'+x
380                 else:
381                     namex = x
382             rybak.showarraysmem(y, namex, n+1)

```

Listing A.6: ModelA.py

```

1 from brian import *
2 from brian.library.random_processes import *
3 from brian.library.synapses import *
4 import MoNeuron as Moto
5 import InNeuron as IN
6 from time import clock
7 from MyConstants import gSynE, gSynI
8 from matplotlib.backends.backend_pdf import PdfPages
9 from Rybak import *
10
11 use_delay = True
12 delay_mean = 2 * ms
13 delay_std = 0.5 * ms
14
15 class modelA(rybak):
16     def __init__(self):
17         self.stype = 'alpha'
18         self.Mstype = 'alpha'
19         super(modelA, self).__init__(1, False)
20
21     def setup_connections(self):
22         self.inputfreq = 30 * Hz

```

## A. APPENDIX

---

```

23
24     self.spiketimes = []
25     for i in xrange(0, 20):
26         self.spiketimes.append((i, 5 * ms))
27
28     self.AfferentInput = SpikeGeneratorGroup(20, self.spiketimes, period
29         =1 / self.inputfreq)
30
31     self.CIN_RGE = Connection(self.AfferentInput, self.RG_E, 'ge', weight
32         =gSynE * 0.08, sparseness=1, structure='dense', max_delay=10 *
33         ms if use_delay else 0 * ms, delay=lambdai, j:delay_mean +
34         randn(20) * delay_std if use_delay else 0 * ms)
35     self.CIN_RGF = Connection(self.AfferentInput, self.RG_F, 'ge', weight
36         =gSynE * 0.075, sparseness=1, structure='dense', max_delay=10 *
37         ms if use_delay else 0 * ms, delay=lambdai, j:delay_mean +
38         randn(20) * delay_std if use_delay else 0 * ms)
39
40     self.CIN_PFE = Connection(self.AfferentInput, self.PF_E, 'ge', weight
41         =gSynE * 0.08, sparseness=1, structure='dense', max_delay=10 *
42         ms if use_delay else 0 * ms, delay=lambdai, j:delay_mean +
43         randn(20) * delay_std if use_delay else 0 * ms)
44     self.CIN_PFF = Connection(self.AfferentInput, self.PF_F, 'ge', weight
45         =gSynE * 0.08, sparseness=1, structure='dense', max_delay=10 *
46         ms if use_delay else 0 * ms, delay=lambdai, j:delay_mean +
47         randn(20) * delay_std if use_delay else 0 * ms)
48
49     self.CIN_MNE = Connection(self.AfferentInput, self.MN_E, 'epsp-Aff',
50         weight=gSynE * 0.4, sparseness=1)
51     self.CIN_MNF = Connection(self.AfferentInput, self.MN_F, 'epsp-Aff',
52         weight=gSynE * 0.4, sparseness=1)
53
54     self.net.add(self.AfferentInput, self.CIN_RGE, self.CIN_RGF, self.
55         CIN_PFE, self.CIN_PFF, self.CIN_MNE, self.CIN_MNF)
56     super(modelA, self).setup_connections(use_delay=use_delay)
57     self.IA_F_MN_E.__init__(self.IA_F, self.MN_E, 'gi', weight=gSynI *
58         0.8, sparseness=1, structure='dense', max_delay=10 * ms if
59         use_delay else 0 * ms, delay=lambdai, j:delay_mean + randn(21)
60         * delay_std if use_delay else 0 * ms);
61     self.IA_E_MN_F.__init__(self.IA_E, self.MN_F, 'gi', weight=gSynI *
62         0.8, sparseness=1, structure='dense', max_delay=10 * ms if
63         use_delay else 0 * ms, delay=lambdai, j:delay_mean + randn(21)
64         * delay_std if use_delay else 0 * ms);
65     self.PF_E_INPF_F.__init__(self.PF_E, self.INPF_F, 'ge', weight=gSynE
66         * 0.6, sparseness=1, structure='dense', max_delay=10 * ms if
67         use_delay else 0 * ms, delay=lambdai, j:delay_mean + randn(20)
68         * delay_std if use_delay else 0 * ms);
69     self.PF_F_INPF_E.__init__(self.PF_F, self.INPF_E, 'ge', weight=gSynE
70         * 0.6, sparseness=1, structure='dense', max_delay=10 * ms if
71         use_delay else 0 * ms, delay=lambdai, j:delay_mean + randn(20)
72         * delay_std if use_delay else 0 * ms);
73
74     def setup_monitors(self):
75         super(modelA, self).setup_monitors()
76         self.spikesAffIn = SpikeMonitor(self.AfferentInput, record=True)
77         self.Spikelist.append(self.spikesAffIn)
78         self.SPMonitorNames.append("AffIn")
79         self.net.add(self.spikesAffIn)
80
81     def __call__(self, filename='rand_run', infrq=30 * Hz, j=0.75, k=1, l
82         =0.8, para=[], value=[], DUR=20 * second, display=False, report=0,
83         run=True):
84         self.inputfreq = infrq
85         filename = filename + ', GK = 2, ' + str(infrq) + ', j = ' + str(j) +
86             ', k = ' + str(k) + ', l = ' + str(l) + ' exp'
87         self.AfferentInput.__init__(20, self.spiketimes, period=1 / self.
88             inputfreq)
89
90         # increasing afferent input to motoneurons
91         self.CIN_MNE.__init__(self.AfferentInput, self.MN_E, 'epsp-Aff',
92             weight=gSynE * 0.4 * j, sparseness=1)
93         self.CIN_MNF.__init__(self.AfferentInput, self.MN_F, 'epsp-Aff',
94             weight=gSynE * 0.4 * j, sparseness=1)

```

```

63
64
65     # changing afferent input to RG/PF
66     self.CIN_RGE._init_(self.AfferentInput, self.RG_E, 'ge', weight=
        gSynE * 0.08 * 1, sparseness=1, structure='dense', max_delay=10
        * ms if use_delay else 0 * ms, delay=lambda i, j: delay_mean +
        randn(20) * delay_std if use_delay else 0 * ms)
67
68     self.CIN_RGF._init_(self.AfferentInput, self.RG_F, 'ge', weight=
        gSynE * 0.075 * 1, sparseness=1, structure='dense', max_delay=10
        * ms if use_delay else 0 * ms, delay=lambda i, j: delay_mean +
        randn(20) * delay_std if use_delay else 0 * ms)
69
70     self.CIN_PFE._init_(self.AfferentInput, self.PF_E, 'ge', weight=
        gSynE * 0.08 * 1, sparseness=1, structure='dense', max_delay=10
        * ms if use_delay else 0 * ms, delay=lambda i, j: delay_mean +
        randn(20) * delay_std if use_delay else 0 * ms)
71
72     self.CIN_PFF._init_(self.AfferentInput, self.PF_F, 'ge', weight=
        gSynE * 0.08 * 1, sparseness=1, structure='dense', max_delay=10
        * ms if use_delay else 0 * ms, delay=lambda i, j: delay_mean +
        randn(20) * delay_std if use_delay else 0 * ms)
73
74
75     super(modelA, self)._call_(para, value, DUR=DUR, report=report,
76         display=display, filename=filename, run=False)
77     # self.MN.dyn = 0
78
79     self.INFactory.SG_RG.drive = 0
80     self.INFactory.SG_PF.drive = 0
81     self.INFactory.SG_RG.GK = 2 * msiemens * cm ** -2
82     self.INFactory.SG_PF.GK = 2 * msiemens * cm ** -2
83     # self.INFactory.SG_INRG.Eleak = (-60+randn(self.INFactory.N_INRG)
        * 2.875*0) * mV
84
85     self.inject_assignments(para, value)
86     if run:
87         self.run()

```

Listing A.7: ModelB.py

```

1  from brian import *
2  from brian.library.random_processes import *
3  from brian.library.synapses import *
4  import MoNeuron as Moto
5  import InNeuron as IN
6  from time import clock
7  from MyConstants import gSynE, gSynI
8  from matplotlib.backends.backend_pdf import PdfPages
9  from ModelA import *
10
11  use_delay=True
12
13  class modelB(modelA):
14      def setup_neurons(self):
15          super(modelB, self).setup_neurons()
16
17      def setup_connections(self):
18          delay_mean=2*ms
19          delay_std=0.5*ms
20
21          self.INPF_E_preMN_E=Connection(self.INPF_E, self.MN_E, 'xprsyn', weight
          =0.8, sparseness=1, structure='dense', max_delay=10*ms if use_delay
          else 0 * ms, delay=lambda i, j: delay_mean+randn(21)*delay_std if
          use_delay else 0*ms);
22          self.INPF_F_preMN_F=Connection(self.INPF_F, self.MN_F, 'xprsyn', weight
          =0.8, sparseness=1, structure='dense', max_delay=10*ms if use_delay
          else 0 * ms, delay=lambda i, j: delay_mean+randn(21)*delay_std if
          use_delay else 0*ms);
23          self.net.add(self.INPF_E_preMN_E, self.INPF_F_preMN_F)
24          super(modelB, self).setup_connections()
25
26
27      def setup_monitors(self):

```

## A. APPENDIX

---

```

28         super(modelB, self).setup_monitors()
29
30         self.tracePresynMNE=StateMonitor(self.MN_E, 'Prsyn', record=[0])
31         self.traceXpresynMNE=StateMonitor(self.MN_F, 'Prsyn', record=[0])
32         self.traceHnapRGE=StateMonitor(self.RG_E, 'hnap', record=True)
33         self.traceHnapRGF=StateMonitor(self.RG_F, 'hnap', record=True)
34         self.spikeINPF_F=SpikeMonitor(self.INPF_F, record=True)
35         self.spikeINPF_E=SpikeMonitor(self.INPF_E, record=True)
36         self.spikeINRG_F=SpikeMonitor(self.INRG_F, record=True)
37         self.spikeINRG_E=SpikeMonitor(self.INRG_E, record=True)
38
39         self.Tracelist.append(self.tracePresynMNE)
40         self.Tracelist.append(self.traceXpresynMNE)
41         self.Tracelist.append(self.traceHnapRGE)
42         self.Tracelist.append(self.traceHnapRGF)
43         self.Spikelist.append(self.spikeINPF_E)
44         self.Spikelist.append(self.spikeINPF_F)
45         self.Spikelist.append(self.spikeINRG_E)
46         self.Spikelist.append(self.spikeINRG_F)
47         self.TrMonitorNames.append("PrsynMNE")
48         self.TrMonitorNames.append("PrsynMNF")
49         self.TrMonitorNames.append("HnapRGE")
50         self.TrMonitorNames.append("HnapRGF")
51         self.SPMonitorNames.append("INPFE")
52         self.SPMonitorNames.append("INPFF")
53         self.SPMonitorNames.append("INRGE")
54         self.SPMonitorNames.append("INRGF")
55         self.net.add(self.tracePresynMNE, self.traceXpresynMNE, self.spikeINPF_E
56             , self.spikeINPF_F, self.spikeINRG_E, self.spikeINRG_F, self
57             .traceHnapRGE, self.traceHnapRGF)
58
59     def __call__(self, filename='modelB', infreq=30*Hz, j=1.5, k=1, l=0.8, para=[],
60         value=[], DUR=20*second, display=False, report=0, run=True):
61         super(modelB, self).__call__(filename, infreq, j, k, l, para, value, DUR,
62             report=report, display=display, run=False)
63
64         self.MN_E.f_presyn=0.65
65         self.MN_F.f_presyn=0.65
66         if run:
67             self.run()

```

Listing A.8: ModelC.py

```

1  from brian import *
2  from brian.library.random_processes import *
3  from brian.library.synapses import *
4  import MoNeuron as Moto
5  import InNeuron as IN
6  from time import clock
7  from MyConstants import gSynE, gSynI
8  from matplotlib.backends.backend_pdf import PdfPages
9  from ModelB import *
10
11  use_delay=True
12
13  class modelC(modelB):
14      def setup_neurons(self):
15          self.additional_in=100
16          super(modelC, self).setup_neurons()
17          self.APath1 = self.INFactory.SG_IN.subgroup(20)
18          self.APath2 = self.INFactory.SG_IN.subgroup(20)
19          self.InPath = self.INFactory.SG_IN.subgroup(20)
20          self.APath2in = self.INFactory.SG_IN.subgroup(20)
21          self.Pois = PoissonGroup(20, rates=75 * hertz)
22          self.net.add(self.Pois)
23
24      def setup_connections(self):
25          delay_mean=2*ms
26          delay_std=0.5*ms
27          super(modelC, self).setup_connections()
28          self.Pois_InPath=Connection(self.Pois, self.InPath, 'ge', weight=gSynE

```

```

    *0.5, sparseness=1, structure='dense', max_delay=10*ms if use_delay
    else 0 *ms, delay= lambda i, j: delay_mean+randn(20)*delay_std if
    use_delay else 0*ms);
29 self.InPath_APath1=Connection(self.InPath, self.APath1, 'gi', weight=
    gSynI*2, sparseness=1, structure='dense', max_delay=10*ms if
    use_delay else 0 *ms, delay= lambda i, j: delay_mean+randn(20)*
    delay_std if use_delay else 0*ms);
30 self.InPfe.InPath=Connection(self.INPF_E, self.InPath, 'gi', weight=
    gSynI*2, sparseness=1, structure='dense', max_delay=10*ms if
    use_delay else 0 *ms, delay= lambda i, j: 5*ms+randn(20)*2*ms if
    use_delay else 0*ms);
31 self.CIN_APath1=Connection(self.AfferentInput, self.APath1, 'ge', weight
    =gSynE*0.75, sparseness=1, structure='dense', max_delay=10*ms if
    use_delay else 0 *ms, delay= lambda i, j: delay_mean+randn(20)*
    delay_std if use_delay else 0*ms);
32 self.APath1_APath2=Connection(self.APath1, self.APath2, 'ge', weight=
    gSynE*0.75, sparseness=1, structure='dense', max_delay=10*ms if
    use_delay else 0 *ms, delay= lambda i, j: delay_mean+randn(20)*
    delay_std if use_delay else 0*ms);
33 self.APath2_APath2in=Connection(self.APath1, self.APath2in, 'ge', weight
    =gSynE*0.75, sparseness=1, structure='dense', max_delay=10*ms if
    use_delay else 0 *ms, delay= lambda i, j: delay_mean+randn(20)*
    delay_std if use_delay else 0*ms);
34 self.APath2_MNF=Connection(self.APath2, self.MNF, 'ge', weight=gSynE
    *0.75, sparseness=1, structure='dense', max_delay=10*ms if
    use_delay else 0 *ms, delay= lambda i, j: delay_mean+randn(21)*
    delay_std if use_delay else 0*ms);
35 self.APath2in_MNF=Connection(self.APath2in, self.MNF, 'xprsyn', weight
    =0.8, sparseness=1, structure='dense', max_delay=10*ms if use_delay
    else 0 *ms, delay= lambda i, j: delay_mean+randn(21)*delay_std if
    use_delay else 0*ms);
36
37 self.net.add(self.Pois_InPath, self.InPath_APath1, self.InPfe.InPath,
    self.CIN_APath1, self.APath1_APath2, self.APath2_APath2in, self.
    APath2_MNF, self.APath2in_MNF)
38
39 def setup_monitors(self):
40     super(modelC, self).setup_monitors()
41
42     self.spikePois=SpikeMonitor(self.Pois, record=True)
43     self.spikeAPath1=SpikeMonitor(self.APath1, record=True)
44     self.spikeAPath2=SpikeMonitor(self.APath2, record=True)
45     self.spikeInPath=SpikeMonitor(self.InPath, record=True)
46
47     self.Spikelist.append(self.spikePois)
48     self.Spikelist.append(self.spikeAPath1)
49     self.Spikelist.append(self.spikeAPath2)
50     self.Spikelist.append(self.spikeInPath)
51
52     self.SPMonitorNames.append("Pois")
53     self.SPMonitorNames.append("APath1")
54     self.SPMonitorNames.append("APath2")
55     self.SPMonitorNames.append("InPath")
56
57     self.net.add(self.spikePois, self.spikeAPath1, self.spikeAPath2, self.
    spikeInPath)
58
59 def __call__(self, filename='modelC', infreq=30*Hz, j=1.5, k=1, l=0.8, para=[],
    value=[], DUR=20*second, display=False, report=0, run=True):
60     super(modelC, self).__call__(filename, infreq, j, k, l, para, value, DUR,
    report=report, display=display, run=False)
61     self.MNF.f_presyn=0.95
62     if run:
63         self.run()

```

Listing A.9: sampleRun.py

```

1 import matplotlib
2 matplotlib.use('Agg')
3
4 from ModelC import *

```

## A. APPENDIX

---

```
5 from brian.tools.datamanager import *
6 from brian.tools.taskfarm import *
7
8 if __name__ == '__main__':
9
10     lst = list()
11
12     for i in [2, 5, 10, 20, 25, 30, 35, 40, 45, 50, 55, 60]:
13         lst.append(('modelC', i*Hz, 1.5, 1, 0.8))
14
15     print lst
16
17     dataman = DataManager('modelC')
18     run_tasks(dataman, modelC, lst, True, 4)
```

### A.3 Curriculum vitae

See following pages.

## Simon M. Danner

CONTACT INFORMATION	Vienna University of Technology I. f. Analysis & Scientific Computing Operngasse 11/DF 01 06 1040 Vienna Austria	Phone: +43 1 58801 799 026 45 E-mail: simon.danner @ {gmail.com, meduniwien.ac.at, tuwien.ac.at}
POSITION	Research associate at the Institute for Analysis and Scientific Computing, Vienna University of Technology, Vienna, Austria and the Center for Medical Physics and Biomedical Engineering, Medical University of Vienna, Vienna, Austria.	
CITIZENSHIP	Austria	
DAY OF BIRTH	December 26, 1985	
PLACE OF BIRTH	Bregenz, Austria	
EDUCATION	<b>Vienna University of Technology</b> , Vienna, Austria	
	Doctoral studies in Engineering Sciences	<b>since March 2010</b>
	Thesis working title: <i>Biologically based simulation of human locomotor neural circuits activated by spinal cord stimulation</i> (Supervisor: Frank Rattay)	
	Master studies in Computer Science Management	<b>Mar. 2009 to Apr. 2011</b>
	Graduation with distinction, Degree: Mag.rer.soc.oec. equiv. to MSocEcSc Thesis: <i>An application for learning and teaching extracellular stimulation of axons</i> (Supervisor: Frank Rattay)	
	Master studies in Medicine and Computer Science	<b>Oct. 2008 to Feb. 2010</b>
	Graduation with distinction, Degree: Dipl.-Ing. equivalent to MSc Thesis: <i>Computer simulation of electrically stimulated nerve fibers in the human spinal cord</i> (Supervisor: Frank Rattay)	
	Bachelor studies in Medicine and Computer Science	<b>Oct. 2005 to July 2008</b>
	Degree: BSc Thesis: <i>Cartoon style rendering</i> (Supervisor: Muhammad Muddassir Malik)	
	<b>Bundesgymnasium Dornbirn</b> , Dornbirn, Austria	
	Oberstufenrealgymnasium (highschool with focus on mathematics)	<b>September 2000 to June 2004</b>
	Matura mit Auszeichnung (Graduation with distinction)	
	Gymnasium Unterstufe (junior highschool)	<b>September 1996 to July 2000</b>
	<b>Volksschule Mittelfeld</b> , Dornbirn, Austria	
	Volksschule (elementary school)	<b>September 1992 to July 1996</b>
EXPERIENCE	<b>Institute for Analysis and Scientific Computing, Vienna University of Technology</b> , Vienna, Austria	
	<i>Research associate</i>	<b>since Sept. 2011</b>
	Computational Neuroscience and Restorative Neurology	
	<b>Center for Medical Physics and Biomedical Engineering, Medical University of Vienna</b> , Vienna, Austria	
	<i>Research associate</i>	<b>since August 2011</b>
	Computational Neuroscience and Restorative Neurology	

## A. APPENDIX

---

	<p><b>International Society for Restorative Neurology (ISRN)</b>, Washington, DC</p> <p><i>Organizing Committee Inaugural Meeting of the ISRN</i> since <b>March 2011</b></p> <p>Member</p>
	<p><b>M. L. Zumtobel Liegenschaftsbeteiligungs GmbH</b>, Vienna, Austria</p> <p><i>Custom real management application</i> <b>May 2011 to June 2011</b></p> <p>Development</p>
	<p><b>Baylor College of Medicine</b>, Houston, TX</p> <p><i>Study stay</i> <b>Nov. 2010 to Apr. 2011</b></p> <p>Trainee of Em. Prof. Dr. Milan R. Dimitrijevic and assistant editor of Dimitrijevic et al. <i>Principles of Restorative Neurology for Spinal Cord Injury Motor Control</i>. New York: Oxford University Press.</p>
	<p><b>Medicinska fakulteta Univerza v Ljubljani</b>, Ljubljana, Slovenia</p> <p><i>Study stay</i> <b>Sept. 2010 to Oct. 2010</b></p> <p>Trainee of Em. Prof. Dr. Milan R. Dimitrijevic</p>
	<p><b>Lehman Brothers International, London-Zurich Branch</b>, Zurich, Switzerland</p> <p><i>Accounting and client-management tool</i> <b>June 2007 to December 2007</b></p> <p>Planning and development; role as the project manager in a team of two</p>
	<p><b>Ausbildungszentrum Vorarlberg</b>, Bregenz, Austria</p> <p><i>Alternative civilian service</i> <b>October 2004 to September 2005</b></p> <p>Care and help for handicapped adolescents</p>
TEACHING EXPERIENCE	<p><b>Vienna University of Technology</b>, Vienna, Austria</p> <p>Computer simulation in medicine; lecture with demonstrations <b>WS2011, WS2012</b></p> <p>Computer simulation; exercises <b>WS2011</b></p>
AWARDS AND SCHOLARSHIPS	<p>Travel award for the <i>22nd Annual Computational Neuroscience Meeting (CNS*2013)</i>, Paris, France, 2013 (\$400).</p> <p>Grad student travel award for <i>Cellular and Network Functions in the Spinal Cord</i>, Madison, WI, 2012 (\$300).</p> <p>Advancement award for the best master thesis presentation of the Austrian Society for Biomedical Engineering at the <i>Medizinische Physik 2011, 3 Ländertagung der ÖGMP, DGMP und SGSMP</i>, Vienna, Austria (€250).</p> <p>Merit scholarship from the Vienna University of Technology for the academic year of 2008/2009 (€730) and 2009/2010 (€900)</p>
MEMBERSHIPS	<p>International Society for Restorative Neurology, Society for Neuroscience, Organization for Computational Neuroscience, Austrian Society for Biomedical Engineering</p>
LANGUAGES	<p>German (native), English (fluent)</p>
PUBLICATIONS	<p><b>Danner, S. M.</b>, Hofstoetter U. S. and Minassian K. (2013). Finite Element Models of Transcutaneous Spinal Cord Stimulation. In: Jaeger D., Jung R. (Eds.) <i>Encyclopedia of Computational Neuroscience</i>: SpringerReference (www.springerreference.com). Berlin Heidelberg: Springer-Verlag. DOI: 10.1007/SpringerReference_348669</p>



Rattay F., **Danner, S. M.**, Hofstoetter U. S. and Minassian K. (2013). Finite Element Modeling for Extracellular Stimulation. In: Jaeger D., Jung R. (Eds.) Encyclopedia of Computational Neuroscience: SpringerReference (www.springerreference.com). Berlin Heidelberg: Springer-Verlag. DOI: 10.1007/SpringerReference.348658

Hofstötter U. S., **Danner, S. M.** and Minassian K.: Paraspinal Magnetic and Transcutaneous Electrical Stimulation. In: Jaeger D., Jung R. (Eds.) Encyclopedia of Computational Neuroscience: SpringerReference (www.springerreference.com). Berlin Heidelberg: Springer-Verlag. DOI: 10.1007/SpringerReference.348668 2013-03-27

**Danner, S. M.**, Wenger, C. and Rattay, F. (2011). *Electrical stimulation of myelinated axons: An interactive tutorial supported by computer simulation*. Saarbrücken: VDM Verlag.

Száva, Z., **Danner, S. M.** and Minassian, K. (2011). *Transcutaneous electrical spinal cord stimulation: Biophysics of a new rehabilitation method after spinal cord injury*. Saarbrücken: VDM Verlag.

**Danner, S. M.**, Hofstoetter, U. S., Ladenbauer, J., Rattay, F. and Minassian, K. (2011). Can the human lumbar posterior columns be stimulated by transcutaneous spinal cord stimulation? A modeling study. *Artificial Organs* 35(3), 257–262.

CONFERENCE  
PRESENTATIONS

**Danner, S. M.**, Rattay, F., Hofstoetter, U. S., Dimitrijevic, M. R. and Minassian, K. (2013). Modeling locomotor pattern generating networks of the human lumbar spinal cord. *Neuroscience 2013, Nov. 9–13, San Diego, CA*.

Dimitrijevic, M. R., Hofstoetter, U. S., Mayr, W., Minassian, K., Rattay, F. and **Danner, S. M.** (2013). Epidural stimulation of the human lumbar spinal cord can elicit characteristic tonic motor outputs. *Neuroscience 2013, Nov. 9–13, San Diego, CA*.

Hofstoetter, U. S., Minassian, K., **Danner, S. M.**, Rattay, F. and Dimitrijevic, M. R. (2013). Alternating modulations of posterior root-muscle reflexes of the human lumbosacral spinal cord: Inhibitory circuits outside the lumbar locomotor pattern generator. *Neuroscience 2013, Nov. 9–13, San Diego, CA*.

Minassian, K., **Danner, S. M.**, Hofstoetter, U. S., Rattay, F. and Dimitrijevic, M. R. (2013). Central rhythm and pattern generating capabilities of the human lumbar spinal cord. *Neuroscience 2013, Nov. 9–13, San Diego, CA*.

Krenn, M., Toth, A., **Danner, S. M.**, Hofstoetter, U. S., Minassian, K. and Mayr, W. (2013). Selectivity of transcutaneous lumbar spinal cord stimulation for eliciting posterior root-muscle reflexes in humans. *Neuroscience 2013, Nov. 9–13, San Diego, CA*.

**Danner, S. M.**, and Dimitrijevic, M. R. (2013). Segmental and plurisegmental processing capabilities of the human lumbar cord isolated from brain motor control. *52nd Annual Scientific Meeting of ISCOS, October 28–30, Istanbul, Turkey*.

**Danner, S. M.**, McKay, W. B., Minassian, K., Hofstoetter, U. S., Mayr, W., Rattay, F. and Dimitrijevic, M. R. (2013). Neurophysiology model of the human lumbar cord separated from brain control by traumatic injury. *SiNAPSA Neuroscience Conference '13 (SNC'13), September 27–29, Ljubljana, Slovenia*.

Krenn, M., Minassian, K., Hofstoetter, U. S., **Danner, S. M.**, Dimitrijevic, M. R. and Mayr, W. (2013). Electrophysiology of posterior roots-muscle reflex of the human lumbosacral cord. *SiNAPSA Neuroscience Conference '13 (SNC'13), September 27–29, Ljubljana, Slovenia*.

**Danner, S. M.**, Rattay, F., Hofstoetter, U. S., Dimitrijevic, M. R. and Minassian, K. (2013). Locomotor rhythm and pattern generating networks of the human lumbar spinal cord: an electrophysiological and computer modeling study. *22nd Annual Computational Neuroscience meeting: CNS\*2013, July 13–18, Paris, France. BMC Neuroscience, 14* (Suppl 1), P274. DOI: 10.1186/1471-2202-14-S1-P274

Mayr, W., **Danner, S. M.**, Hofstoetter, U. S., Krenn, M., Minassian, K., Tansey, K., Freundl, B. and Binder, H. (2013). Non-invasive spinal cord stimulation and assisted treadmill stepping to generate rhythmic activities in motor complete spinal cord injured people. Wings for Life scientific meeting, April 23-24 2013, Salzburg, Austria

**Danner, S. M.** (2013). Locomotor rhythm and pattern generating networks of the human lumbar spinal cord: Computer modeling study *Workshop on Recent advances in the pathophysiology and neurorehabilitation of spinal lesions, April 13, 2013, Trieste, Italy.*

**Danner, S. M.**, Sarabon, N., Panjan, A., Mayr, W., Hofstoetter, U. S., Minassian, K., Krenn, M., Rattay, F., Tansey, K. E. and Dimitrijevic, M. R. (2012). Modification of posterior root-muscle reflexes by volitional motor tasks. *Program Number 890.01. Neuroscience Meeting Planner Neuroscience, New Orleans, LA.*

**Danner, S. M.**, Hofstoetter, U. S., Rattay, F., Mayr, W. and Minassian, K. (2012). Simulation transkutaneer Aktivierung neuronaler Strukturen am Beispiel der Rückenmarkstimulation. *ÖGBMT Jahrestagung 2012 und Tiroler Medizintechnik-Forum, Hall in Tirol, Austria.*

Mayr, W., Minassian, K., Tansey, K., Rattay, F., **Danner, S.**, Krenn, M., Hofstoetter, U., Dimitrijevic, M. R. (2012). Non-invasive transcutaneous stimulation of the human lumbar spinal cord facilitates locomotor output in spinal cord injury. *DGBMT Jahrestagung (BMT 2012), Jena, Germany.*

**Danner, S. M.**, Hofstoetter, U. S., Minassian, K., Rattay, F., Mayr, W. and Dimitrijevic, M. R. (2012). The human lumbar cord circuitry disconnected from the brain can generate a variety of motor outputs in response to non-patterned spinal cord stimulation at different frequencies. *Cellular and Network Functions in the Spinal Cord, Madison, WI.*

Mayr, W., **Danner, S. M.**, Sarabon, N., Panjan, A., Krenn, M., Hofstoetter, U. S., Minassian, K., Rattay, F. and Dimitrijevic, M. R. (2012). Effect of functional electrical stimulation on the central state of excitability of the spinal cord. *World Congress for Medical Physics and Biomedical Engineering, Beijing, China.*

**Danner, S. M.**, Rattay, F., Bijak, M., Mayr, W., Minassian, K., Hofstoetter, U. S. and Dimitrijevic, M. R. (2011). Human lumbar cord can process spinal cord stimulation of different frequencies. *Program No. 182.06. 2011 Neuroscience Meeting Planner. Washington, DC: Society for Neuroscience, 2011. Online.*

**Danner, S. M.** and Rattay, F. (2011). An application for learning and teaching extracellular stimulation of axons. *Medizinische Physik 2011, 3 Ländertagung der ÖGMP, DGMP und SGSM, Vienna, Austria.*

**Danner, S. M.** (2011). An application for learning and teaching extracellular stimulation of axons. *EPLOG, Präsentation der Diplomarbeiten der Fakultät Informatik, Sommersemester 2011, Vienna, Austria, 82.*

Dimitrijevic, M. R. and **Danner, S. M.** (2011). Spinal interneuronal network activity elicited by epidural lumbar posterior root stimulation. *8th International Symposium on Experimental Spinal Cord Repair and Regeneration, Brescia, Italy.*

Dimitrijevic, M. R. and **Danner, S. M.** (2011). Neurocontrol of gait in patients with initial complete upper motor neuron lesion after spinal cord injury. *8th international symposium on experimental spinal cord repair and regeneration, Brescia, Italy.*

Rattay, F., Minassian, K., Hofstoetter, U. S., **Danner, S. M.**, Mayr, W. and Dimitrijevic, M. R. (2010). Computation in neuroscience of conducting and processing capabilities of the human nervous system. *10th Vienna international workshop on functional electrical stimulation and 15th annual conference of the international FES society, Vienna, Austria.*

**Danner, S. M.** (2010). Biologically based simulation of human locomotor neural circuits activated by spinal cord stimulation. *MEiCogSci Conference, Dubrovnik, Croatia, 14.*

- Danner, S. M.** (2010). Computer simulation of electrically stimulated nerve fibers in the human spinal cord. *EPILOG, Präsentation der Diplomarbeiten der Fakultät für Informatik, Sommersemester 2010, Vienna, Austria*, 80.
- PAPERS IN  
CONFERENCE  
PROCEEDINGS
- Danner, S. M.**, Rattay, F., Hofstoetter, U. S., Dimitrijevic, M. R. and Minassian, K. (2013). Pattern generating networks in the human lumbar spinal cord: electrophysiology and computer modeling. *BMT 2013, Sept. 19–21, Graz, Austria*.
- Hofstoetter, U. S., **Danner, S. M.**, Dimitrijevic, M. R., Hofer, C., Kern, H., Mayr, W. and Minassian, K. (2013). Effects of transcutaneous spinal cord stimulation on voluntary locomotor activity in an incomplete spinal cord injured individual. *BMT 2013, Sept. 19–21, Graz, Austria*.
- Minassian, K., Hofstoetter, U. S., **Danner, S. M.**, Mayr, W., McKay, W. B., Tansey, K. and Dimitrijevic, M. R. (2013). Mechanisms of rhythm generation of the human lumbar spinal cord in response to tonic stimulation without and with step-related sensory feedback. *BMT 2013, Sept. 19–21, Graz, Austria*.
- Krenn, M., Toth, A., **Danner, S. M.**, Hofstoetter, U. S., Minassian, K. and Mayr, W. (2013). Selectivity of transcutaneous stimulation of lumbar posterior roots at different spinal levels in humans. *BMT 2013, Sept. 19–21, Graz, Austria*.
- Danner, S. M.**, Hofstoetter, U. S., Rattay, F., Mayr, W. and Minassian, K. (2012). Simulation transkutaner Aktivierung neuronaler Strukturen am Beispiel der Rückenmarkstimulation. In: C. Baumgartner, W. Mayr (eds.) *Proceedings der ÖGBMT Jahrestagung 2012 und Tiroler Medizintechnik-Forum*, 15–16. ISBN: 978-3-9503191-1-8.
- Danner, S. M.** and Dimitrijevic, M. R. (2012). Spasticity: Pathophysiology and neural control. In: P Kusumastuti, A.B.M. Tular (eds.) *Proceedings of the 3rd Asia-Oceanian Conference of Physical and Rehabilitation Medicine*, 9–15. Pianoro: Medimond. ISBN: 978-88-7587-655-5.
- Mayr, W., **Danner, S. M.**, Sarabon, N., Panjan, A., Krenn, M., Hofstoetter, U. S., Minassian, K., Rattay, F. and Dimitrijevic, M. R. (2012). Effect of functional electrical stimulation on the central state of excitability of the spinal cord. In Long, M., editor, *World Congress on Medical Physics and Biomedical Engineering May 26-31, 2012, Beijing, China*, volume 39 of IFMBE Proceedings, pages 2240–2243. Springer Berlin Heidelberg. DOI: 10.1007/978-3-642-29305-4\_588
- Rattay, F., Minassian, K., Hofstoetter, U. S., **Danner, S. M.**, Mayr, W. and Dimitrijevic, M. R. (2010). Computation in neuroscience of conducting and processing capabilities of the human nervous system. *Proceedings of the 10th Vienna international workshop on functional electrical stimulation and 15th annual conference of the international FES society*, 268–270. ISBN: 978-3-900928-09-4.
- Danner, S. M.** (2010). Biologically based simulation of human locomotor neural circuits activated by spinal cord stimulation. *Proceedings of the MEiCogSci Conference 2010*, 14.
- CONFERENCE  
WORKSHOPS
- Hofstoetter, U. S., Minassian, K., **Danner, S. M.**, Mayr, W., Rattay, F. and Dimitrijevic, M. R. (2010). Spinal cord Stimulation. *10th Vienna international workshop on functional electrical stimulation and 15th annual conference of the international FES society, Vienna, Austria*.

